PERFORMANCE BASED MECHANISTIC-EMPIRICAL APPROACH TO ASSESS JOINT SEALANT EFFECTIVENESS ON SUSTAINABILITY OF CONCRETE PAVEMENT INFRASTRUCTURE

A Dissertation

by

KEIVAN NESHVADIAN BAKHSH

Submitted to the Office of Graduate and Professional Studies of
Texas A&M University
in partial fulfillment of the requirements for the degree of

DOCTOR OF PHILOSOPHY

Chair of Committee,	Dan Zollinger
Committee Members,	Robert Lytton
	Dallas Little
	Bruce Herbert
Head of Department,	Robin Autenrieth

August 2014

Major Subject: Civil Engineering

ABSTRACT

The primary purpose of sealing joints in rigid pavement is to prevent or reduce the amount of water infiltrating into pavement structure. It is well accepted that the presence of moisture in a pavement structure is a contributor to a variety of governing distress types that eventually deteriorates the pavement structure and decreases the pavement service life. Effectiveness of joint sealants to protect jointed concrete pavement against water related distresses has been a focus of great interest recently. An experimental program was carried out on the Riverside Campus of Texas A&M University to study the effectiveness of different sealant types to limit drainage related infiltration of the joint under different joint openings and bonding conditions. Results confirmed that if joint seals are properly installed, they can be very effective in preventing moisture infiltration. Unsealed joints had significantly higher flow rates compared to joints with damaged sealants. The test results in this study have also demonstrated the effect of sealant proper installation on performance. Using experimental data the actual number of wet days was defined and analyzed.

A faulting prediction model was developed. The erosion resistance of materials, number of wet days and traffic load were precisely defined and considered in this model. The mechanistic empirical model presented in this dissertation can effectively analyze the faulting and erosion in jointed concrete pavements. The model is capable to be calibrated for local conditions as a distinct advantage over other faulting models. The model was successfully implemented and calibrated into a computerized format. Results

show that the model fits well with the field data and can be implemented for design and maintenance management purposes.

By using the model the effectiveness of sealant in pavement sustainability can be determined. The most valuable outcome of this study is the demonstration mechanistically of the role of joint sealing on service life of jointed concrete pavements. Sealants, by limiting water infiltration into the pavement sublayers, can greatly improve concrete pavement performance.

DEDICATION

To my parents,

Pouran and Farzad

ACKNOWLEDGEMENTS

I would like to express great appreciation to my advisor and chair of committee, Professor Dan G. Zollinger, for his guidance and continuous encouragement during the course of this work. Special thanks are extended to Dr. Robert Lytton, Dr. Dallas Little, and Dr. Bruce Herbert for their useful suggestions and for serving as advisory committee members. I would also like to thank Dr. Jose Rafael Menendez for his great friendship and support.

Finally, thanks to my parents, Pouran and Farzad and my brother, Kamyar, for their encouragement and love.

NOMENCLATURE

AASHTO	American Association of State Highway and Transportation Officials
ACI	American Concrete Association
ADOT	Arizona Department of Transportation
ADT	Average daily traffic
ADTT	Average daily truck traffic
ASTM	American Society of Testing Materials
CRC	Continuously reinforced concrete
CRCP	Continuously reinforced concrete pavement
DC	Dielectric constant
DOT	Department of Transportation
ESAL	Equivalent single axle load
FHWA	Federal Highway Administration
FWD	Falling weight deflectometer
GPR	Ground penetration radar
HWTD	Hamburg wheel-tracking device
JPCP	Jointed plain concrete pavement
LTE	Load transfer efficiency
LTPP	Long-term pavement performance
MEPDG	Mechanistic-Empirical Pavement Design Guide
NCHRP	National Cooperative Highway Research Program

PCC	Portland cement concrete
SHRP	Strategic Highway Research Program
SPS	Specific Pavement Study
TxDOT	Texas Department of Transportation
WisDOT	Wisconsin Department of Transportation

TABLE OF CONTENTS

Page

ABSTRACT ii

DEDICATION iv

ACKNOWLEDGEMENTS v

NOMENCLATURE vi

TABLE OF CONTENTS viii

LIST OF FIGURES xi

LIST OF TABLES xv

1. INTRODUCTION 1

1.1 Statement of the Problem 1
1.2 Research Approach 2
1.3 Structure of Dissertation 5

2. LITERATURE REVIEW 7

2.1 Joints in Concrete Pavements 7
2.2 Early Use of Sealant in PCC Pavements 8
2.3 Main Sealant Material Types 9
2.4 Current Sealant Practice 12
2.5 Sealant Adhesive and Cohesive Failure 15
2.6 Questioning the Need for Joint Sealing 20

3. FIELD TESTING ON JOINT SEALANT PERFORMANCE 25

3.1 Pavement Test Area 25
3.2 Field Test Conditions 28
3.3 Flow Test (Infiltration Test) 29
3.4 Evaluate Infiltration Rates of Sealed Joints 30
3.5 Flow Test Using a Movable Joint System 32
3.6 Test Results of Movable Joint Systems 34
3.7 Tests on Joint Sealant Installation 38

4. EVALUATION OF NUMBER OF WET DAYS FOR DESIGN PURPOSES 41

4.1 Pavement Drainage 41
4.2 Transmission of Water into the Pavement Sublayer 43
4.3 Rainfall Inflow 45
4.4 Water Surface Flow and Joint Infiltration 46
4.5 Infiltration Coefficient of the Sealant 49
4.5.1 Sealant Damage Test and Flow Factor 50
4.5.2 Sealant Installation Test and Installation Factor 56
4.5.3 Calculation of Infiltration Coefficient 59
4.6 Water Movement in the Subbase 60
4.7 Calculation of Number of Wet Days 66

5. FAULTING PREDICTION MODEL FOR DESIGN OF CONCRETE PAVEMENT STRUCTURES 75

5.1 Introduction 75
5.2 Faulting, a Major Distress Type in Concrete Pavements 75
5.2.1 Traffic Loads and Pavement Strength 77
5.2.2 Existence of Water underneath the Slab 77
5.2.3 Erosion Potential of the Subbase 78
5.3 Faulting/ Erosion Model 79
5.3.1 General Form of the Model 80
5.3.2 Calculations for Equivalent Traffic Level 82
5.3.3 Calculations for Effective ESALs, N_i 83
5.3.4 Ultimate Load and Shear Strength, Nf 84
5.4 Computerization of the Model 87
5.5 Sensitivity Analysis 88
5.6 Field Data 92
5.7 Conclusions and Discussion 96

6. SUBBASE EROSION CHARACTERISTICS 97

6.1 Material Selection 98
6.1.1 Gradation and Classifications 99
6.1.2 Maximum Density and Optimum Moisture 104
6.2 Method of Testing Erosion 104
6.2.1 Hamburg Wheel-Tracking Device 104
6.2.2 Test Program 106
6.2.3 Stabilized Samples 109
6.3 Test Results 110
6.3.1 Dry and Wet Erosion Tests (At Optimum Moisture) 110
6.3.2 Erosion Tests on Clays 115
6.3.3 Stabilized Clay Samples 118
6.3.4 Stabilized Sand Samples 121

7. CONCLUSIONS AND DISCUSSIONS....124

REFERENCES....128

APPENDIX A. SOIL SAMPLES CLASSIFICATIONS....136

Sample Number 1....136
Sample Number 2....137
Sample Number 3....138
Sample Number 4....139
Sample Number 5....140
Sample Number 6....141
Sample Number 7....142
Sample Number 8....143

APPENDIX B. SOIL SAMPLES ATTERBERG LIMITS....144

APPENDIX C. LIME STABILIZATION ON CLAY SAMPLES....145

APPENDIX D. HAMBURG TEST RESULTS....147

APPENDIX E. EVAPORATION OF TRAPPED WATER IN A JOINT WELL....151

LIST OF FIGURES

Page

Figure 1 Cohesive Failure in Sealants. 16

Figure 2 Adhesive Failure in Sealants. 16

Figure 3 Layout of Joint Sealant Test Area. 26

Figure 4 Joint Sealant Layouts. 26

Figure 5 Joint Sealing Process. 27

Figure 6 Flow Test on Existing Joint. 30

Figure 7 Damaged Sealing Condition. 31

Figure 8 Flow Test Results on Damaged Sealants. 32

Figure 9 Schematic of the Movable Joint System. 33

Figure 10 Installation of the Movable Joint System. 34

Figure 11 Flow Test Results for Various Joint Sealant Types. 35

Figure 12 Slope of Flow Rate Increase with Joint Opening. 37

Figure 13 Increasing Rate of Flow with Joint Opening. 38

Figure 14 Water Infiltration Rates for Different Joint Dirtiness Levels. 40

Figure 15 Water Related Damages; Potholes, Corner Breaking and Wide Cracks. 42

Figure 16 Three Stages of Water Transmission into Subbase Layer. 44

Figure 17 Maximum 1-H-Duration/1-Y-Frequency Precipitation in the U.S [44]. 47

Figure 18 Open Graded Granular Subbase Used for Test Program. 50

Figure 19 Fifty Percent Debonded Sealant 51

Figure 20 Infiltration Test Results on Damaged Sealants. 53
Figure 21 Infiltrations for Different Damage Levels Compared to 100% Damaged. 53
Figure 22 Modulus Aging Parameter versus Time [48]. 55
Figure 23 Adhesive Strength Aging Parameter versus Time [20]. 56
Figure 24 Water Infiltration Rates for Different Joint Dirtiness Levels. 57
Figure 25 Average Infiltration Rates for Different Dirtiness Levels. 58
Figure 26 Flow Net for Water Seepage from the Concrete Joints into the Subbase. 64
Figure 27 Regression to Fit the Ratio of Flow Net Lines to Base Thickness. 65
Figure 28 Example of Subbase Seepage Distribution. 69
Figure 29 Algorithm to Calculate the Number of Wet Days. 70
Figure 30 Computer Spreadsheet Program that Calculates the Number of Wet Days. 71
Figure 31 P_2 Distribution for the Example Analysis. 73
Figure 32 P_2 Cumulative Distribution for the Example Analysis. 73
Figure 33 P_{sb} Distribution for the Example Analysis. 74
Figure 34 P_{sb} Cumulative Distribution for the Example Analysis. 74
Figure 35 Three Main Elements Contributing in Subbase Erosion and PCC Faulting. 76
Figure 36 Sample Gumbel S-Shaped Distribution. 81
Figure 37 Shear Strength and Angle of Friction Determinations. 86
Figure 38 The Design Program Main Page. 88
Figure 39 Sensitivity Analysis on Base Curve. 90
Figure 40 Changes of Load Transfer Efficiency With and Without Dowel Bars. 91
Figure 41 Calibration of the Model Using the Field Data. 94

Figure 42 Modeled versus Measured Faulting of LTPP Data. 95
Figure 43 The Soil Classification Triangle and U.S. Soil Classification Map [63]. 99
Figure 44 Comparison between Two of the Sample's Gradation. 101
Figure 45 PI for Each Sample along with the Percent of Minus 200 (Silt and Clay). ... 102
Figure 46 Grading Curves for Collected Samples. 103
Figure 47 Hamburg Wheel-Tracking Device (HWTD) [59]. 106
Figure 48 Schematic View to Compare the Permeability of Sand versus Clay. 108
Figure 49 Erosion Tests Results for all Samples (Wet and Dry Tests). 111
Figure 50 Dry Erosion Tests Results for all Samples. 112
Figure 51 Wet Erosion Tests Results for all Samples. 112
Figure 52 Hamburg Test Results for One Sample of Each Subcategory. 114
Figure 53 Dry Hamburg Test Results. 114
Figure 54 Wet Hamburg Test Results. 115
Figure 55 Results for Hamburg Test on Lean Clay and Fat Clay. 116
Figure 56 Hamburg Tests for Lean Clay, Sample Number 7. 117
Figure 57 Hamburg Tests for Fat Clay, Sample Number 8. 118
Figure 58 Results for Hamburg Test on Stabilized Clays. 119
Figure 59 Hamburg Tests for Stabilized Lean Clay, Sample Number 7. 120
Figure 60 Hamburg Tests for Stabilized Fat Clay, Sample Number 8. 120
Figure 61 Results for Hamburg Test on Stabilized Sand. 122
Figure 62 Hamburg Tests for Stabilized Sand, Sample Number 1. 122
Figure 63 Gradation Curve for Sample No. 1, Poorly Graded Sand. 136

Figure 64 Gradation Curve for Sample No. 2, Poorly Graded Sand with Silt. 137
Figure 65 Gradation Curve for Sample No. 3, Silty Sand. 138
Figure 66 Gradation Curve for Sample No. 4, Sandy Silt. 139
Figure 67 Gradation Curve for Sample No. 5, Sandy Lean Clay. 140
Figure 68 Gradation Curve for Sample No. 6, Sandy Lean Clay with Gravel. 141
Figure 69 Gradation Curve for Sample No. 7, Lean Clay with Sand. 142
Figure 70 Gradation Curve for Sample No. 8, Fat Clay with Sand. 143
Figure 71 Fine Particles Classifcation for Samples (ASTM D2487). 144
Figure 72 PH Measurement Device. 145
Figure 73 PH Test Plot for Lean Clay, Sample No. 7. 146
Figure 74 PH Test Plot for Fat Clay, Sample No. 8. 146
Figure 75 Erosion Test Results for Poorly Graded Sand. 147
Figure 76 Erosion Test Results for Poorly Graded Sand with Silt. 147
Figure 77 Erosion Test Results for Silty Sand. 148
Figure 78 Erosion Test Results for Sandy Silt. 148
Figure 79 Erosion Test Results for Sandy Lean Clay. 149
Figure 80 Erosion Test Results for Sandy Lean Clay with Gravel. 149
Figure 81 Erosion Test Results for Lean Clay with Sand. 150
Figure 82 Erosion Test Results for Fat Clay with Sand. 150
Figure 83 Evaporation of Trapped Water in a Joint. 151

LIST OF TABLES

Page

Table 1 Factors and Causes of Sealant Failure. 18

Table 2 Test Controlling Factors for Joint Sealant Field Study. 28

Table 3 Flow Test Results for Various Joint Sealant Types. 36

Table 4 Infiltration Test Results on Damaged Sealants. 52

Table 5 Flow Factor for Different Sealant Conditions. 56

Table 6 Dirtiness Levels, Installation Qualities and Calculated Installation Factor. 59

Table 7 Installation Factor as a Function of Installation Quality. 59

Table 8 Number of Flow and Equpotential Lines for Different Base Thicknesses. 64

Table 9 Input Values for the Example Pavement. 71

Table 10 Output Values for the Example Pavement. 72

Table 11. Input Parameters for the Base Analysis. 89

Table 12. Changed Parameter for Each of the Five Case Studies. 90

Table 13. Sensitivity Analysis Results. 92

Table 14. Construction Information on LTPP Sections. 93

Table 15. Statistical Analysis for Sampled LTPP Faulting Data. 95

Table 16 Soil Samples Location and Classification (NP for Non-Plastic). 103

Table 17 Compaction Test Results for Samples. 104

Table 18 Erosion Tests Using Hamburg Wheel-Tracking Device (HWTD). 108

Table 19 Results of Dry and Wet Erosion Tests (Optimum Moisture) for all Samples. 111

Table 20 Results for Hamburg Test on Lean Clay and Fat Clay. 116

Table 21 Results for Hamburg Test on Stabilized Clays. 119

Table 22 Results for Hamburg Test on Stabilized Sand. 121

Table 23 Gradation Table for Sample No. 1, Poorly Graded Sand. 136

Table 24 Gradation Table for Sample No. 2, Poorly Graded Sand with Silt. 137

Table 25 Gradation Table for Sample No. 3, Silty Sand. 138

Table 26 Gradation Table for Sample No. 4, Sandy Silt. 139

Table 27 Gradation Table for Sample No. 5, Sandy Lean Clay. 140

Table 28 Gradation Table for Sample No. 6, Sandy Lean Clay with Gravel. 141

Table 29 Gradation Table for Sample No. 7, Lean Clay with Sand. 142

Table 30 Gradation Table for Sample No. 8, Fat Clay with Sand. 143

Table 31 Atterberg Limits for Samples. 144

1. INTRODUCTION

1.1 Statement of the Problem

Joints in concrete pavements are intended to provide freedom of movement of the slab relative to concrete volume changes due to drying shrinkage, temperature changes and moisture differences. The primary purpose for sealing rigid pavement joints is to prevent or reduce the amount of water infiltrating into a pavement structure, which results in slab erosion, loss of support and other water related distresses.

It is well accepted that the presence of moisture in a pavement structure is a contributor to a variety of governing distress types that eventually deteriorates it and decreases the useful service life. Effectiveness of sealants to protect jointed concrete pavement against water related distresses has been a focus of great interest recently. There have been a number of research studies, field observations and testing programs that has been performed on joint sealants in concrete pavements. State and other DOT's have adopted a wide variety of joint sealing practices and policies for jointed pavements, derived from local experience, climate, and traffic conditions. In response to an NCHRP survey, "nine state highway agencies reported that they seal joints, but do not provide positive subsurface drainage in every instance. Thirty states reported that they sealed joints but also use a permeable base layer, a subsurface drainage system, or both. The remaining eleven states reported that they took the position that water will inevitably enter the pavement system and sought only to control it through use of a drainage layer or other subsurface drainage, or both rather than relying on the capability of joint

sealant. And one of the eleven states, Wisconsin, reported that it had dispensed with joint sealing entirely" [1].

This research aims to evaluate the effect of joint sealant on jointed concrete pavement sustainability and performance. The outcome of this study should help state DOT's, contractors, maintenance agencies and pavement designers to make better decisions on using sealants in respect to long term performance of a pavement. The right decision on using sealant can save maintenance effort and cost and improve performance and pavement serviceability.

1.2 Research Approach

An experimental program was carried out on the Riverside Campus of Texas A&M University to study the effectiveness of different sealant types to limit drainage related infiltration of the joint under different joint openings. The experiments included three main sealant types; silicon based sealants, hot pour asphalt based sealants, and compression sealants with different sealant debonding conditions and joint reservoir geometries. A unique system of concrete joints, movable joint system, was employed to simulate joint widening. The experiment also addressed the importance of installation on joint sealants effectiveness. A flow test was introduced as an easy, quick and reliable in situ test method to evaluate the amount of water infiltration in to a joint and therefore to evaluate the effectiveness of the sealant to keep the water away from the sublayers.

The aim of this extensive test program is listed as follows;

- To evaluate how effectual is a joint sealant to prevent water from infiltrating into the sublayer

- To evaluate the difference of an unsealed joint versus a sealed joint in terms amount of water infiltration
- To assess the sealant bond quality under different joint openings (a movable joint system was used as a simulation of joint sealant's behavior during hot and cold seasons when joint width changes)
- To compare different types of sealants in different joint opening and debonding conditions in respect to water infiltration
- To determine the importance of installation quality and joint reservoir's cleanness prior to sealing the joints

The test program led to fruitful results and solid conclusions on sealants effectiveness in respect to water infiltration.

Furthermore, the sealant effectiveness in terms of concrete pavement long term performance was analyzed. Beside the importance of sealant capability to keep water away from the sublayer, it is of a great interest of project owners, designers, contractors and maintenance agencies to determine how sealing or not sealing may affect the sustainability of a concrete pavement. Sealant effectiveness was placed in a concrete pavement performance model so the effect of sealing or no sealing could be determined for any particular pavement structure in terms of damage commencement and distress development during the service life.

One of the most important consequences of water infiltration through joints in concrete pavement is the inevitable erosion at the interface of sublayers. Subbase erosion directly contributes to the process of joint faulting which can involve several

factors. Faulting is considered as a major distress type in jointed concrete pavements and as a result is a major criteria for designing concrete pavements. The effects of faulting have implications on the pavement both structurally and in terms of serviceability. Faulting if not maintained in a timely manner can also lead to other distresses and impose considerable repair costs.

A mechanistic-empirical faulting prediction model was developed .The effect of joint seal effectiveness is directly employed within the faulting model. The three main elements of erosion, the rate of erosion of the base/subbase, existence of moisture under the slab (as reflected by the number of wet days), and traffic are included in the model. The model is calibrated with lab and field data and is widely useful for design and maintenance purposes.

Using this model, sealant effectiveness with respect to concrete pavement long term performance and sustainability can be evaluated. This makes agencies and designers capable of determining if sealing is necessary for a given project.

There have been two other studies to support modeling the connection of the sealant effectiveness to erosion related distresses. One important factor that was addressed was a mean to evaluate the number of wet days. Number of wet days is defined here as the actual number of days per year that water resides underneath the slab along the slab/subbase interface. This number is thought to be a function of the annual rainfall but likely is also a function of surface infiltration, sealants effectiveness and subbase drainage ability. The number of wet days was determined as probability functions that can be used for each site to evaluate the actual number of days that water

exist underneath the slab. Another study was to evaluate the resistance of different subbase materials against erosion. The study was required in order to calibrate the erosion/faulting model. An extensive laboratory tests on different subbase materials was performed. Data from this test program was used for erosion model calibration. This outcome of this study is also very helpful for future use of designers to determine erosion resistance for a certain subgrade type.

Finally this process is embroidered within a spreadsheet computer program that analyzes a concrete pavement structurally and predicts the erosion and faulting at slab joints considering sealant effects. This program is capable to be calibrated with field performance or laboratory erosion data. Results show that the model fits well with the field data and can be implemented for design and maintenance management purposes.

1.3 Structure of Dissertation

This dissertation consists of seven sections, each with specific objectives. Section one is the introduction, statement of the problem and brief review of the approach. Section two is the literature review where background information, history of joints and sealing, different agencies approach and policies regarding sealing, overview of sealant failure modes and causes and seal or no seal issue is discussed.

Field testing on joint sealant performance in regards to infiltration is discussed in section three. This section includes thorough explanation of test area, test method and test variants. Flow test is introduced as a very effective field test method. Moreover test results are shown using figures and tables and the results and conclusions were discussed and analyzed.

An important design factor, number of wet days, is defined and analyzed in section four. This section includes discussions on how water transmits into the sublayers. Infiltration coefficient is defined and determined using results from test program in section three. Water seepage into subbase has been calculated. The number of wet days is presented as a probability function that counts for annual rainfall, surface inflow, sealants effectiveness and subgrade permeability.

A mechanistic-empirical faulting model that was developed is explained in section five in a step by step format. Three major factors contributing in erosion/faulting process is considered in this model. Passing traffic, existence of water in the subbase/slab interface and erodibility of the base material are the three major factors. Sensitivity analysis on the model and calibration of the model using field data is presented to demonstrate the sensitivity and accuracy of the model.

Section six includes the extensive erosion test program on different subbase materials. The explanation on type and diversity of the samples and materials properties is provided. Test results on stabilized and non-stabilized samples are explained and results are shown in graphs and tables. Test conclusions extracted and discussed.

Finally, a summary of the major findings and conclusions are summarized in section seven. In the appendices, detailed of material samples for erosion tests, erosion test results and erosion test procedure are explained.

2. LITERATURE REVIEW

2.1 Joints in Concrete Pavements

Joints in concrete pavements are primarily intended to provide freedom of slab movement relative to concrete volume changes due to drying shrinkage, temperature changes and moisture differences. Functionally speaking, joints are designed to control cracking, minimize stresses in the pavement caused by volume change as well as prevent damage to immovable structures.

Joints have always played an integral part in concrete pavement construction but joint geometry and design has been improved over the years [2]. Joints were typically placed at regular intervals mainly determined by experience. The first specifications regarding the placement of joints in concrete pavements was included in guidelines for transverse joint spacing by the American Concrete Institute (ACI) in 1914 [1]. Discontinuities in portland cement concrete (PCC) pavements such as joints have been a major performance concern since they are major planes of weakness; in many instances, distresses often initiate and propagate at or near the joint.

Therefore, attempts have been made to reduce the number of joints by extending the joint spacing. Using better curing techniques, construction methods and the proper concrete properties, PCC pavements with longer joint spacing have been constructed. Accordingly, field observations have suggested and led to improved joint systems to help avoid the early distresses at the joint. Other improvement led to the use of joint sealants [3].

2.2 Early Use of Sealant in PCC Pavements

Sealing the joints is widely believed to be beneficial to concrete pavement performance in two ways [4]; first by minimizing water infiltration into the pavement structure. This effect would result in a low occurrence of moisture-related distresses since moisture can cause support issues that may decrease the pavement service life. Secondly, sealed joints reduce the infiltration of incompressibles (i.e., sand and small stones, debris) into the joints, therefore reducing the possibility of joint distresses such as spalling due to the pressure in the joint reservoir under the load. Incompressibles are thought to create point loading when slabs expand due to temperature induced expansions possibly leading to spalling but this type of damage is more likely propagated under load rather than temperature effects [4].

Water infiltrating in to the pavement structure could result in slab erosion, loss of support and loss of joint stiffness [5]. Faulting for instance, considered as a major failure criteria in jointed concrete pavements is directly associated with the presence of water. Accumulation of water under the slab combined with traffic loading can initiate erosion on the base material if the slab is separated from the subbase. Corner breaks and freeze-thaw damage (D cracking) are other examples of distresses related to moisture trapped in the pavement joints.

In 1871, a U.S. patent represented the use of gum, tar or rubber materials as joint fillers in between concrete joints [2]. Later and in the early 1900s, it was common construction practice to use bituminous materials in order to fill the joints. Bituminous materials were relatively inexpensive and easy to produce and place. In 1912, the first

reinforced concrete pavement was constructed in Port Huron, Michigan consisted of expansion joints throughout the entire project. Asphalt cement was used to fill the joints [1]. Sealing the cracks as a part of maintenance program was also considered in the early 1910s; the material was a mixture of sand coated with tar [1].

In the early 1920s, many states studied various tar and asphaltic filler materials in repairing cracks in concrete pavements. One of these studies was sponsored by the Iowa State Highway Commission in 1923 to identify grades of tars and asphalts suitable for use in crack maintenance. The experimental sections were located outside of Des Moines, Iowa. Different materials were tested, including three tars, nine asphalts and blown oils, an emulsified bitumen and a single light-colored material [1]. The cracks were pressure-cleaned and dried before installation of the filler material. After the final inspection, all three grades of tar were nearly 100 percent intact, adhering well to the concrete joint wall. These were the only materials exhibiting excellent performance.

2.3 Main Sealant Material Types

Currently, there are mainly three kinds of sealant materials used for rigid pavement applications; asphalt based sealants, silicon based sealants, and compression sealants. Historically, the hot-applied asphalt based materials have been the most commonly sealant materials used in concrete pavement joints. However, silicone based sealants (ASTM D5893) and preformed compression seal materials (ASTM D2628) have gained increased acceptance for use in rigid pavements and have become the preferred choice of a significant number of state DOTs [6] [7] [8] [9].

Hot pour rubberized asphalt materials typically possess good sealing characteristics and flexibility at a relatively low cost, however; as they age over time the possibility of water infiltration increases due to reduction of flexibility and bond along the seal/joint wall interface [10]. Hot pour rubberized joint sealants if installed well may last for a long time. A study by Federal Highway Administration, FHWA, showed that hot pour sealants last over 110 months (about 9 years) with overall 75% effectiveness [11]. This study also showed that service life of sealants varies and might not always be as long. Several factors such as installation practice, climatic condition, traffic level, etc. play role in joint sealant's serviceability. The study includes the Strategic Highway Research Program (SHRP) H-106 maintenance experiment and the FHWA Long-Term Monitoring (LTM) of Pavement Test Sites [11]. Another sealant study by California Department of Transportation (Caltrans), in their Caltrans/ industry joint sealing field review, stated that rubber joint seals placed over 10 years were still in good condition [12].

Silicon based materials developed much later provide better bonding and expansion characteristics. The application of this type of sealants is easier and safer than the asphalt based sealants. Silicon sealants typically have excellent adhesive characteristics as well as having less sensitivity to changes in flexibility due to aging and temperature effects [13, 14]. Cost is higher than hot pour rubberized asphalt while expected service life is longer. A study conducted on silicon based joints in Arizona showed excellent performance over long period of time (about 20 years) [15]. The Arizona Special Pavement Studies (SPS - 2) jointed concrete pavement test site, was

constructed in 1993 with 12 LTPP and 9 ADOT test sections. Each test section included 33 transverse joints which were sealed using Crafco 34902 non-sag RoadSaver Silicone sealant. Various combinations of base type, concrete strength, slab width, and slab thickness were designed to allow statistical analysis of the contributions of each factor. A March 2013 evaluation of the condition of the joints and seals indicated that overall performance of the SPS-2 joint seal systems was extraordinarily good, considering the seals have been in place for 20 years and the truck lane has carried about 31 million Equivalent Single Axle Loads (ESALs).

The third major category of sealants along with asphaltic base and silicone base materials is the compression sealant, also called preformed sealants. The compression sealants are designed to remain tight in the joint well when the joint is at its maximum opening and are able to bear the compressive force when the opening are at the smallest as would occur in the summer time. The important consideration when using compression sealants is they should remain in compression. Compression sealants are probably more resistant than other sealant types to deterioration from exposure to weather, sunlight, oils, chemicals, heat, abrasion and impact and hydrostatic pressure. Preformed compression seals normally provide a long service life if the sealant remains in compression (in the appropriate range between 20 to 50 percent of its original width); therefore, these types of sealants must be sized based on expected joint movements in order to function properly. From the economical perspective, the compressed sealants are the most expensive choice and the asphalt base sealants are comparatively cheap. A study by Michigan Department of Transportation on various concrete pavement joint

sealants concluded that preformed compression sealant performed better than other sealant types [16].

Even though some field investigations reported that sealants may not provide a long service life, results from two recent unique studies confirm that sealants if installed properly can achieve service life of 20 years. One of the two studies was at the Federal Highway Administration's Long-Term Pavement Performance (LTPP) SPS-2 Experiment in Phoenix, Arizona as mentioned previously [15]. The other study was coordinated by pavement preservation product manufacturer Crafco, and took place at Fairchild Air Force Base in Spokane, Wash [17]. In 1989, the U.S. Army Corp of Engineers Construction Productivity Advanced Research (CPAR) conducted a sealant performance study consisting of both laboratory and field evaluations. The study evaluated both hot-pour and silicone sealants. A silicone sealant installed in a conventional manner and a low-modulus, hot-applied asphalt sealant installed using flush-fill geometry. Sealants exhibited a performance period of more than 21 years [17].

Findings of these two studies indicate that properly installed sealants can provide at least a 20 year service life. Previously, there has not been any factual evidence to prove the long-term effectiveness of sealant's serviceability but these findings confirm and document that sealants can last a long period of time.

2.4 Current Sealant Practice

In recent years, states have adopted a wide variety of joint sealing practices for jointed pavements, based on local experience, climate, and traffic conditions. Generally, where there is naturally positive drainage in the sub layers or where climates are very hot

and dry, joints experience minimal distress and likely hold less moisture. This may allow agencies to think they could get by with narrower saw cuts without sealing, while in wet climates and less drainable subgrade materials, agencies prefer to have sealed joints [4]. Transverse contraction joints in PCC pavements are traditionally constructed in the following sequence of steps:

- Making an initial saw cut to control cracking.
- Making a second saw cut to create a reservoir for joint sealant.
- Cleaning and preparing the reservoir faces.
- Placing a backer rod in the reservoir, to keep the sealant from adhering to the bottom of the reservoir and to create a curved bottom surface for the sealant.
- Placing sealant material in the reservoir (which may include tooling the sealant into place).

It was reported that saw and sealing operations are estimated to be between 2 and 7 percent of the initial construction cost [1]. A study on relative cost of concrete highway features by American Concrete Pavement Association, ACPA, indicated the relative cost of the unsealed joint is approximately seven percent less than the silicone sealed joint [18]. According to the study this cost is even higher if more expensive sealant materials are used (The most expensive sealant option found to be ½ inch compression sealant) [18].

This is one reason that several State Departments of Transportation (DOTs) have been suggesting alternative methods; the most prevalent alternative is to cut the joints narrowly with the single saw cut and leave them unsealed. This approach is used by the

State of Wisconsin DOT where they avoid having wide saw cuts and sealants. In 1990, WisDOT passed a policy eliminating all PCC joint sealing, in new construction and maintenance. According to the report by Shober, 1997, this "no-seal" policy has saved Wisconsin $6,000,000 annually with the claim of no loss in pavement performance while achieving increased customer safety and convenience [19].

A second alternative is to use narrow joints but to fill them with sealant. In this configuration, the sealant adheres to the sides and bottom of the saw cut; although this configuration saves the expense of a second saw cut, it puts the sealant in a high state of debonding stress. A third alternative is to have the narrow sealed joints, consisting of single saw cuts with a narrow backer rod and sealant installed. Backer rod helps the sealant to lay with a structurally better shape which can distribute the stresses more effectively.

These alternatives are intended to reduce the initial cost not necessarily to enhance the performance. All three alternatives (mentioned in order of increasing cost) eliminate the second sawing operation needed to form a joint sealant reservoir, and the additional joint sealant material that would be required to fill the reservoir. This also makes the installation procedure faster and could save the time [4].

Resealing operations tend to be costly, due to the expenses of the material, labor, construction, joint widening, and lane closures. Lane closure costs depend on both time and traffic level. Shober stated that the cost for maintaining a sealed pavement for 10 years (sawing a joint reservoir and sealing it to resealing the joint whenever it was needed) amounted to as much as 45 percent more than the cost for a similar unsealed

pavement [19]. Of course there is a cost associated with base erosion damage that should be considered when comparing sealed and unsealed pavements.

2.5 Sealant Adhesive and Cohesive Failure

This section discusses the sealant failure causes and mechanism. In order to evaluate sealant effectiveness during the service life, there is a need to identify and evaluate the effects of different factors on sealants failure mechanism. As discussed previously there are mainly three different sealant types currently used; asphalt based sealants, silicon based sealants and preformed compression sealants. There are basically two types of mechanism for sealant failure; cohesive failure and adhesive failure.

Cohesive failure is defined as the failure of the sealant material itself when stresses within the sealant exceed the sealant's tolerance. Stresses on sealants caused by several factors such as joint movements, traffic load, etc. Over the time, combination of horizontal and vertical stresses coupled with the aging of the sealant may cause internal micro-cracking. Once micro cracking has begun, the problem often grows in scale. Smaller micro cracks lead to larger and larger micro cracks and so on until eventually macro cracks develop. Consequently, such a macro crack may form along the entire sealant depth until the sealant fails [20-22].

Adhesive failure is defined as a failure at the sealant-concrete interface. Adhesive failure in joint sealants is more common than the cohesive failure. Adhesive failure should take some time to develop in properly installed sealants. Aging of the sealant material can make the sealant stiffer and less flexible. Therefore sealants receive higher stresses at the interface that leads to debonding and failure [23]. Another type of

adhesive failure may occur when joint reservoir walls are not properly cleaned and dried prior to installation. If there is debris or moisture at the interface, sealant will adhere to the debris instead of the concrete slab, thereby decreasing the amount of contact area between slab and sealant. This makes the initial bond between sealant and joint wall weak that leads to debonding. This type of adhesive failure happens in early ages therefore it is called premature failure [20, 21]. Figure 1 and Figure 2 show the cohesive and adhesive failures in sealants. Table 1 shows common factors and causes of sealant failure.

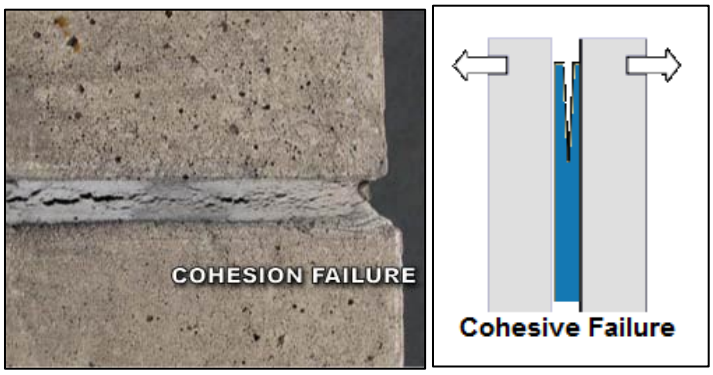

Figure 1 Cohesive Failure in Sealants.

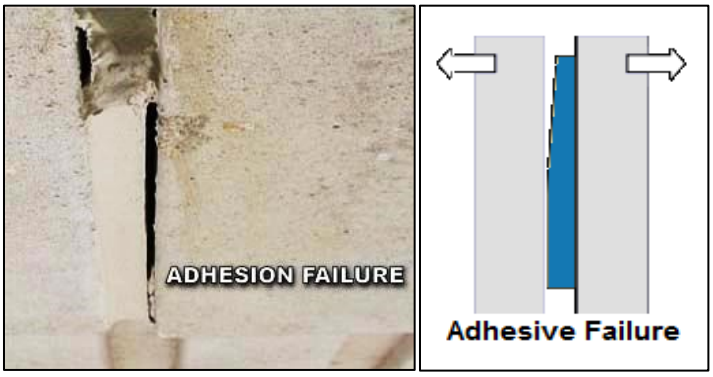

Figure 2 Adhesive Failure in Sealants.

Sealant installation is a critical factor as many researchers have showed that if sealants installed properly they can last very long [3, 17]. Improperly installed sealants are subjected to premature debonding from weather and traffic effects [21, 24]. The sealant must be installed under suitable weather conditions, with virtually no moisture present in any form. Existence of humidity causes a problem in achieving the full adhesion potential. Moisture, likely from condensation, present between the substrate and sealant will result in a poor wetting surface for sealant and lowers the adhesion [23]. Given the stringency of cleaning and installation procedures, these operations should be inspected as they proceed. Without such inspection, a great deal of effort and money could be wasted on ineffective seals. Before the installation, joint well walls should be cleaned to prevent contamination of the sealant materials affecting the bond to the joint wall [4].

There are many popular techniques for surface preparation and to achieve better installation that are used to clean and prepare the concrete substrate for sealing purposes. These pretreatments of the substrate generally include one or more techniques such as water-blasting, sand-blasting, air-blasting, etc. [23, 25].

Moreover, if sealants are installed too far below the pavement surface, incompressible materials are likely to enter the joints. Conversely, sealants installed at or slightly above the pavement surface are likely to be damaged or destroyed by passing vehicle tires.

Table 1 Factors and Causes of Sealant Failure.

Factor	Cause	Failure Type
Factors related to sealant material properties	Low bond strength between sealant material and joint reservoir	Adhesive Failure
	Low cohesiveness quality	Cohesive Failure
	Lack of sealant material's extension capacity	Adhesive/Cohesive Failure
Climatic factors (Solar radiation, temperature changes, etc.)	Weathering and aging (Stiffening and losing flexibility)	Crack initiation in the middle of the sealant - Cohesive Failure
Factors related to construction/installation	Existence of moisture at the joint wall prior to installation	Premature Failure (Adhesive)
	Joint wall dirtiness prior to installation	Premature Failure (Adhesive)
Pavement/Joint and sealant design related factors	Sealant size and geometry (depth to width ratio)	Affects stress distributions, lead to fatigue - Cohesive Failure
	Joint width too wide; preformed sealant not in compression	Sealant displacement
	Joint width too narrow during summer; Sealant in excessive compression	Sealant press/damage
Traffic/Load related factors	Slabs vertical displacements while traffic passes (Particularly in case of joints with faulting) - sealants elongation cycles	Adhesive /cohesive Failure
Joint distresses	Spalling, corner breaks, etc. directly damage the sealant	Sealant damages and failures
Sealants chemical reactions	Destructive chemical reactions between sealant materials and fuel/engine oils particularly the jet fuels in airfields	Stiffening - Cohesive Failure

As it shown in Table 1, although the sealant material plays an important role, the failure of the sealant is not always related to sealant material properties. Sometimes failure occurs due to the poor design of the slab and joint system. Researchers found that sealant failures could often be attributed to unestimating the characteristics of a joint rather than to deficiencies of the sealant material itself [26]. This might happen when the joint opening is wider than the sealant extension properties (during winters), or when the joint becomes too narrow causing the sealant material to be over compressed (during summers). The design of a joint should ensure the joint movement without failure of the joint sealant. The main failure mechanism in compressed sealants occurs when the joint opens too wide. Sealant geometry and size also influence the sealants performance. A 1992 study based on finite element analyses showed the advantage of using seals with low depth to width ratios. Sealants with better geometry distribute the stresses and may last longer. The researchers also found that for seals with higher depth-to-width ratios, adhesion failure is likely to originate at the center of the contact region between the seal and joint wall, rendering the failure undetectable [26-29].

Based on measurements taken on more than 100 expansion joints in concrete pavements in Massachusetts, a study concluded that although the effect of vertical movements on joint seal performance may be negligible, the effect of horizontal displacements was not. Three distinct stress or strain states were recognized in sealants:

- Stress reversals: sealant alternating between tension and compression,
- Sealant always in compression, and
- Sealant always in tension.

The stress reversal case was cited as the most detrimental condition to joint seal performance. The author stated that "many joints sealed in the past with the sealants alternating through compressive and tensile stress-strain cycles have shown adhesion failure and distortion in the sealant shape". Apparently a sealant in a continuous state of compression was desirable, since this produced no adverse stresses at the bond interface between the sealant and joint wall [30].

Joint sealant failure cause could be construction related. A common joint distress is spalling which accelerates joint sealant's failure. Another construction related factor is the non-uniform distribution of broken saw cut joints. Inconsistent, jointing often leads to irregular joint movement causing some joints to open more than others. In Pennsylvania, for example, some projects experience only every third joint at 6-m (20-ft) cracking full-depth. The detrimental result of this phenomenon is that the joints that do crack are not contracting according to the theoretical joint movement calculated for the designed joint spacing. So the adjacent joints experience wider movements than can be sustained by the sealant. Problems experienced by many joint-seal designs result from inadequate construction quality control [4].

2.6 Questioning the Need for Joint Sealing

At the 16th World Congress of the Permanent International Association of Road Congresses (PIARC), the Technical Committee on Concrete Roads presented a report concluding that for joint spacing of 4 to 6 m, there was no disadvantage in leaving narrow transverse joints unsealed when: (a) traffic is light, (b) traffic is heavy but the climate is dry, or (c) traffic is heavy and the climate is wet, but the pavement is doweled

[24]. Earlier published literature from Europe had suggested similar conclusions [19, 31].

As early as 1967, S. E. Hicks addressed the Highway Research Board concerning 20 years of observations that illustrated the lack of benefits from joint sealing [19]. After that in 1987, another study by Karl Dunn of the Wisconsin DOT indicated the similar results [32]. Followed by two test programs, one in the period of 1958-1966, in the southbound lanes of US-41 in Washington County, Wisconsin and the other one which was a larger experimental project between 1966 and 1977 in Columbia County, Wisconsin researchers found that there is no difference in measurable pavement performance between the sealed and unsealed sections. A paper by Shober from the Wisconsin DOT stated that regular joint resealing was judged to have no benefit to overall pavement performance compared to not resealing [19]. Shober also reported the performance of sealed and unsealed sections that were 8 to 22 years old. In order to measure distresses, Wisconsin used the pavement distress index (PDI), which measures all distresses (extent and severity) and combines them into one index. Each distress is weighted to account for its significance on pavement performance. The PDI scale ranges from 0 to 100; with 100 being the worst score. The report indicates that almost in all cases the performance of the unsealed sections is better than the performance of the sealed sections. A statistical analysis of pavement ride (in terms of IRI), concluded that joint sealing has no significant effect on pavement ride qualities.

While Wisconsin has officially passed the policy not to seal the joints, researchers from other states criticized the Wisconsin's findings. In 1996 two

independent teams visited Wisconsin's field sections and tried to verify the WisDOT's findings. They noted that the sealed sections had not been maintained properly during the experiment and did not reflect a sealed condition. Obviously if the joint seals were not maintained properly then the comparison between sealed and unsealed conditions would not be reasonable.

Later in 2002, Burke et al. in response to Wisconsin research findings stated that valid generalized conclusions about the suitability of unsealed pavements cannot be made based on extrapolations of short-term visual performance observations. This study also reported that pavement specialists of transportation agencies with the most long-term unsealed pavement experience (California and most Western European countries), have concluded that well-maintained pavement with doweled and sealed joints, and stabilized well-drained bases provide the most functional, durable and cost-effective pavement applications [33].

An analysis of LTPP Database on relative performance of sealed and unsealed joints concluded that "despite the conventional wisdom concerning the need to keep concrete pavement joints well sealed, studies on the subject have not demonstrated that JPCP with sealed joints and JPCP with unsealed joints perform differently in terms of spalling, faulting, IRI, or deflections" [34].

A joint seal study was funded by the U.S Department of Transportation, August 2008, in which data were collected from a total of 117 test sections in 11 states (Arizona, Colorado, Florida, Georgia, Illinois, Indiana, Iowa, Minnesota, New York, Ohio, and Wisconsin). Statistical analyses of the collected distress data detected no significant

difference between average pavement performance in the unsealed-joint test sections and the silicone-sealed, hot-pour-sealed, or preformed-sealant test sections at the same site [1]. An evaluation report in 2009 by North Dakota Department of Transportation on unsealed joint performance showed the sealed joints would reduce the amount of water intrusion into the pavement and base section. This study did not recommend to leave the concrete joints unsealed [35].

As it has been discussed, research over the past decade on the efficiency of the sealing has involved several field studies. The main problem with all these studies is the lack of comprehensive approach and proper methodology to evaluate the degree of damage or erosion that has occurred as a result of condition or effectiveness of the joint sealing, making extension of results to other situations a challenge. Even though most of the studies considered different types of sealants (hot pour, silicone and preformed plus unsealed joints) and involved variables such as age, traffic, climate etc., there has not been a process to account for the sealants effect on long term pavement performance and sustainability.

Despite these shortcomings, these studies have been helpful to answer some of the questions in the seal no seal debate. Research shows that for some situations there is no need to seal the joint, particularly in dry areas or those that have drainable structures. Some studies show that considering a particular base material, traffic and climate there is no difference between the performance of the sealed and unsealed PCC pavement. Faulting, spalling and cracking are the main criteria that have been considered in these

studies. So understanding of "seal no seal" question is "where or in what conditions warrant sealing?"

The major factor in this debate is the cost and whether the elimination of the seal and reseal process is more beneficial cost-wise compared to the costs of not having them sealed. If joint sealing does enhance pavement performance, it is necessary to determine if the enhancement is cost-effective. Cost effectiveness must include costs of joint well cutting, sealing and resealing over the life of the pavement, and user delay and safety costs caused by those activities. Thus, it is not enough just to prove an enhancement in performance; the enhancement must equal the costs [19].

From a risk prospective the consequences of not sealing maybe too high if the expense of reconstruction is too high. Therefore sealing is only beneficial if it can be shown to be necessary. Therefore, the key to answer the seal-no seal question in most cases is determining the probability that the cost and risk are both reasonable. Like many other engineering decisions there is no intent in wasting money on a very low risk situation while on the other hand, there is no intent in saving a little money by ignoring a huge risk. By changing the influential factors such as base type, climate, traffic, etc. the pavement configuration would change, meaning for different combinations there would be a different probability for the need of sealing. Hence, answer to the "seal-no seal" question is in what conditions should sealing be done? When and where does joint sealing achieve a cost-effective improvement in pavement performance?

3. FIELD TESTING ON JOINT SEALANT PERFORMANCE

An experimental program was carried out on the Riverside Campus of Texas A&M University to study the effectiveness of different sealant types to limit drainage related infiltration of the joint under different joint openings.

3.1 Pavement Test Area

The pavement test area consists of a concrete segment that is 38 ft long and 12 feet wide, with four existing transverse joints spaced at 15 foot intervals. The 12 foot wide lane includes a curb on one side. The concrete slab is 6 inches thick with an open graded high permeable subbase beneath. The test area was divided into four test areas as shown in Figure 3.

In addition to the four existing transverse joints, four additional full-depth sawn joints were made on 2 ft intervals in each test area as shown in Figure 4. Each full depth cut was 1/8 inch wide with wells cut 1/4 inch wide and 1.5 inch deep. After sawing the joint wells, washing operations were conducted to clean the joint reservoir.

Figure 3 Layout of Joint Sealant Test Area.

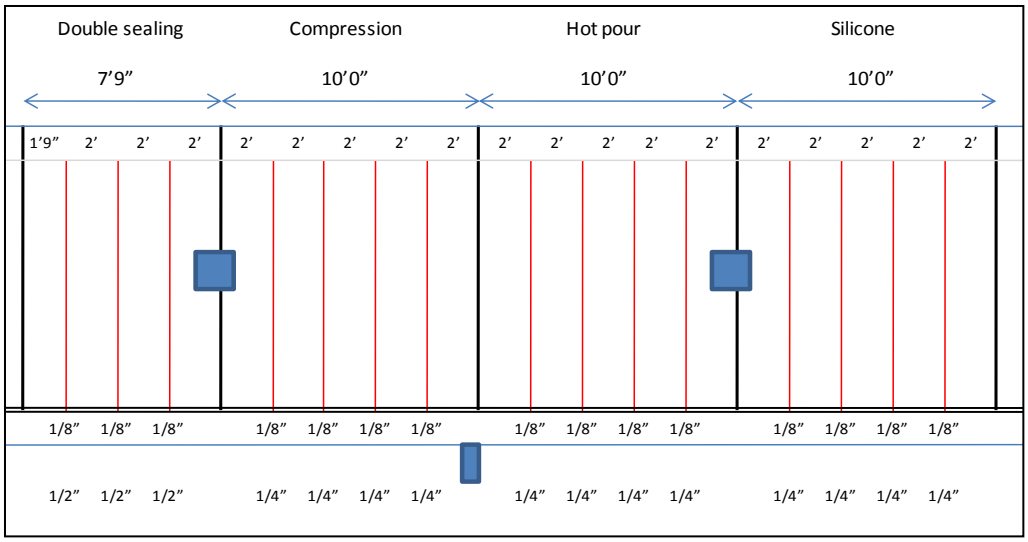

Figure 4 Joint Sealant Layouts.

Figure 5 shows the process of joint sealing. Joints walls were cleaned and completely dried before placing the sealants. Sufficient time (at least one day) was provided to ensure that adequate drying of the joint wells took place. The sides of the new joints

were sandblasted and then air blasted before sealing (Figure 5-a). Preformed compression sealant were placed using an adhesive and an installation machine (Figure 5-b). For the liquid type sealants, backer rods were used to shape sealant reservoirs. They were placed to a depth of 3/4 inch using a wheeled roller (Figure 5-c). Both, hot pour rubberized asphalt materials and silicon sealants were placed with backer rods and were placed with care to avoid trapping air bubbles (Figure 5-d).

a) Sand and Air Blasting

b) Compression Seal Placement

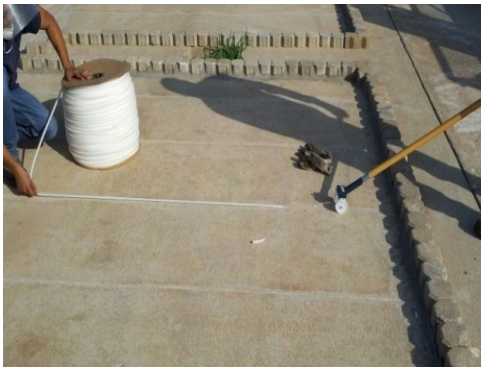

c) Backer Rod Placing

d) Silicon and Hot-pour Placement

Figure 5 Joint Sealing Process.

3.2 Field Test Conditions

The project work is focused on advancing the understanding of the sealant effectiveness related to moisture infiltration. Many factors can influence the performance of a joint sealant some which has been included in an experimental design for examination in this project are shown in Table 2. The three most popular types of joint sealants are being tested under different sealing conditions.

Table 2 Test Controlling Factors for Joint Sealant Field Study.

Sealant Type	Hot pour rubberized asphalt
	Silicone self-leveling
	Preformed compression
Sealant Condition	100% sealed (No debonding)
	75% sealed (25% debonding)
	50% sealed (50% debonding)
	25% sealed (75% debonding)
	0% sealed (No bonding)
Joint Configuration	1/4 inch wide by 1-¼ inch deep
	3/8 inch wide by 1-¼ inch deep
	1/2 inch wide by 1-¼ inch deep

Generally, joints are well sealed immediately after installation and are highly effective in blocking the infiltration of water. Joint seal materials generally deteriorate over time

which accordingly leads to a higher possibility of moisture infiltrating the pavement substructure. The rate of surface water infiltration is thought to be governed by the degree of degradation that has taken place in the joint sealant. The seal condition is represented in part by the amount of debonding that has taken place. Sealants were carefully debonded along the joints prior to the tests of different debonding levels; 100%, 75%, 50%, 25% and 0% debonding. Hundred percent debonding represents the condition in which sealant is not bonded to the joint wall as one side of the sealant has been carefully cut along the joint wall. Next phases of the experiments consider effects of joint width change and installation on sealant performance.

3.3 Flow Test (Infiltration Test)

Infiltration or flow testing was performed using a falling head permeameter. The edge of the permeameter is completely sealed prior to the test. Then the device is filled with the water and the time for water head drops are recorded. Using time for certain head drops the infiltration (permeability) of the joint is calculated. The initial water level (initial head) is 5 inches. If the joint system has high permeability water may infiltrate into the joint quickly. In this case, greater initial head may apply in order to have enough time to record the head drop. This test method is quick, cheap and sufficiently adaptable to allow measurements to be made at multiple locations along the sealed joint in a relatively short period of time in the field condition.

Figure 6 shows an infiltration test on an existing joint. The original saw cut width was 1/8 inch and the crack widths were approximately 0.04 inch. Since the pavement is constructed over 15 years ago, saw cut joints and cracks may have become clogged with

debris and dust resulting in a low infiltration rate of 0.11 gal/hr/ft. After pressure washing the joint, the infiltration rate increased to 0.14 gal/hr/ft. Cleaning through the full depth of the existing joint (if that can be accomplished) may increase the infiltration rate greatly.

Figure 6 Flow Test on Existing Joint.

3.4 Evaluate Infiltration Rates of Sealed Joints

After 3 weeks of cure time, a series of infiltration tests were conducted for each of the three joint sealant types. Under fully sealed conditions, no infiltration occurred for any of the three types of seals since all joints were sealed completely without any defects. This is an important observation that shows sealants when installed properly are potentially very effective to block the water from infiltration into the joints.

In order to better represent the type of deterioration that occurs under normal wear due to weathering and traffic, as a second series of testing, thin slots were cut along the interface between the joint sealant and the joint well wall to create varying degrees of debonding. Sealants were carefully cut along the joint wall to make different debonding levels. Figure 7 shows 25% and 50% debonding for silicone joint sealants.

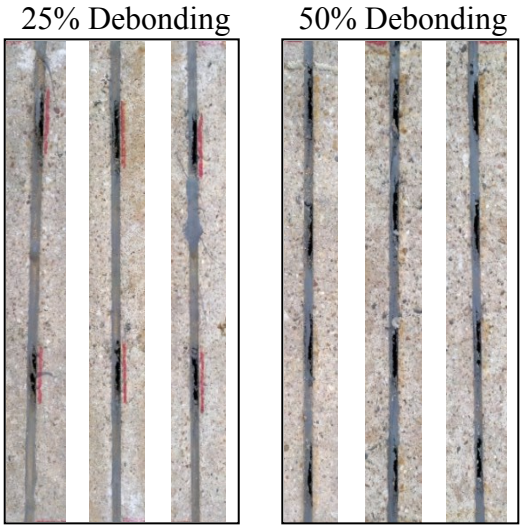

Figure 7 Damaged Sealing Condition.

Flow test results on damaged sealants are shown in Figure 8. The measured flow rates were higher due to the increased amount of sealant damage. The hot pour sealants showed the highest flow rate while the silicon sealants showed the lowest flow rate.

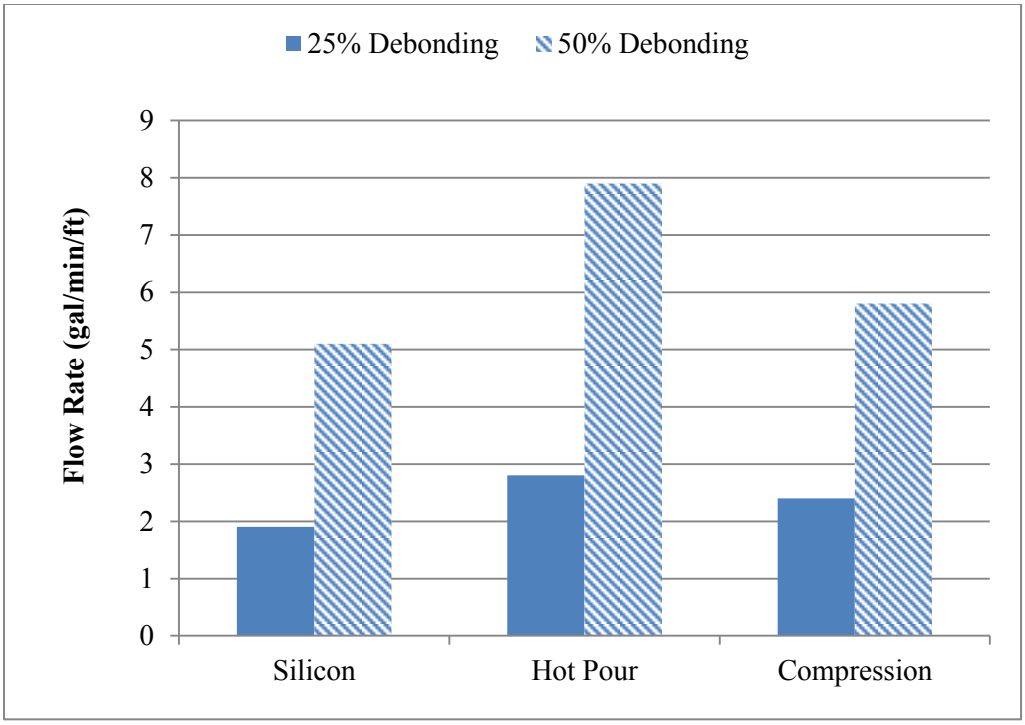

Figure 8 Flow Test Results on Damaged Sealants.

3.5 Flow Test Using a Movable Joint System

With the original test setup, the feasibility of representing realistic joint movements under field conditions was limited; therefore a movable joint system was designed and installed. Joint seals subjected to tensile strains (as would occur under widening conditions) most likely will yield larger amounts of flow over a given amount of debonding, similar as what would occur under temperature contraction, causing the joint to be subjected to greater moisture infiltration. To consider joint movement and debonding effects on subsequent moisture penetration, the field experiments considered variable joint openings for different joint widths and degrees of debonding. Such system is helpful to simulate different joint opening widths that occur during the year due to

temperature changes under field conditions. Figure 9 and Figure 10 show the schematic view and pictures of the installed movable joint system. Using this system, the opening of the joint reservoir was controlled for different joint widths to cause different amounts of flow to take place.

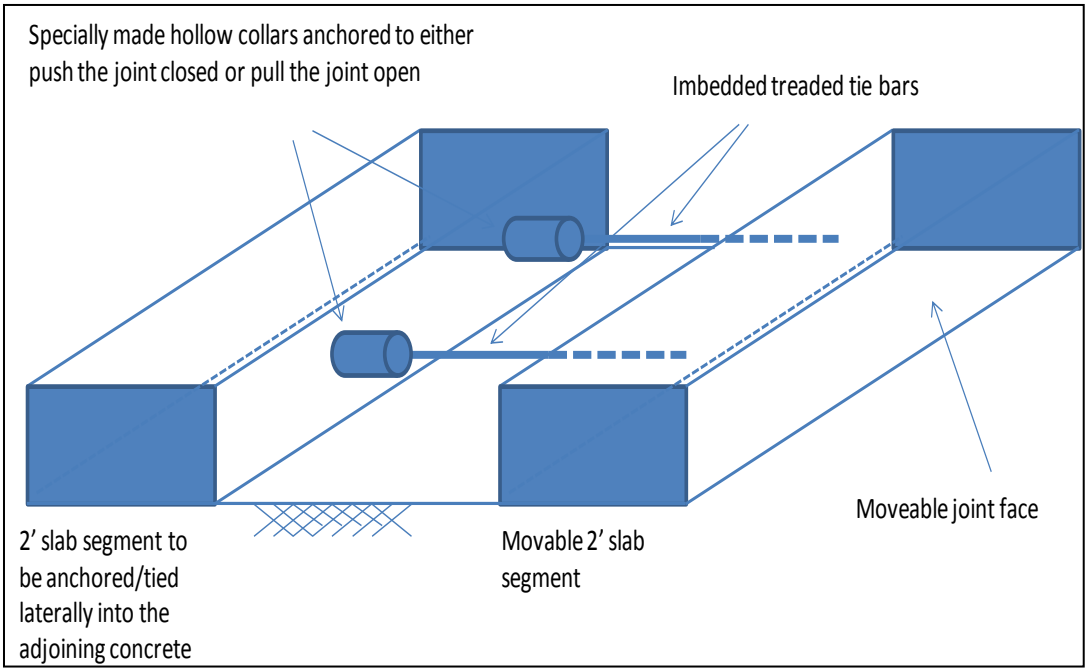

Figure 9 Schematic of the Movable Joint System.

Figure 10 Installation of the Movable Joint System.

3.6 Test Results of Movable Joint Systems

Test results from joints with 1/4 inch wide joint reservoirs using the three types of sealants (hot pour, silicon, and preformed compression) as well as an existing unsealed joint that was approximately 1/8 inch wide are subsequently provided. Sealants were debonded from the joint wall using a sharp knife with minimum disturbance of the original shape and opened gradually under controlled testing to measure the corresponding water infiltration rate.

Table 3 and Figure 11 show the infiltration rates versus joint openings for three sealant types and the unsealed joint (the zero opening represents the original joint width which is 1/4 inch for the sealed joints and 1/8 inch for the unsealed joint).

The unsealed joint showed the highest infiltration rate. Infiltration of the joint sealed with silicon sealant initiated at joint opening less than 0.04 inch (1 mm) while flows for the joint sealed with hot pour sealant started with an opening greater than 0.04 inch (1 mm) joint opening; joint sealed with preformed compression sealant initiated the flow after the openings were greater than 1/8 an inch (3 mm) as shown in Figure 11.

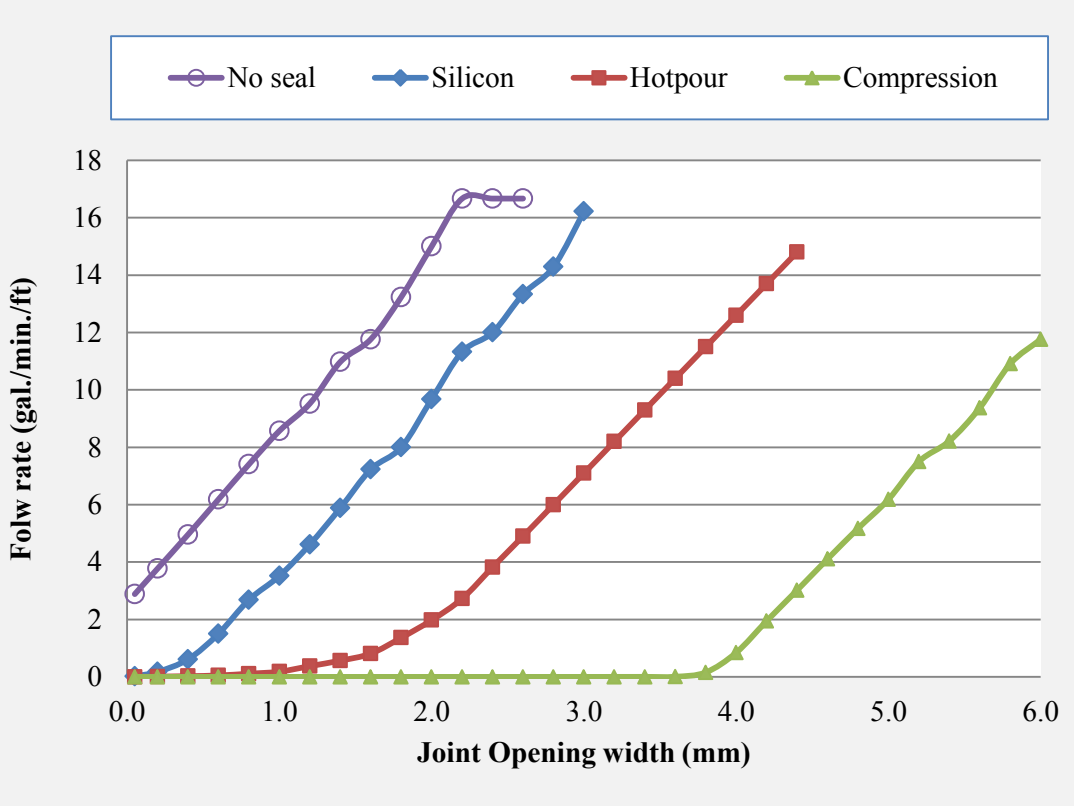

Figure 11 Flow Test Results for Various Joint Sealant Types.

Table 3 Flow Test Results for Various Joint Sealant Types.

Joint opening width (inch)	Joint opening width (mm)	Flow rate (gallon/min./ft)			
		No seal	Silicon	Hot pour	Compression
0.002	0.1	2.88	0.020	0.001	0
0.008	0.2	3.77	0.18	0.010	0
0.016	0.4	4.96	0.61	0.025	0
0.024	0.6	6.19	1.50	0.050	0
0.031	0.8	7.41	2.69	0.11	0
0.039	1.0	8.57	3.52	0.18	0
0.047	1.2	9.52	4.62	0.38	0
0.055	1.4	10.98	5.88	0.57	0
0.063	1.6	11.76	7.23	0.81	0
0.071	1.8	13.24	8.00	1.36	0
0.079	2.0	15.00	9.68	1.98	0
0.087	2.2	16.67	11.32	2.73	0
0.094	2.4	16.67	12.00	3.82	0
0.102	2.6		13.33	4.90	0
0.110	2.8		14.29	6.00	0
0.118	3.0		16.22	7.10	0.000
0.126	3.2			8.20	0.001
0.134	3.4			9.30	0.002
0.142	3.6			10.40	0.005
0.150	3.8			11.50	0.16
0.157	4.0			12.60	0.85
0.165	4.2			13.70	1.95
0.173	4.4			14.80	3.02
0.181	4.6				4.11
0.189	4.8				5.17
0.197	5.0				6.19

The increasing rate of water infiltration with the increase of joint opening shows the lowest infiltration occurs with the hot pour sealant and highest for the unsealed joint (as shown in Figure 12 and Figure 13). This means as joint width increases, the unsealed

joint will allow a greater infiltration rate than joints with sealants will. Among the sealant types, silicon type sealant allowed greater infiltration than the hot pour sealant; the hot pour sealant allowed relatively lower rates of infiltration than the other sealants. Preformed compression sealants tended to recover their original shape; infiltration initiated only when the opening width exceeded its recoverable range (recoverable range was gradually reduced with time due to creep recovery under continuous compressed conditions).

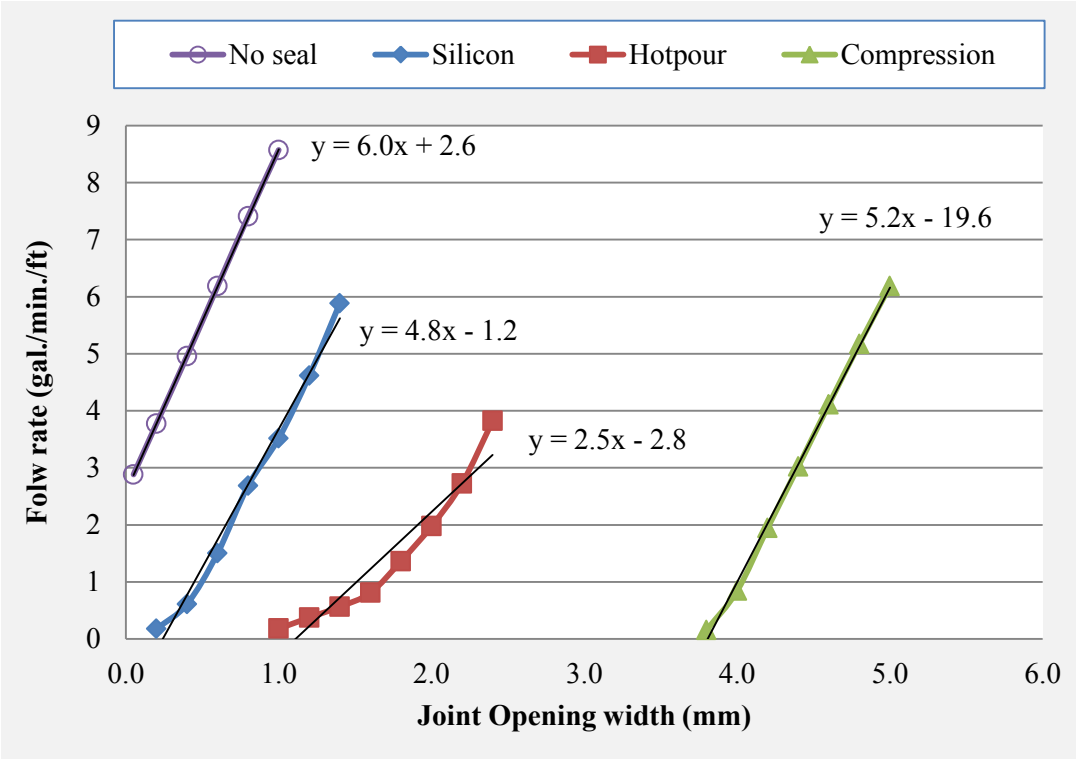

Figure 12 Slope of Flow Rate Increase with Joint Opening.

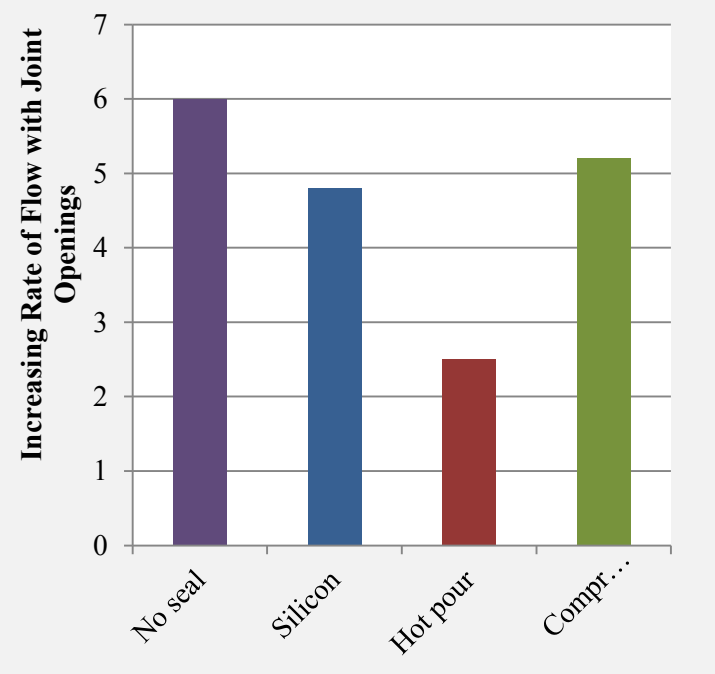

Figure 13 Increasing Rate of Flow with Joint Opening.

3.7 Tests on Joint Sealant Installation

The most common form of failure in a joint seal is the adhesive type of failure where the seal debonds from the joint wall; this type of failure is principally thought to be premature and is mainly due to installation factors.

The procedure of sealing or resealing involves sawing, and refacing the sides of joint reservoir. The cutting blade is cooled with water which forms a watery mix with the saw cuttings which when dried can leave a heavy residue on the face of the joint. This residue must be thoroughly removed in order for a sealant to have proper bond to the joint wall. Any residue can significantly decrease the bond strength between the sealant material and the joint. Even though water blasting or sandblasting is done in

order to clean the joint prior to sealing, these procedures may not be carried out well enough in the field as effectively as needed. It should be mentioned that water blasting or sandblasting may contribute to the dirtiness of the joint wall if they are not done correctly. Field observations and investigations from contractors and others indicate that the installation process has a major impact on bond capacity of the joint [10].

The testing program addressed the importance of installation quality associated with joint sealing. As previously noted, a main element of joint preparation is cleaning of the joint side walls prior to placing the joint seal. Tests were conducted using a slurry of saw dust with density of 68041.5 grains per gallon (1164.74 kg/m^3) varied to make three different concentration levels (Slurry to water ratios of 1:1, 1:1/5 and 1:2). Results were then analyzed with respect to dirtiness or the degree of contamination and sealant performance. After cleaning the joints, joints were prepared with four different dirtiness levels:

1. Clean joints, no dirt (0% slurry),
2. Dusty joints (33% concentration of slurry),
3. Dirty joints (40% concentration of slurry), and
4. Very dirty joints (50% concentration of slurry)

Slurry mixes were brushed on the joint reservoir walls. Application of the slurry in this manner allowed for the needed accuracy and consistency of the contamination and distributed the dirtiness equally along the joints. Sealants were placed and later the joints were moved to various openings to perform flow testing. The results for the silicon sealants are shown in Figure 14. There is a significant difference when the

dirtiness level was zero. Results also show that after a certain level of dirtiness the joint allowed a greater amount of water into it.

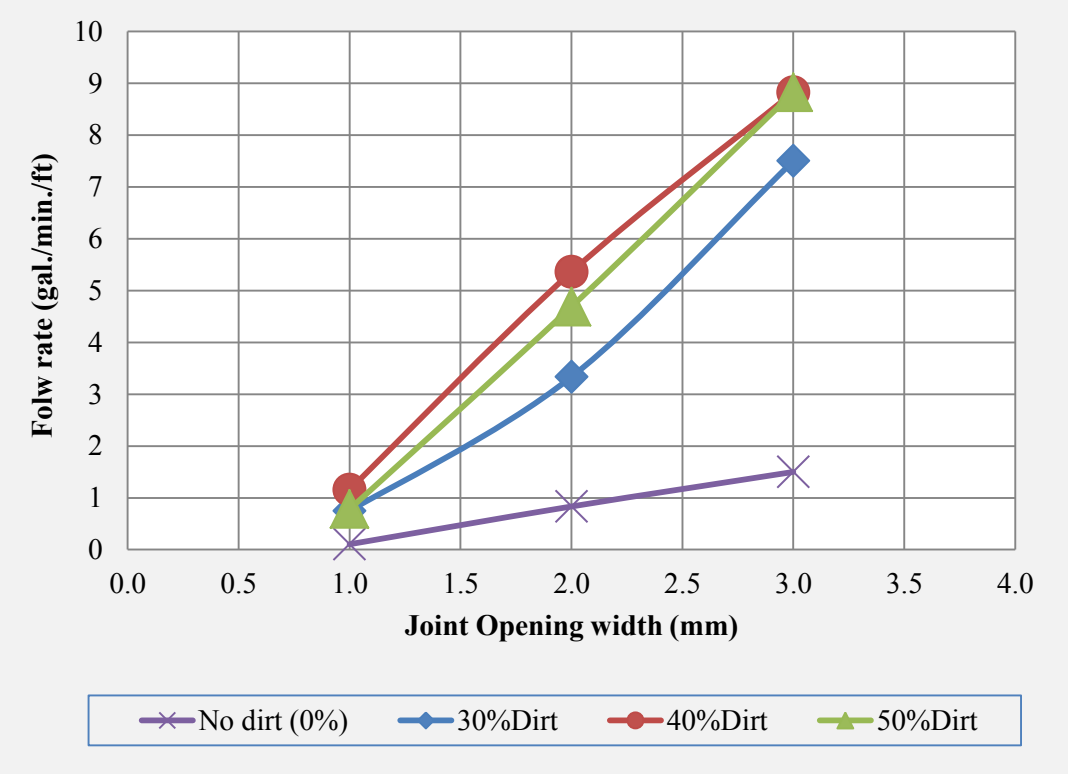

Figure 14 Water Infiltration Rates for Different Joint Dirtiness Levels.

4. EVALUATION OF NUMBER OF WET DAYS FOR DESIGN PURPOSES

Number of wet days is defined here as the actual number of days per year that water resides underneath the slab along the slab/subbase interface. This number is thought to be only a function of the annual rainfall but is also a function of surface infiltration, sealants effectiveness and subbase drainage ability. The number of wet days was determined as probability functions. Test results discussed in previous section was used to consider sealants effects on this analysis.

4.1 Pavement Drainage

Drainage is one of the most important factors in concrete design. Water contributes to several major distresses in jointed concrete pavements and can significantly affect concrete pavement's longevity. There are mounting evidences that good drainage will provide better, longer lasting pavements [36]. Forsyth stated that if the excess infiltrated water can be drained quickly, the pavement life can be extended by 50 percent for the rigid pavement system [37]. Some of the major detrimental consequences of trapped water under a concrete slab can be summarized as follows [38]:

1. It reduces the shear strength of the sub layer,
2. It greatly reduces the bond at the slab/subbase interface,
3. It causes pumping effects that subsequent faulting and corner breaks, and
4. It reduces the support of the concrete pavement.

Figure 15 shows how water can accelerate distresses in Jointed Concert Pavement, JCP.

Figure 15 Water Related Damages; Potholes, Corner Breaking and Wide Cracks.

The development of realistic practices to protect pavements from the damaging action of water is one of the biggest and most demanding challenges facing design engineers [36]. The importance of designing an effective drainage system in a pavement was acknowledged by AASHTO guide for design of pavement structure by incorporating the drainage factors in their design [39].

Existence of the moisture underneath the slab is one of the main elements of erosion process. Passing traffic pumps the free water at the base/slab interface and can create voids that lead to occurrence of faulting. Most recent erosion/faulting models address the moisture under the slab in terms of the number of wet days [10, 40, 41]. Since this factor represents existence of water in pavement sublayers, it plays an important role in pavement design and analysis.

The important issue is that by far this factor has not received the attention it merits in concrete pavement design. Most definitions relate the number of wet days only to climatic factors such as rainfall but the actual number of days that water exists underneath the slab is not only a factor of rainfall; several other factors such as surface and subsurface drainage, joint sealants or subbase permeability must take into considerations when defining the actual number of wet days. As an example the Mechanistic-Empirical Pavement Design Guide, MEPDG, defines wet days as number of days with rainfall greater than 0.1 inch without any consideration of joint sealants effects or different base materials drainage capacity [40].

Major factors regarding the water existence in pavement sublayers are discussed in this section in order to better define the number of wet days that can be used for concrete pavement design and analysis purposes.

4.2 Transmission of Water into the Pavement Sublayer

Water primarily enters the concrete pavement by penetrating through the joints, surface cracks or shoulders. Transmission of water into the pavement sublayer occurs in three steps:

1. Rainfall as the main source of the water
2. Water flow on pavement surface and infiltration into the joint wells
3. Water infiltration or seepage in to the subbase

Accordingly there is a possibility to avoid water being trapped underneath the slab by using proper drainage design. In order to redefine the number of wet days, each of the three steps needs to be considered. In other words, the number of wet days for a

particular pavement section relates to the local precipitation and how effective the drainage system is with respect to surface drainage, joint and sealant's effectiveness and subbase layer permeability. Rainfall is the main source of water. Once the rain water encounters the slab surface a portion of water flow away from the joints due to cross sectional slope. The other parameters to account for in defining the number of wet days is the size of the joint well and joint sealants effectiveness. Figure 16 schematically shows the three stages of water transmission into a subbase layer.

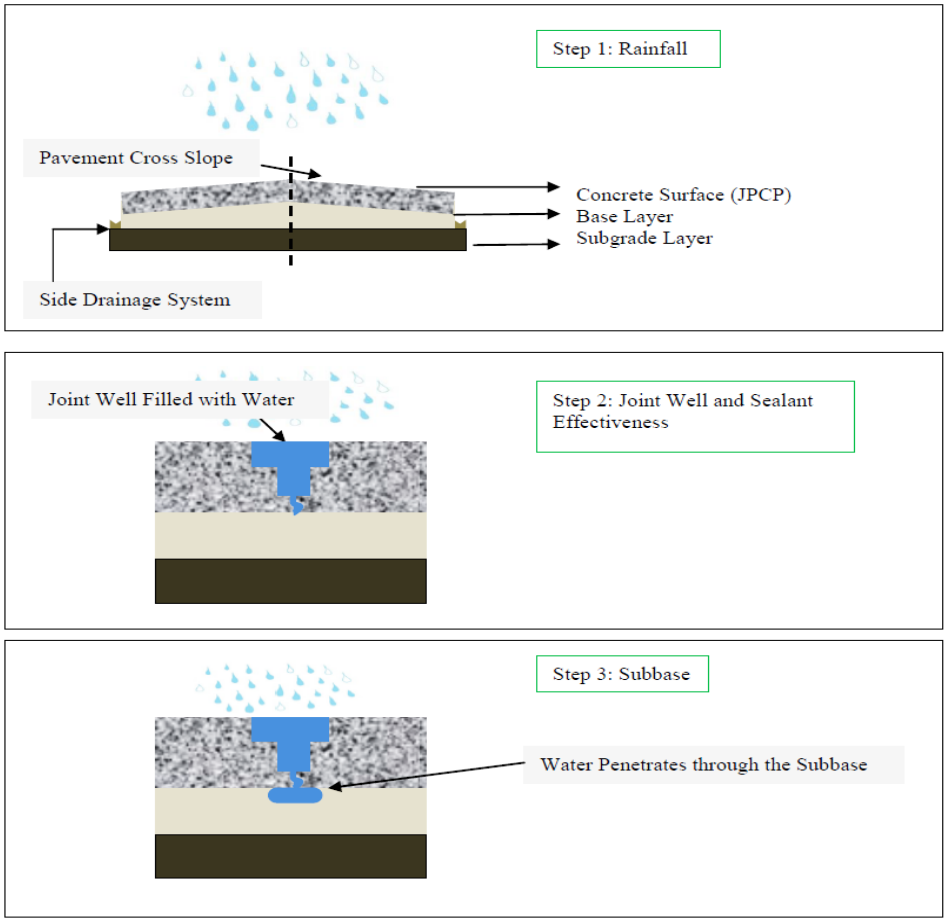

Figure 16 Three Stages of Water Transmission into Subbase Layer.

4.3 Rainfall Inflow

The source of water contributing to inflow into the pavement systems is mainly due to rainfall. With a simple calculation assuming an average slab and joint geometry it can be shown that approximately 0.02 inch of rainfall is needed to completely fill an unsealed joint well. Therefore, the amount of precipitation to be considered for wet day's calculation must be significantly higher than 0.02 inch knowing the surface drainage potential, blocking effects of the sealant and the water head needed to penetrate into the sublayer. The Mechanistic-Empirical Pavement Design Guide, MEPDG, defines wet days as number of days with rainfall greater than 0.1 inch [40]. As a climatic factor this intensity of inflow is quite reasonable as a minimum amount of rainfall to be counted that can potentially infiltrates into sublayers. In fact a rainfall less than 0.1 inch (2.5 mm) is not enough to overcome the surface drainage and sealant system. Rainfall less than 0.1 inches is either completely prevented by surface drainage system, or even if water gets to the joints the amount of water is not enough to be of any consequence. Similar findings were obtained using the computer program DRIP. DRIP is a design program that was developed in research funded by the United States Department of Transportation and Federal Highway Administration (FHWA) for the design and analysis of pavement subsurface drainage [42].

Therefore in the calculation of number of wet days, the number of days with rainfall greater than 0.1 inch will be considered as the minimum amount for infiltration to take place.

4.4 Water Surface Flow and Joint Infiltration

Water inflow into a pavement substructure is mainly by precipitation. Surface drainage is mainly due to cross slope of the pavement system, shoulders, exiting into longitudinal side drainage channels, side ditches or culverts. In designing surface drainage systems, the primary objective is to properly accommodate run-off along and across the pavement surface through the application of hydraulic principles and fluid mechanics.

According to TxDoT, the recommended minimum pavement cross slope is 2 percent. In areas of high rainfall or along the curves, steeper cross slopes may be used. The algebraic difference of cross slope between the traveled way and shoulder grades should not exceed 7 percent. Maximum shoulder slope should not exceed 10 percent [43]. Surface drainage can divert 35 to 50 percent of the amount of total rainfall water from the pavement structure. Cedergren recommended that the design infiltration rate to be found by multiplying precipitation by a coefficient varying from 0.5 to 0.67 for concrete pavements [38, 44, 45]. Hence to estimate the surface inflow Cedergren recommended the design infiltration to be by multiplying the 1-hour-duration/1-year-frequancy precipitation rate by a coefficient varying from 0.50 to 0.67 for jointed concrete pavements [44, 45]. . Figure 17 shows the 1-hour-duration/1-year-frequancy precipitation rate in the Unites States.

Given the results of field infiltration tests, Ridgeway [46], indicated that the duration of rainfall is a more critical factor than the intensity. He found that the amount of infiltration can be calculated by the following equation;

$$q_i = I_C \left(\frac{N_C}{W_p} + \frac{W_C}{W_p C_s}\right) + k_p \quad (4\text{-}1)$$

Where

q_i = Infiltration rate per unit area, $ft^3/day/ft^2$

I_c = Joint infiltration rate (2.4 $ft^3/day/ft$)

N_c = Number of longitudinal joints

W_p = Width of pavement lane subjected to infiltration

W_c = Length of transverse joints

C_s = Joint spacing

K_p = Concrete infiltration rate

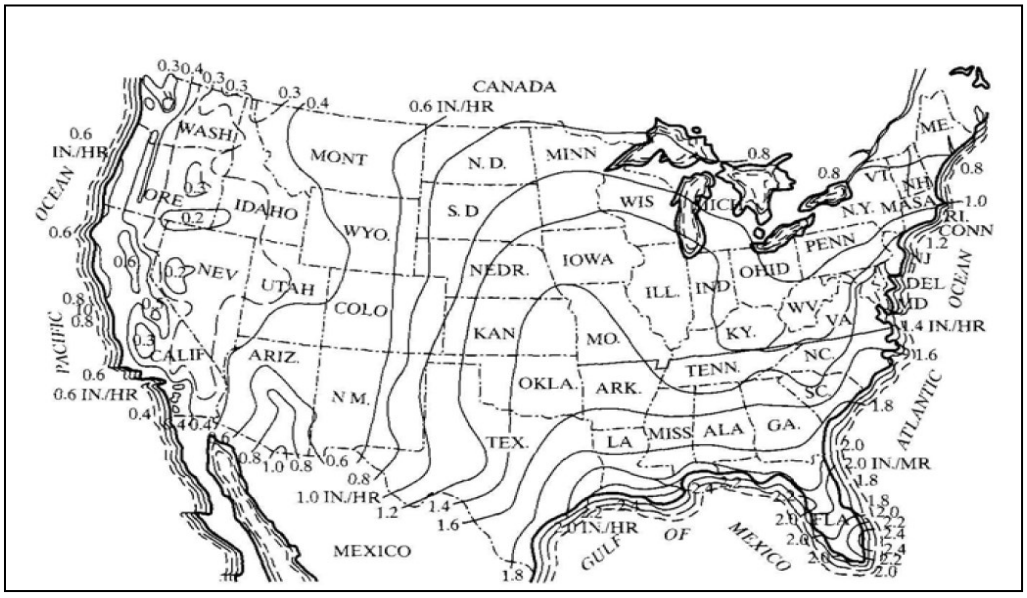

Figure 17 Maximum 1-H-Duration/1-Y-Frequency Precipitation in the U.S [44].

Apparently the K_p value for concrete slab is exceedingly small and negligible. N_c is equal to number of lanes plus one, and W_p is equal to W_c. Therefore inflow rate can be written as [47]:

$$q = q_i W_p = I_C \left(N + 1 + \frac{W_p}{C_s}\right) \quad (4\text{-}2)$$

Where N is the number of lanes and q is the inflow rate in ft^3/day/linear ft of pavement and Cs is the slab joint spacing.

The equations developed by Ridgeway mainly were to address infiltration from cracks in asphalt pavements or unsealed joints in concrete pavements. Therefore a main problem with these equations in applying them for drainage calculations on jointed concrete pavement is that they do not account for the joint sealant effect. Sealants can significantly affect the infiltration rate. Therefore Ridgeway's equation can be adjusted in to the followings;

$$q_i = F * I_j * \left(\frac{N+1}{W} + \frac{1}{S}\right) \quad (4\text{-}3)$$

Where

q_i = Infiltration rate per unit area, ft^3/day/ft^2

F = Infiltration coefficient (function of joint sealant effectiveness)

I_j = Joint infiltration rate, 2.4 ft^3/day/ft

N = Number of the lanes

W = Length of transverse joints, ft

S = Joint Spacing, ft

Infiltration coefficient of the sealant is a function of sealants installation and sealant damage in percent. The infiltration coefficient of the sealant ranges between 0 to 100.A value of zero represents a perfectly bonded condition along the joint where no infiltration can occur, and a value of hundred represents a no seal condition. The equation for the no sealed condition faults to the original Ridgeway equation. Another possible factor to account for in order to modify the Ridgeway equation is the evaporation effect that is discussed in Appendix E.

4.5 Infiltration Coefficient of the Sealant

Results from joint sealant infiltration testing were used to define the infiltration coefficient of the sealant. These tests were all performed in Riverside campus of Texas A&M University. The important consideration about these tests is the choice of subbase material; the subbase layer for all these tests is an open graded subbase (Figure 18). Subbase material permeability can affect the results of the infiltration tests. The advantage of a high permeable base is to isolate the joint sealant from any other effects.

Figure 18 Open Graded Granular Subbase Used for Test Program.

Infiltration coefficient consists of two factors; flow factor and installation factor. Flow factor pertains to sealant bond to the joint wall while installation factor pertains to installation quality prior to application of the sealants.

Two sets of testing were performed to address the infiltration coefficient: sealant damage tests (in order to define flow factor) and sealant installation tests (in order to define installation factor). Details of the pavement test sections and test procedures were discussed previously.

4.5.1 Sealant Damage Test and Flow Factor

Sealants were carefully separated (debonded) from the face of the joint well prior to testing in different levels of 100%, 75%, 50% and 25% of the joint seal length. Hundred percent separation, represents the condition in which sealant is completely debonded from the joint well on one side. Figure 19 shows 50 percent debonded sealant.

Using the movable joint system as previously explained, allowed for the joint opening to be varied. This was done in order to simulate the effects of seasonal changes

on the joint opening. Infiltration tests were performed for each level of separation (debonding) at different joint openings. The original joint width was 3/8 inches. Table 4 and Figure 20 show the results for these infiltration tests.

As it is shown sealants with higher percentage of separation are more sensitive to joint opening. Sealants with 100% separations were totally deboned and not capable of preventing infiltration. As sealants are less damaged they are more effective. Rate of infiltration for different amount of separation were compared to the one for 100% separated seal for each opening. Results are shown in Figure 21.

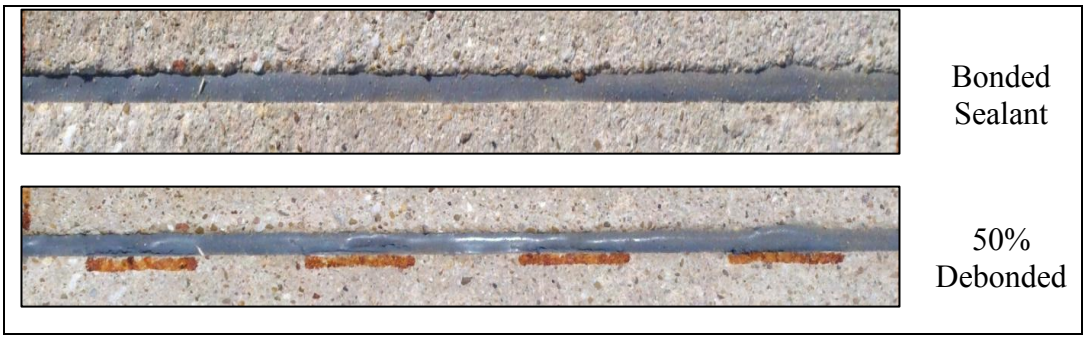

Figure 19 Fifty Percent Debonded Sealant.

Table 4 Infiltration Test Results on Damaged Sealants.

Joint opening width (inch)	Joint opening width (mm)	Flow rate (gallon/min./ft)			
		100% damaged	75% damaged	50% damaged	25% damaged
0.002	0.05	0.000	0.000	0.000	0.000
0.008	0.20	0.002	0.000	0.000	0.000
0.016	0.40	0.349	0.075	0.000	0.019
0.024	0.60	1.107	0.324	0.089	0.079
0.031	0.80	2.076	0.775	0.246	0.270
0.039	1.00	3.125	1.435	0.579	0.432
0.047	1.20	4.196	2.113	1.024	0.668
0.055	1.40	5.357	2.791	1.463	0.901
0.063	1.60	6.522	3.550	1.923	1.186
0.071	1.80	7.407	4.348	2.381	1.415
0.079	2.00	8.738	5.202	2.821	1.744
0.087	2.20	9.836	6.061	3.429	1.961
0.094	2.40	10.909	6.452	3.774	2.128
0.102	2.60	11.765	7.317	4.167	2.419
0.110	2.80	13.043	8.696	4.800	2.679
0.118	3.00		9.836	5.357	3.030

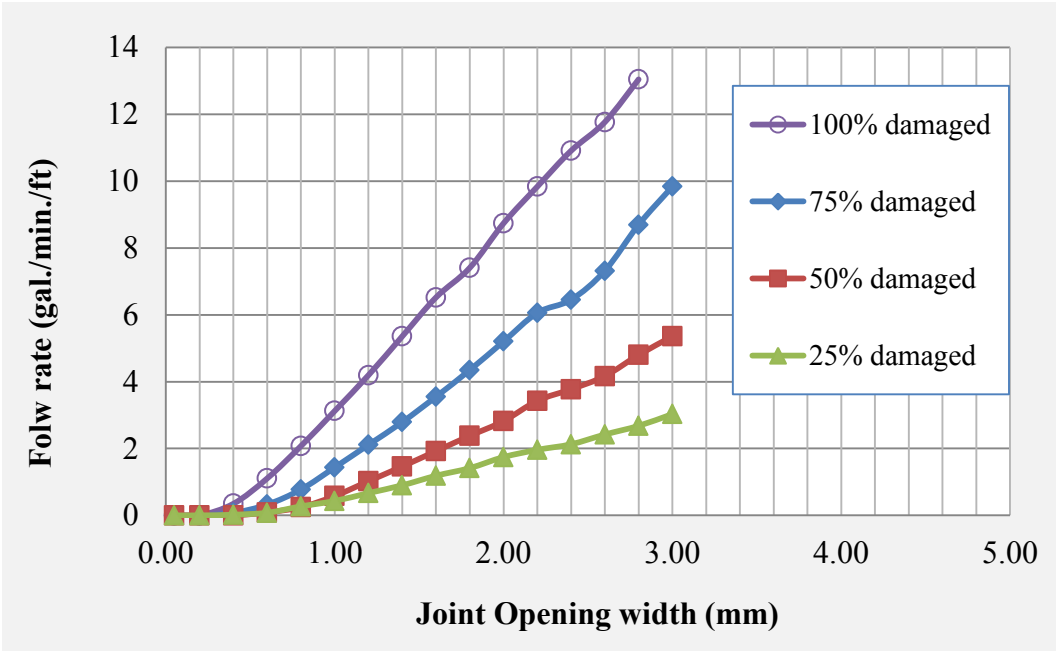

Figure 20 Infiltration Test Results on Damaged Sealants.

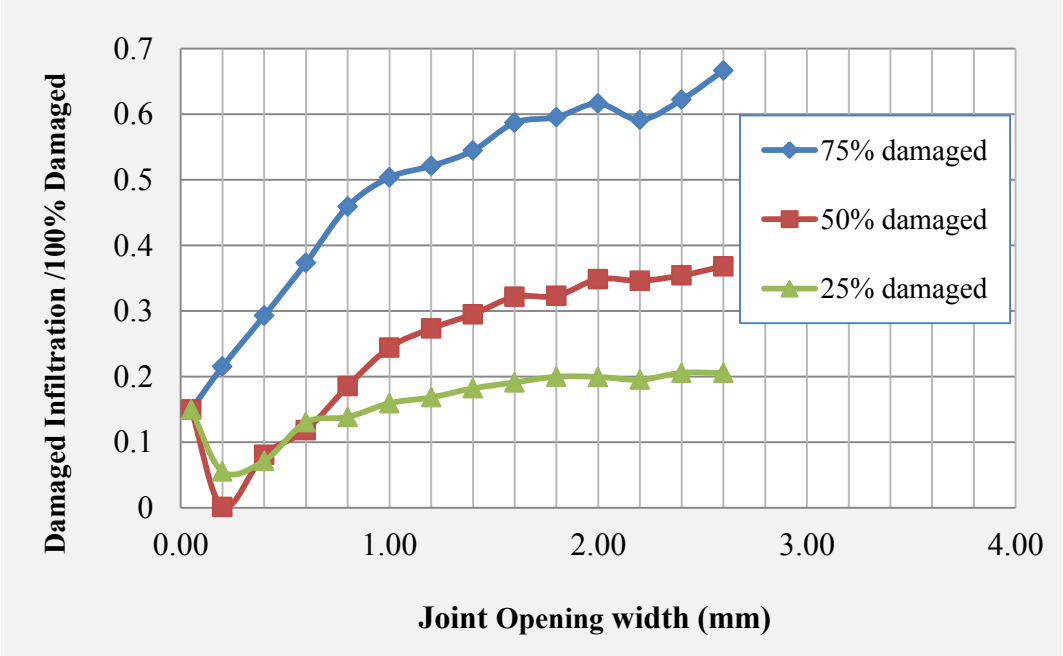

Figure 21 Infiltrations for Different Damage Levels Compared to 100% Damaged.

The weight average of this analysis (infiltration rates versus joint opening for each separation level) can be used in order to assign a flow factor for sealants. Sealants bond condition can be classified from very poor to good condition. Very poor rating is given to the sealant that is fully debonded, ineffective and 100% separated. Poor rating is given to sealants with 75% separation; fair condition represents sealants with around 50% separation and a good rating is given to sealants that have less than 25% separation. Sealants deterioration could be a result of aging. Aging is a continuous process that results from the effect of exposure to ultraviolet (UV) radiation from sunlight and moisture and temperature fluctuation experienced during the service life of the sealant. These factors result in degradation of the material and turn the sealant rigid and stiff with time [22]. Aging of the sealant material can make the sealant stiffer and less flexible. Therefore, sealants receive higher stresses at the interface that leads to debonding and failure [23]. Field tests indicate that, over time, sealants become stiffer because of aging effects [48]. Silicon based sealants after five years of exposure was reported to show tensile strength reductions of 24-54% and elongation at break reductions of 24-50% [48]. Accelerated weathering of a silicone sealant, Dow Corning 781, in an Atlas Weatherometer, for 6000 h produced no change in tensile strength, a decrease in elongation at break of 6% and an increase in hardness of 21%,4 which was equated to a life expectancy of greater than 20 years [48]. Oldfield and Symes studied long-term in-situ aging of silicone sealant in which sealant samples were aged in natural environments for 20 years. Their results indicate that sealant's modulus increases by approximately 60% over 20 years. Oldfield and Symes provided an aging parameter to quantify a

sealant's modulus as a function of time (Figure 22) [20, 48]. A recent study conducted at University of Florida is evaluated the adhesive strength of original field-poured silicone sealants as they are being aged. An adhesive strength aging parameter was developed based on Oldfield and Symes' modulus aging parameter. Results are shown in Figure 23 which indicates the adhesive strength was inversely proportional to modulus of elasticity and the adhesive strength decreases with aging.

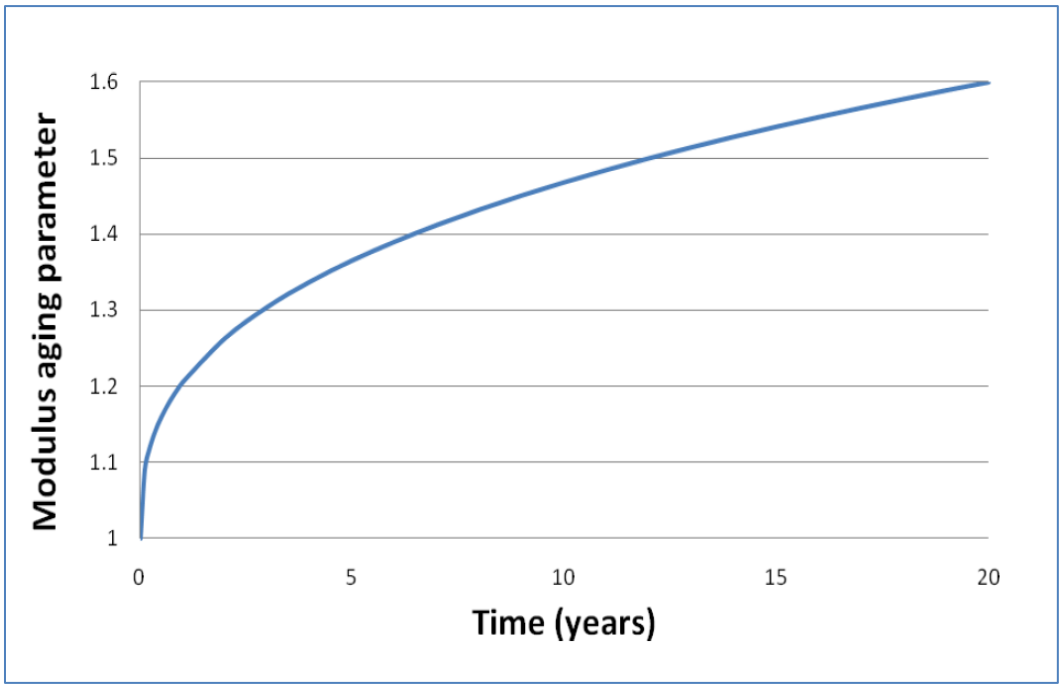

Figure 22 Modulus Aging Parameter versus Time [48].

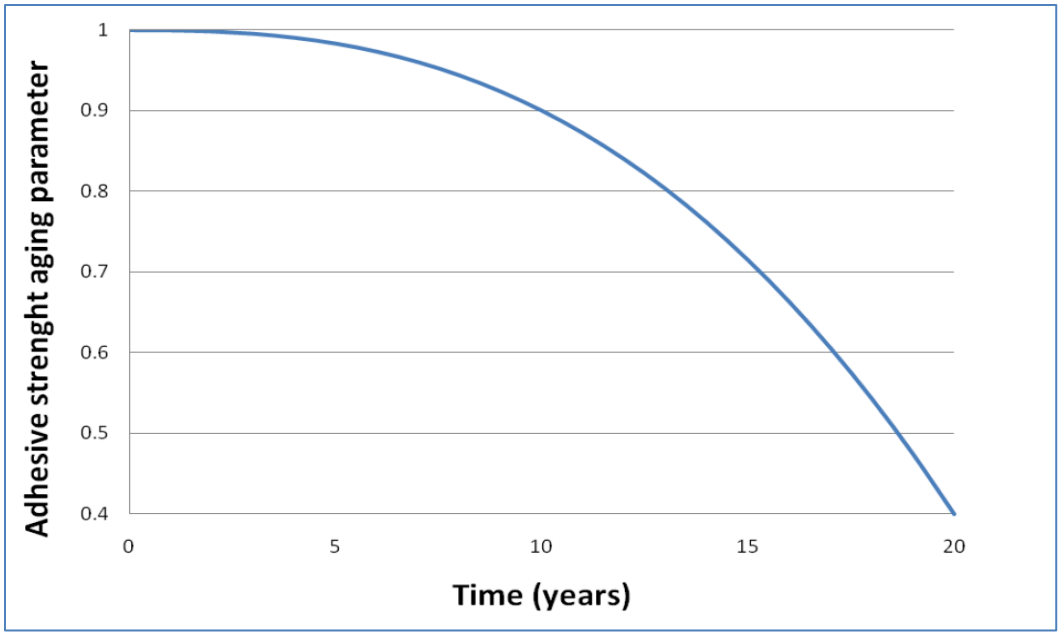

Figure 23 Adhesive Strength Aging Parameter versus Time [20].

Table 5 shows the flow factor for different sealant conditions. The better the sealant condition the lesser the rate of infiltration through the joint.

Table 5 Flow Factor for Different Sealant Conditions.

Sealant Condition	Good	Fair	Poor	Very Poor
Calculated Flow Factor	22%	30%	52%	100.00%

4.5.2 Sealant Installation Test and Installation Factor

The testing program also addressed the effect of installation quality associated with joint seal effectiveness. As previously mentioned, tests were conducted using saw dust slurry to make three different concentration levels. Results were then analyzed with respect to dirtiness or the degree of contamination and sealant performance. The results

shown in Figure 24 shows a significant difference when the dirtiness level is zero (completely clean joint walls).

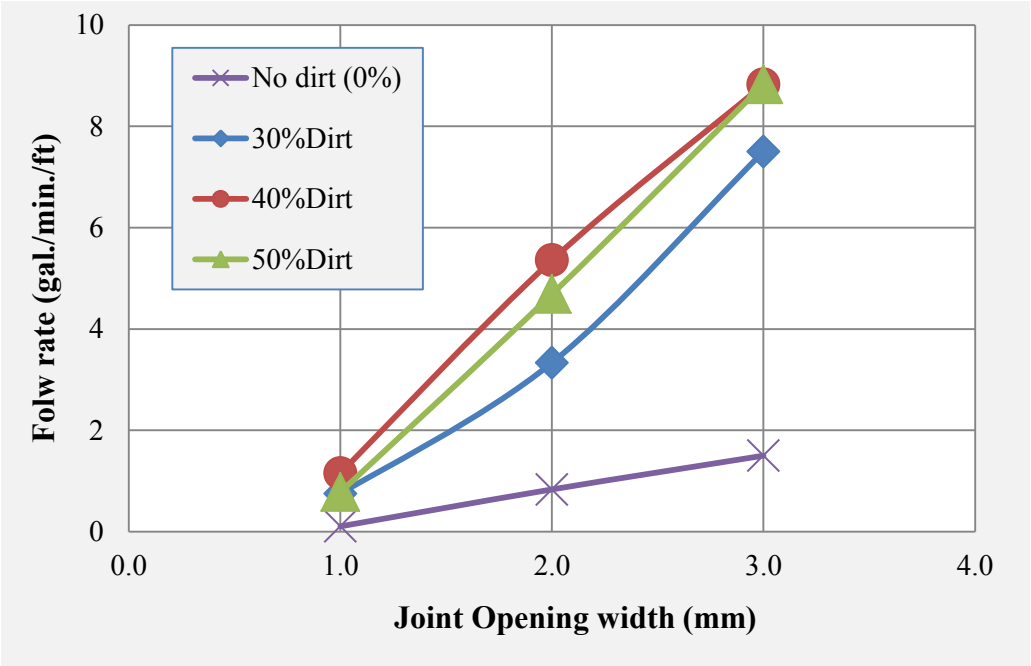

Figure 24 Water Infiltration Rates for Different Joint Dirtiness Levels.

Same as for separated sealants, the weighted average of these results for different installation qualities and different joint openings can be used to assign an installation factor. Sealants installation quality can be classified from very poor to very good. Very poor rating is given to the sealant installation that leads to premature debonding shortly after installation. 50% dirtiness, the highest level of dirtiness in the test program, represents the condition where one side of the joints is totally contaminated and debonded. Figure 25 shows the average infiltration rate for different dirtiness levels. Table 6 shows the installation quality factor for different installation qualities; dirtiness

levels were scaled from 0 to100 and each dirtiness level assigned to an installation quality rating. Installation factor for clean joints with absolutely no dirtiness defined as 100% and other sealant installation factors were calculated in respect to a given infiltration rate scaled to the infiltration rate of a clean joint. A greater value of the installation factor corresponds to a greater sealant bond quality and lower infiltration through the joint. Table 7 shows installation factors as a function of installation quality.

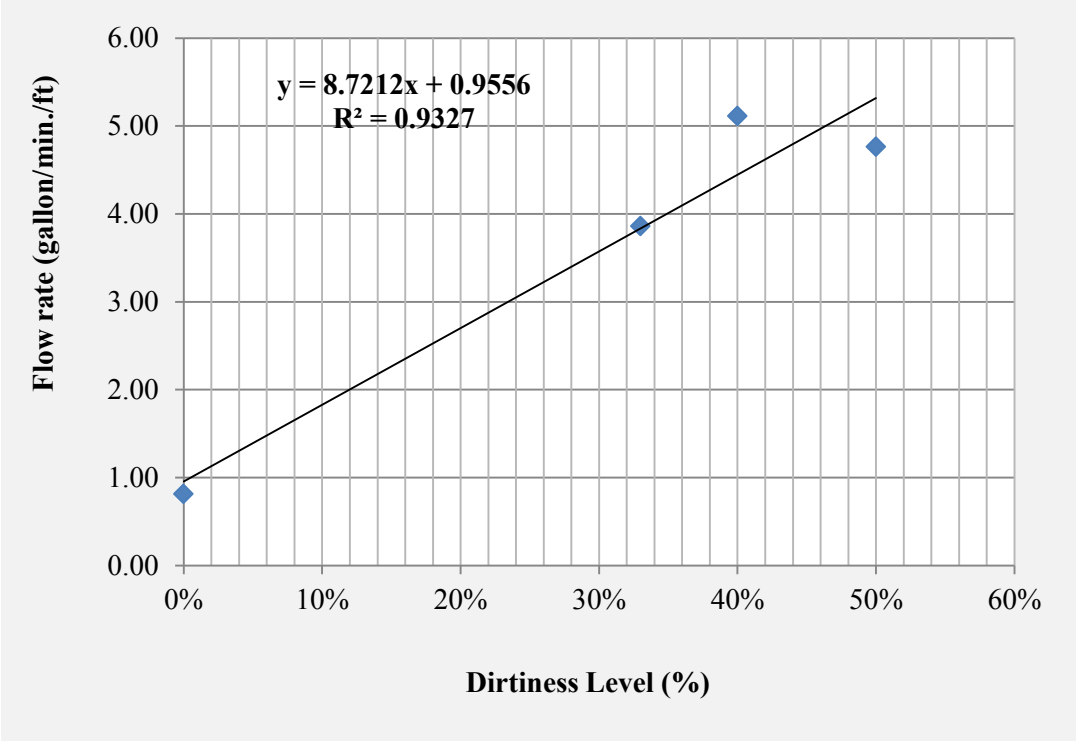

Figure 25 Average Infiltration Rates for Different Dirtiness Levels.

Table 6 Dirtiness Levels, Installation Qualities and Calculated Installation Factor.

Installation Quality	Dirtiness levels in the test (%)	Scaled Dirtiness in 0-100 Range	Inflow Rate (gallon/min./ft)	Installation Factor
Very Good	0	0	0.9	100.00
Good	15	30	2.3	70.00
Fair	30	60	3.6	40.00
Poor	40	80	4.4	20.00
Very Poor	50	100	5.3	0.00

Table 7 Installation Factor as a Function of Installation Quality.

Sealant Installation Quality	Very Good	Good	Fair	Poor	Very Poor
Installation Factor	100%	70%	40%	20%	0%

4.5.3 Calculation of Infiltration Coefficient

Given the results from testing program, the infiltration coefficient, F that was added to Ridgeway's equation can be defined as follows;

$$F = i * (1.4 - d) \quad (4\text{-}4)$$

Where *i* is the flow factor according to Table 5 and *d* is the installation factor according to Table 7. The installation factor, *d*, has an inverse effect on *F*. Since the tests on separated seals were performed at a level of fair installation quality (installation factor of 40%), the infiltration coefficient must be equal to flow factor at that installation quality

(F=i). It should be noticed that infiltration coefficient has a maximum value of 100%. So equation 4-4 can be modified as;

$$F = Min\,[i * (1.4 - d)\,,\ 1] \tag{4-5}$$

Where

F = Infiltration coefficient

i = Flow factor

d = Installation factor

4.6 Water Movement in the Subbase

The movement of water in the sublayer is mainly due to gravity and obeys Darcy's law of flow [38] [49];

$$v = ki \tag{4-6}$$

$$Q = kiA \tag{4-7}$$

In which v is the discharge velocity, i is the hydraulic gradient, k is the coefficient of permeability, A is the total cross sectional area normal to the direction of flow and Q is the seepage quantity. The hydraulic gradient is the head loss between two points divided by the distance between them. The hydraulic conductivity of a subbase material depends on several factors:

- Fluid viscosity
- Pore size distribution
- Grain size distribution
- Void ratio
- Degree of saturation

K can be determined in the field or in the lab. K is determined in the lab using two methods: Constant-Head Test and Falling-Head Test. The constant head test is used primarily for coarse-grained materials. This test applies a constant head of water to each end of a sample in a "permeameter" (ASTMD2434). The falling head test is used for both coarse-grained soils as well as fine-grained soils in which initial and final head is recorded.

Darcy's law can be used in conjunction with the continuity equation to form the differential equation governing ground water flow. A convenient and practical way to solve the equation is by drawing the flow nets, as illustrated by Cedergren, 1977 [36]. In simple application Darcy's law can be applied directly in order to define the amount and timing of seepage. In a more precise way Darcy's law could be applied in order to solve the Laplace equations of water flow nets. In case of water flow from the joints in to the subbase, flow nets are more accurate and practical as the water flow under slab is not only in one direction.

A flow net is a graphical representation of two dimensional steady-state groundwater flows through an aquifer. To develop the Laplace equations for flow underneath a slab, following assumptions are used:

1. The subbase material is homogeneous
2. The voids are completely filled with water
3. The subbase and water are incompressible

The two dimensional form of the Laplace equation for water flow is as follows:

$$\frac{\partial^2 h}{\partial x^2} + \frac{\partial^2 h}{\partial z^2} = 0 \tag{4-8}$$

In which *h* is the water head and x and z are Cartesian coordinates. The equation can be represented by two families of curves that intersect at right angles to form a pattern of square figures know as flow net [36]. One set of lines is called the streamline or flow lines and the other that are perpendicular to flow are called equipotentials. The flow lines represent paths along which water can flow through a cross section. The equipotentials lines are lines of equal energy level or head. Flow nets must meet certain requirements as follows:

1. Flow lines and equipotential lines must intersect at right angles to form areas that are basically squares,
2. Certain entrance and exit requirements must be met,
3. A basic deflection rule must be followed in passing from a soil of one permeability to a soil with different permeability,
4. Adjacent equipotentials have equal head loses, and
5. The same quantity of seepage flows between adjacent pair of flows.

From equations 4-6 to 4-8, an expression for the computation of seepage can be found to be as follows [36];

$$Q = kh\frac{N_f}{N_d} \tag{4-9}$$

Where k is the coefficient of permeability, Q is the seepage quantity, N_f is the number of flow channels and N_d is the number of equipotentials drops. The flow net for a concrete pavement joint is shown in Figure 26. For water seepage from the joint into the subbase essentially the water head is equal to the slab thickness. Therefore, for the case of water flow underneath the slab, equation 4-9 can be written as follows in which h_c is the slab thickness.

$$Q = kh_c\frac{N_f}{N_d} \tag{4-10}$$

The flow net was drawn in scale for different base thicknesses. As the base layer becomes thicker the number of equipotential lines increases which means thicker subbases has lower Nf/Nd ratio and so the lower seepage quantity according to equation 4-10. As the base layer becomes thicker water tends to spread more diagonally into the layer that lowers the quantity of seepage. Table 8 shows the number of flow lines and equipotential lines for different base layer thicknesses. Incomplete equipotential lines

were measured carefully as a portion of a full channel. It should be noticed that the Nf/Nd ratio does not depend on slab thickness.

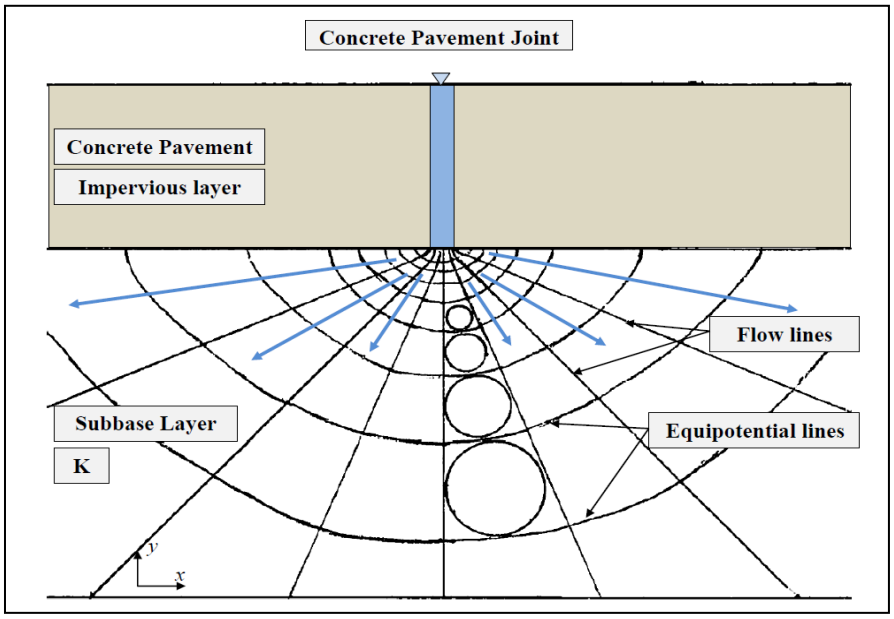

Figure 26 Flow Net for Water Seepage from the Concrete Joints into the Subbase.

Table 8 Number of Flow and Equpotential Lines for Different Base Thicknesses.

Base Thickness (inch)	Nf	Nd	Nf/Nd
1	8.00	4.00	2.000
2	8.00	5.70	1.404
3	8.00	6.65	1.203
4	8.00	7.41	1.080
5	8.00	8.00	1.000
6	8.00	8.41	0.951
7	8.00	8.85	0.904
8	8.00	9.61	0.832

Figure 27 shows a regression model to fit the ratio of flow and equipotential lines to base thickness. The R square value is equal to 0.99 and the fit is highly acceptable. Therefore, for a particular case of flow from a joint into the subbase equation 4-10 can be written as follows;

$$Q = kh_c * 1.92\ h_b{}^{-0.403} \tag{4-11}$$

Where Q is the seepage quantity, k is subbase coefficient of permeability, h_c and h_b are slab and base thicknesses and base thickness has to be put in unit of inch.

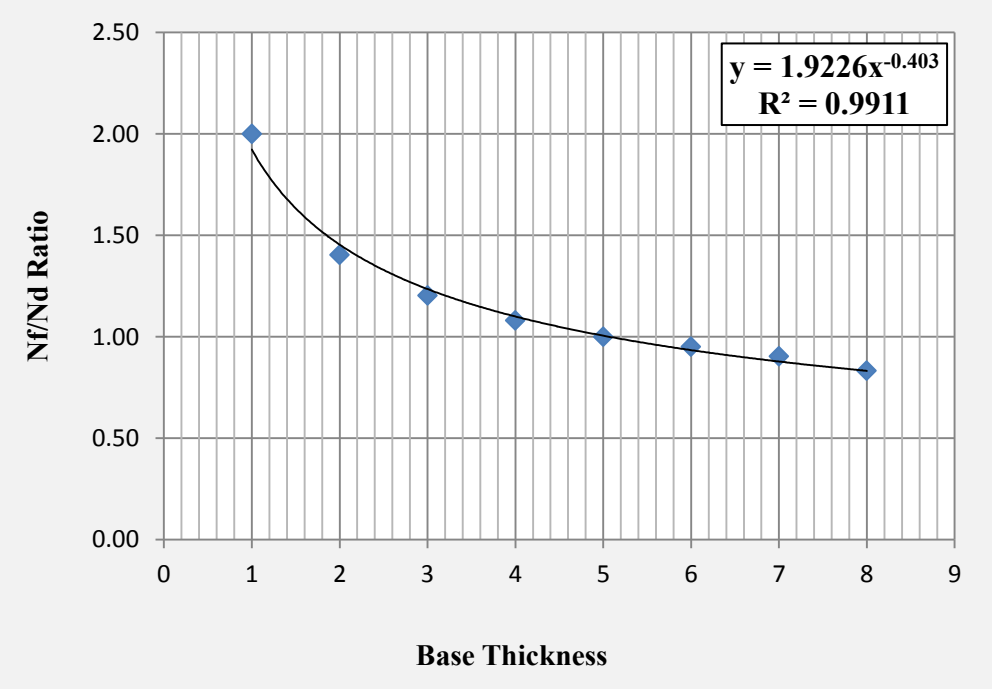

Figure 27 Regression to Fit the Ratio of Flow Net Lines to Base Thickness.

4.7 Calculation of Number of Wet Days

Number of wet days has been used as a climatic factor in the modeling of jointed concrete pavement performance. As mentioned previously number of wet days defined as number of days with rainfall greater than 0.1 inch in a year [40].

But this definition is not explicit. The definition does not take in to consideration the effects of surface drainage, joint sealants effects or different base materials drainage capacities. Surface drainage can decreases the amount of rain that gets into the joint by up to 50 percent therefore the effect of surface inflow cannot be ignored. Also sealant effectiveness and subbase permeability and seepage rate are critical factors that can change the actual number of days that moisture exists underneath the slab.

Number of the wet days is a function of climatic factor, surface inflow, joint and sealant condition and subbase drainage capacity. Number of wet days, N_w, initially is modeled as a probability function of the total number of days in a year;

$$N_W = P\% * 365 \tag{4-12}$$

Considering the previous discussions on surface inflow, joint infiltration and base seepage this probability can be broken down in to three parts;

$$P = p_1 * p_2 * (1 + p_3) \tag{4-13}$$

Where

P = Percent of wet days

p_1 = Probability of the rain,

p_2 = Probability of infiltration in to the joint

p_3 = Probability of wet subbase

All these probability values ranges between zero and one ($0 < p_i < 1$). P_1 defines a climatic probability function. That is simply the number of rainy days greater than 0.1 inch (2.5 mm) in one year divided by the total number of days in a year. In order to calculate P_2, modified form of Ridgeway's equation is used;

$$q_i = F * I_j * \left(\frac{N+1}{W} + \frac{1}{S}\right) \quad (4\text{-}14)$$

Where

q_i = Infiltration rate per unit area, $ft^3/day/ft^2$

F = Infiltration coefficient (function of joint sealant effectiveness)

I_j = Joint infiltration rate, 2.4 $ft^3/day/ft$

N = Number of the lanes

W = Length of transverse joints, ft

S = Joint Spacing, ft

Beta distribution function is assumed to find the probability of infiltration in to a joint. The beta distribution can be used to model events which are constrained to take place

within an interval defined by a minimum and maximum value. Shorthand computations are widely used to estimate the mean and standard deviation of the beta distribution [50].

$$\sigma = \frac{(b-a)}{6} \tag{4-15}$$

$$\mu = \frac{1}{6}(a + 4 * m + b) \tag{4-16}$$

Where

σ = Standard deviation

μ= Expected Value (Mean)

a = Minimum value (Estimation)

b = Maximum value (Estimation)

m = Average value (Estimation)

The above estimate for the mean is known as the PERT three-point estimation. This case makes the distribution symmetric and non-skewed that is very similar to the normal distribution. A Taylor series expansion of the Beta distribution probability density function shows that the Beta distribution can be approximated by the Normal distribution when skewness is equal to zero and the range is sufficiently great.

Equation 4-11 ,$Q = kh_c * 1.92\ {h_b}^{-0.403}$, was applied in order to calculate P3. Same approach applied to estimate extremum values for seepage and to build a

distribution. Since the equation is for water seepage into the subbase layer, the output of this cumulative distribution is the probability of seepage, P_{sb}, which is the probability of the water passing through a subbase layer. Probability of subbase being wet, P_3, is equal to $1-P_{sb}$ since the water that exists in the sublayer is of the interest rather than the water that passes through (Figure 28). Figure 28 shows an example of a relatively permeable subbase. Since the permeability is high the seepage quantity and the probability of subbase seepage, Psb, is high (the colored area under the curve) while the probability of wet subbase, P3, is low (the uncolored area under the curve).

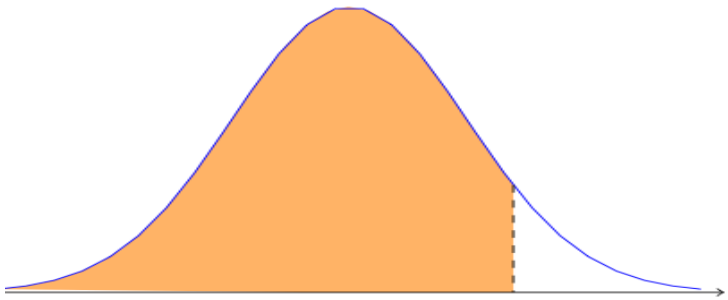

P_{sb} (The probability of the subbase seepage (P_{sb})

P_3 (The probability of the subbase to be wet) ($P_3=1-P_{sb}$)

Figure 28 Example of Subbase Seepage Distribution.

Figure 29 shows an algorithm to calculate the number of wet days. This algorithm along with all related equations is used to make a spreadsheet that is capable to analyze the probability functions, makes distribution graphs and calculate the number of wet days.

Figure 30 shows the main sheet of a computer spreadsheet program that calculates the number of wet days. These calculations can be done without the

spreadsheet using equations that were explained but the spreadsheet makes the analysis faster. It also provides graphs and distributions. In order to better understand the step by step procedure, the analysis is illustrated in an example. Table 9 shows the input values for the example pavement.

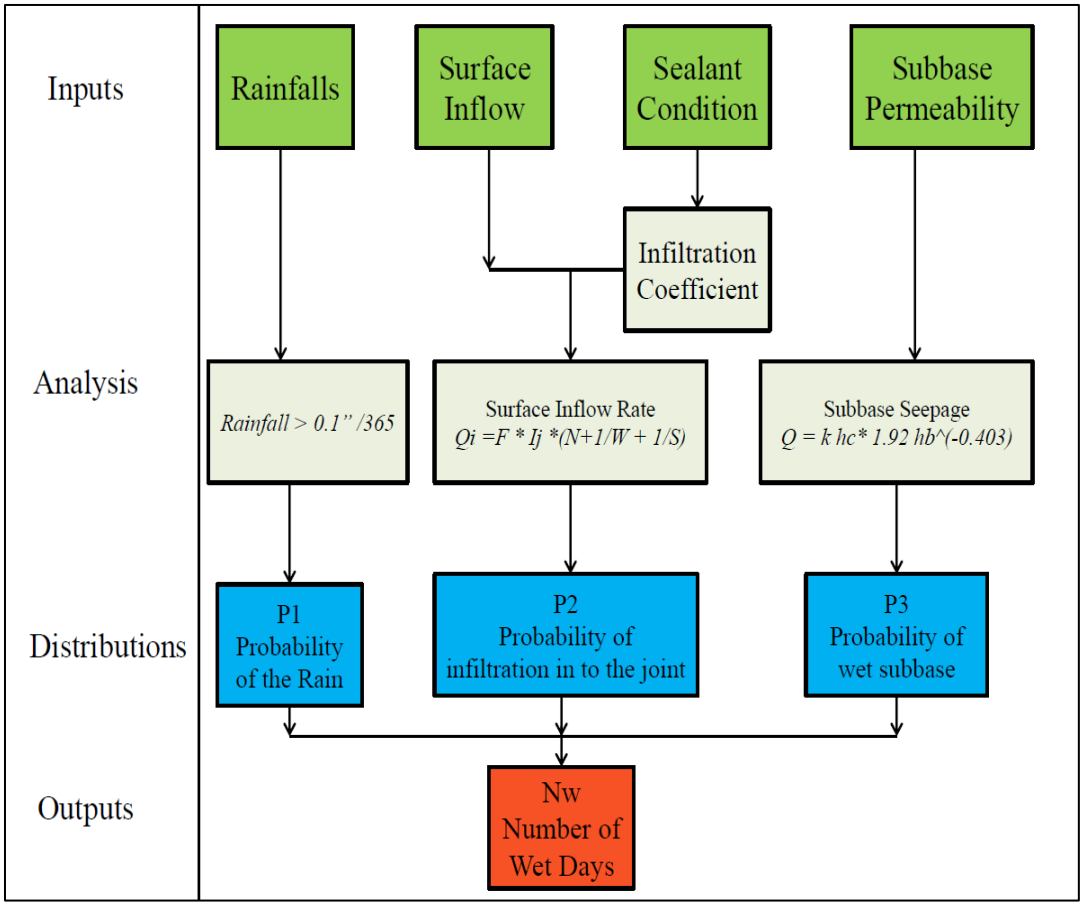

Figure 29 Algorithm to Calculate the Number of Wet Days.

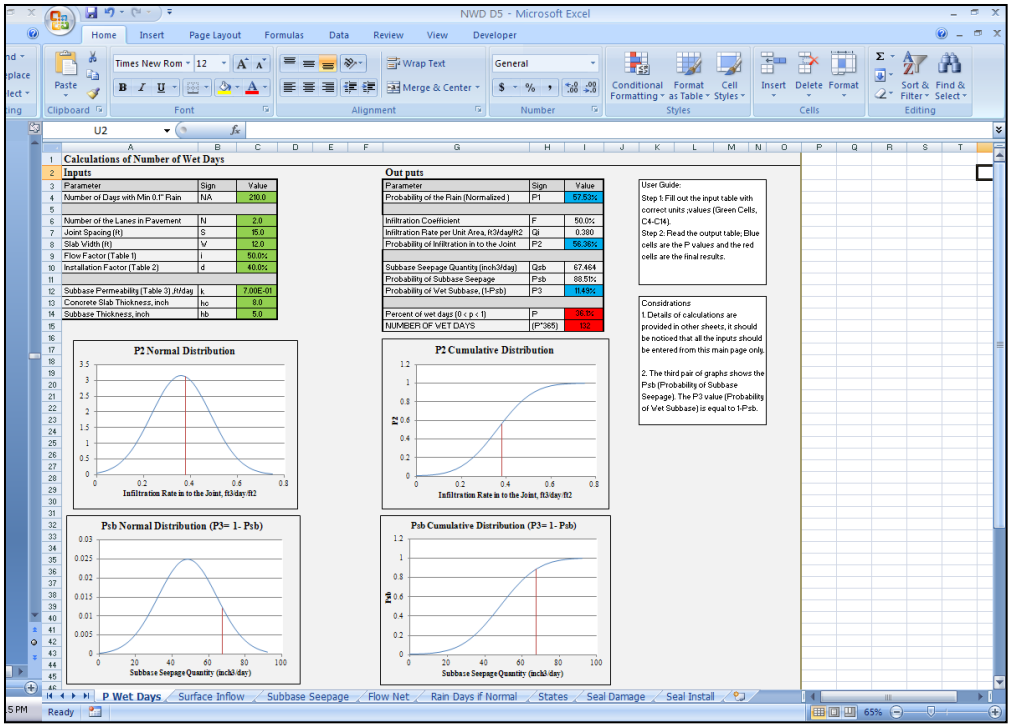

Figure 30 Computer Spreadsheet Program that Calculates the Number of Wet Days.

Table 9 Input Values for the Example Pavement.

Analysis Step	Parameter	Sign	Value
Calculations of P_1	Number of Days with Min 0.1" Rain	NA	210.0
Calculations of P_2	Number of Lanes in Pavement	N	2.0
	Joint Spacing (ft)	S	15.0
	Slab Width (ft)	W	12.0
	Flow Factor	i	50.0%
	Installation Factor	d	40.0%
Calculations of P_3	Subbase Permeability, ft/day	k	7.00E-01
	Concrete Slab Thickness, inch	h_c	8.0
	Subbase Thickness, inch	h_b	5.0

As the number of days with minimum 0.1" rainfall is equal to 210 days (Table 9), the P_1 is simply calculated as 210/365= 57.53%. The infiltration rate per unit area in to a joint is calculated and it is equal to $Q_i = 0.38$ $ft^3/day/ft^2$. From there P_2 is calculated. A P_2 of 56.36% means that a bit more than half of the rainfall water would infiltrate the joint while the rest would be drained by surface drainage or blocked by joint sealants. Last step is to consider the effects of subbase seepage. The subbase, unless it is very permeable would hold the water and increase the total number of the wet days. Table 10 shows the output values of the example analysis. Figure 31 and 32 show the distributions for P_2 for this example calculations and Figure 33 and 34 show the distributions for P_{sb} for this example calculations.

Table 10 Output Values for the Example Pavement.

Parameter	Sign	Value
Probability of the Rain	P_1	57.53%
Probability of Infiltration in to the Joint	P_2	56.36%
Probability of Subbase Seepage	P_{sb}	88.51%
Probability of Wet Subbase, (1-Psb)	P_3	11.49%
Percent of wet days ($0 < p < 1$)	P	36.1%
Number Of Wet Days (P*365)	Nw	132

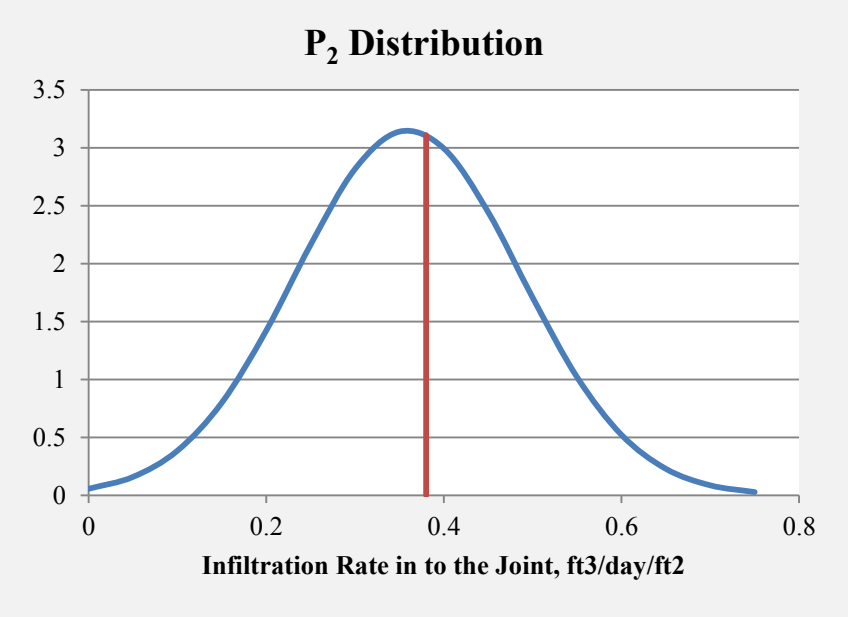

Figure 31 P_2 Distribution for the Example Analysis.

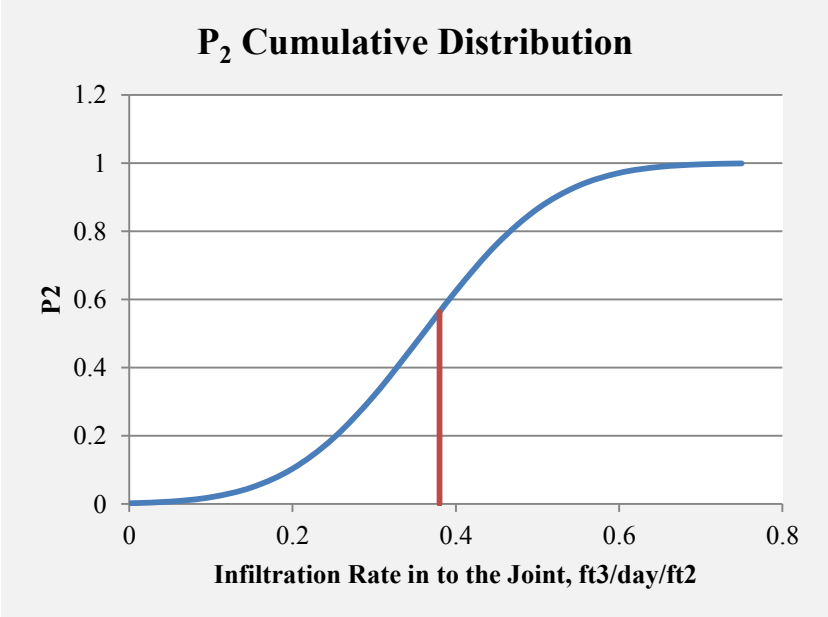

Figure 32 P_2 Cumulative Distribution for the Example Analysis.

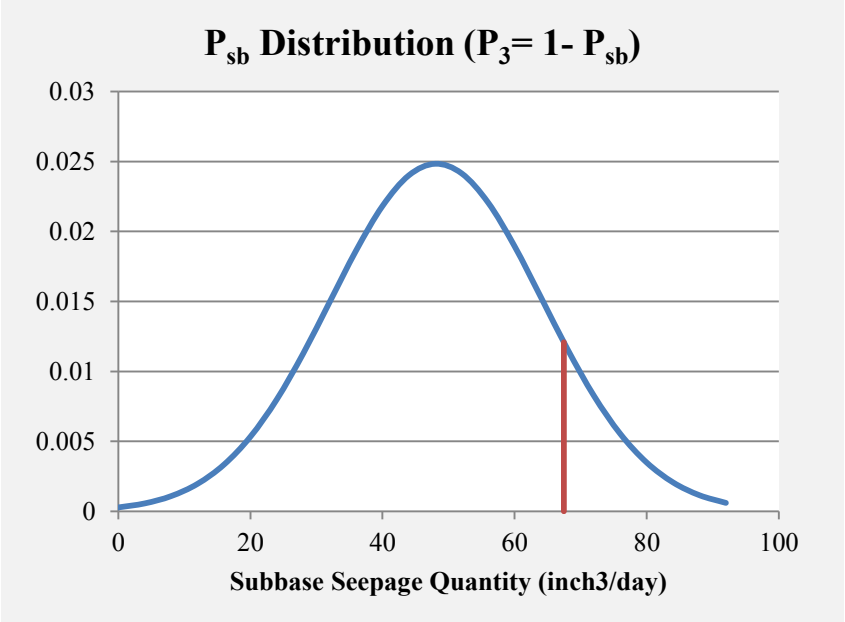

Figure 33 P_{sb} Distribution for the Example Analysis.

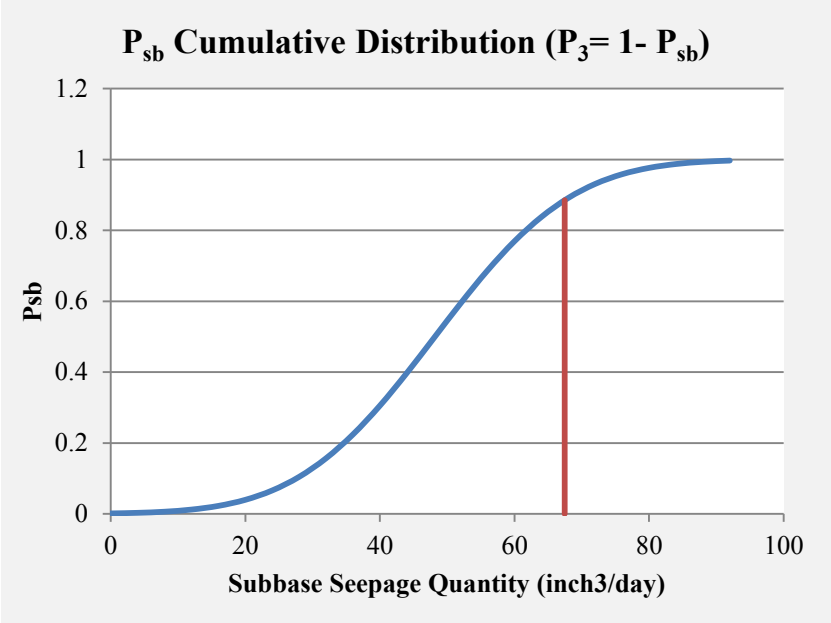

Figure 34 P_{sb} Cumulative Distribution for the Example Analysis.

5. FAULTING PREDICTION MODEL FOR DESIGN OF CONCRETE PAVEMENT STRUCTURES*

5.1 Introduction

Prior to presenting the modeling process, the mechanism of faulting is elaborated with respect to the three main elements that cause erosion. As part of this discussion is the description of the erosion model in a step by step format. Key details of the erosion model are presented keeping the focus on the analysis results and outcomes and the comparison of them to performance data from pavement sections under service. The erosion model is employed in a computer program. Sensitivity analysis of the design results is also discussed.

5.2 Faulting, a Major Distress Type in Concrete Pavements

According to field observations, faulting is typically a major performance issue for jointed concrete pavements [51]. Faulting, when it occurs, also affects drivers safety and decreases the smoothness of the ride [52]. Faulting is costly to repair and difficult to manage often requiring extensive grinding or in some cases full depth repair or slab grouting involving lane closures impacting public delays etc [53-55]. Faulting is addressed as a main performance indicator in the Mechanistic-Empirical Pavement

---

* Part of this chapter is reprinted with permission from "*Faulting Prediction Model for Design of Concrete Pavement Structures*" by K. Neshvadian Bakhsh and D. Zollinger, 2014. Geo Shanghai 2014 Conference Proceedings, Shanghai, China, Copyright 2014 by American Society of Civil Engineers.

Design Guide, MEPDG [40]. Therefore, faulting could be considered as a dominant distress type when designing a jointed concrete pavement.

Subbase erosion is a key to understanding the process of joint faulting which involves factors such as passing traffic, existence of water along the subbase/slab interface, and erodibility of the base material [10] (Figure 35). When slab support layers are saturated, vertical slab movement due to loading propels interlayer surface water back and forth under the slab across the joint creating a pumping action. This action creates voids under the departure slab by transporting loosened or abraded materials which leads to a building up of fine particles under the approach slab resulting in faulting. Erosion of slab support can often lead to high deflections and possibly other types of distress such as spalling of the joint, as well as acceleration of the loss of load transfer and bond between the slab and the base layer shortening the life of the pavement [1, 10].

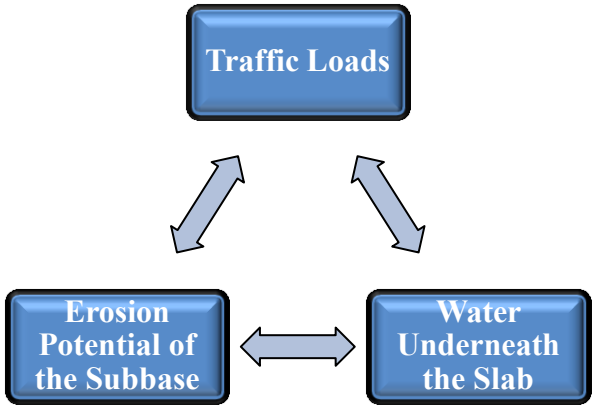

Figure 35 Three Main Elements Contributing in Subbase Erosion and PCC Faulting.

5.2.1 Traffic Loads and Pavement Strength

Heavy trucks continually loading a pavement structure in combination to lift-off of the slab edges and corners that tends to break down the adhesive bond between the slab and the subbase. This bond depends upon the shear strength of the supporting layers which over time can break down and affect the overall quality of the performance. If the slab is thin or if the subbase consists of low shear strength, the interfacial shear stress imposed by the applied loading may exceed the strength of the subbase or subgrade layer and cause erosion damage. Stiffening the pavement along the edges or at the joints may help to lower the shear stresses. This can be done simply by improving the strength of the subbase material (i.e. stabilization of subbase layer) or by using or restoring the integrity of the dowel bars at the joints. Design models with the appropriate sensitivity to shear strength and stress are key advantages to considering the integral effects of loading, subbase strength, and effects of the moisture.

5.2.2 Existence of Water underneath the Slab

It is well accepted that the presence of moisture in a pavement structure is a contributor to a variety of governing distress types related to erosion of the support that eventually deteriorates the pavement structure and decreases the pavement service life. Accumulation of water along the slab/subbase interface in the vicinity of the joint combined with passing traffic can often initiate pumping along the interface transporting eroded material leading to faulting of the joint. Pumping, involves the transportation of abraded interfacial material from beneath slab typically voiding the slab support in the vicinity of a joint [10, 41]. To give consideration to all factors that can affect the

performance of the pavement, climatic conditions that may cause the subgrade or subbase to become wetter over time, such as surface water infiltration, should be determined. Possible trapped water directly beneath the slab greatly increases the potential for erosion. Condition of the drainage system and joint seals considerably affects the existence of moisture underneath the slab [56]. Improving joint seal effectiveness may provide opportunities to improve the cost effectiveness of the pavement structure. Effectiveness of the joint sealants and the drainage system directly affect the number of wet days for design purposes.

5.2.3 Erosion Potential of the Subbase

A variety erosion tests were developed starting in late 1970s using various testing devices, but few of those tests have been successfully used to develop a model or a framework for design. Most of the laboratory tests in this regard involve the application loads on the material and define erosion related to weight loss, a parameter not particularly amenable to mechanistic design analysis. One method known as the brush test takes too long to run for practical purposes and the rotational shear device or jetting device tends to overestimate the loss of aggregate-sized particles. The rolling wheel erosion test device tends to create an erosion mechanism not like the voiding that occurs under an actual concrete slab [41, 57]. Jung and Zollinger developed a new test procedure that represents concrete pavement joint behavior to overcome these limitations and incorporates a parameter that can be transferred from lab to conditions in the field. This new laboratory test protocol involves measuring the erodibility of subbase materials using the Hamburg wheel-tracking device (HWTD) [41, 58]. The test

consists of two component layers, one being a concrete cap on top and the other the material of interest which is placed immediately under the concrete cap. A wheel passes on top of the two layers and the sensors record the deflection versus passes. HWTD testing is mainly conducted under wet conditions in which erosion occurs due to mechanical and hydraulic shearing on the subbase layer generated by slab movement under an applied load [59, 60]. Therefore HWTD can simulate the erosion that occurs underneath the slab due to the shear stress coming from the load in presence of water.

A wide range of subgrade soil materials from seven locations in four states were tested and analyzed in order to evaluate the erosion potential of different subbase materials and the capability of them to perform as a sublayer. The selected samples cover different soil categories; non-plastic pure sands, combination of silt and sand, combination of sand and clay, and clays with high and low plasticity. Results were then plotted as number of load passes versus deflection measured in millimeters. Erosion resistance (ER) is defined as the amount of erosion (in mm) at 1,000,000 load applications under HWTD erosion testing [41]. The greater ER indicates that a subbase or subgrade material has less resistance against erosion. This parameter serves to differentiate different subgrade and base types with respect to erodibility.

5.3 Faulting/ Erosion Model

The faulting/erosion model subsequently explained is a new ME (Mechanistic-Empirical) model formulation for faulting/erosion as a function of number of load repetitions and magnitude in respect to wet days and the erosion resistance of the subbase.

5.3.1 General Form of the Model

The erosion model follows Gumbel cumulative probability function that pertains to structural damage due to aging and loading over time or traffic [61].

$$\%\boldsymbol{E} = \frac{\boldsymbol{f_i}}{\boldsymbol{f_{ult}}} = \boldsymbol{e}^{-(\frac{\boldsymbol{\rho}}{\boldsymbol{D_i}})^{\boldsymbol{\alpha}}} \tag{5-1}$$

$$D_i = \boldsymbol{\Sigma}\frac{\boldsymbol{N_i}}{\boldsymbol{N_f}} \tag{5-2}$$

Where

%E = Percent of erosion

f_i = Level of faulting per load cycle i

f_{ult} = Ultimate faulting

D_i = Damage ratio per load cycle i

α = Erosion rate factor

ρ = Erosion shape factor

N_i = Designed $ESAL_i$ per load cycle i

N_f = Ultimate ESALs to failure

The model calculates erosion in percentage (%E) that is equal to the ratio between the current faulting to the ultimate amount of faulting. There are two calibration factors associated with the erosion model illustrated in Figure 36; erosion rate factor, alpha (α) and erosion shape factor, rho (ρ) are calibration factors that change the rate of the

damage. Figure 36 demonstrates how changing the value of the α or the ρ parameters affects the distribution.

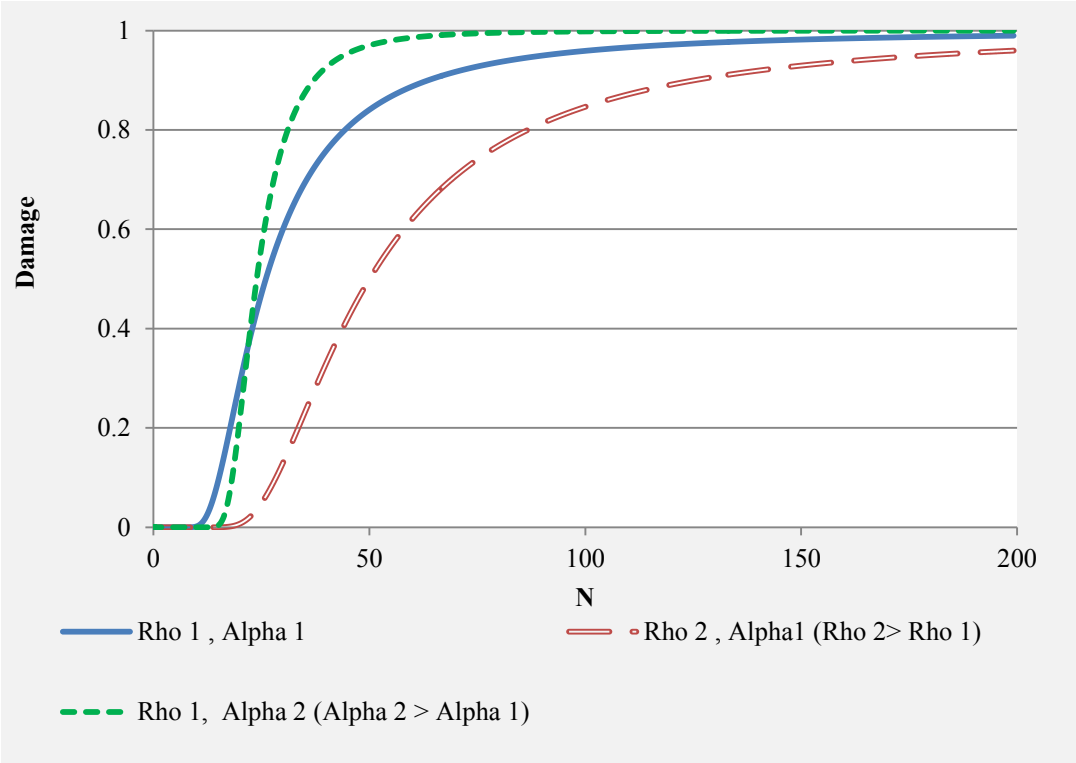

Figure 36 Sample Gumbel S-Shaped Distribution.

These factors are a direct function of erosion resistance (ER) determined for different subgrade categories using extensive lab data on different subgrades and base materials. As previously noted, a useful parameter derived from Hamburg testing device is the erosion resistance (ER) of the material. The pavement designer can use this factor to differentiate one material from another with respect to its erodibility. The factor applies to either the subgrade or the subbase. As was previously mentioned erodibility, traffic loading and existence of water underneath the slab are three main factors affecting the

potential for erosion. Two of these factors are taken in to consideration during the calculation of damage. Damage, D_i, is determined with respect to an equivalent traffic level (i.e. an erosion-based ESAL previously elaborated) and the allowable loads to failure N_f (i.e. $D_i = N_i/N_f$).

5.3.2 Calculations for Equivalent Traffic Level

In order to convert the daily traffic to an erosion-based equivalency, a traffic model was incorporated into this analysis process. The equivalency determination, expressed in terms of an equivalent single axle load (ESAL) in this section is based on an erosive mode of failure using the deformation energy (DE) concept assuming the slab corner to be the critical location. The model, given in equation 5-3 incorporates several parameters such as lane distribution factor (LDF), equivalent load factor (ELF), an equivalent axle factor (EAF), and an equivalent wander factor (EWF). LDF estimates the number of trucks in the design lane; *ELF* converts the different load group to the design single axle load; *EAF* adjusts tandem or tridem axle configurations to a single axle configuration. The equivalent ESAL can be obtained by equation 5-4 using the equivalent wander factor, *EWF* which accounts for the traffic distributed laterally in the lane.

$$\boldsymbol{ESAL_i = \frac{ADT}{2} * GF * LDF * \sum_{j=1}^{3} \left[\left(\%\, \mathbf{a_{i+1,j}} - \%\, \mathbf{a_{i,j}}\right)\mathbf{A_j} * \mathbf{ELF_j}\right] * EAF_i} \qquad (5\text{-}3)$$

$$\boldsymbol{ESAL_d = EWF * \sum ESAL_i} \qquad (5\text{-}4)$$

Where

$ESAL_i$ = ESAL converted from all load groups and axle types (daily)

$ESAL_d$ = Equivalent ESAL as a result of traffic wandering consideration

$\%a_{kj}$ =Percent of loaded radius within a load group

ADT = Average daily traffic

GF = Growth Factor

LDF = Lane distribution factor

i = Per load group

j = Per axle configuration (axle type)

A_j = Load group, (%)

ELF_j = Equivalent load factor

EAF_i = Equivalent axle factor

EWF = Equivalent wander factor

5.3.3 Calculations for Effective ESALs, N_i

The design ESAL is adjusted for the expected pavement drainage conditions. This is accomplished through consideration of the joint sealant condition, drainage characteristics and the potential of rainfall [61]:

$$\boldsymbol{N_i = ESALi * P}\ (\%) \tag{5-5}$$

Where

P = Percent of wet days, [$P = p_1 * p_2 * (1 + p_3)$]

p_1 = Probability of the rain,

p_2 = Probability of infiltration in to the joint

p_3 = Probability of wet subbase

As noted above, the design traffic is moderated by the value of three different factors. The use of these factors basically delineates the portion of traffic distribution to that which is applied to the pavement only when moisture exists underneath the pavement. Probability of rain, P_1, is simply a climatic factor defined as the number of days with rainfall greater than 0.1 inch [41].

One important aspect in this model is the consideration of sealant quality, P_2. The sealant quality affects the infiltration of moisture into the slab/subbase interface. Sealants installed correctly are assumed to have the capability of keeping water from penetrating the joint. Sealants potentially should decrease the number of wet days in order to be effective component of the pavement. P_3 shows the effect of subbase drainage capacity.

This factor considers the effectiveness of drainage system in terms of conducting the moisture out of pavement with respect to subbase permeability. The P values were discussed thoroughly in section four.

5.3.4 Ultimate Load and Shear Strength, Nf

As it mentioned, damage is the ratio between the adjusted traffic load (effective ESALs) and ultimate loads to failure ($D_i = N_i/N_f$). Ultimate load to failure is a function of shear strength of the pavement structure.

$$N_f = \mathbf{10}^{k_1 + k_2 r_i} \quad (5\text{-}6)$$

$$r_i = \frac{\tau_i}{f_\tau} \quad (5\text{-}7)$$

Where:

N_f = Ultimate loads to failure

k_i = Erosion damage coefficients (determined from calibration)

τ_i = Interfacial Shear Stress (FL^{-2})

$f\tau$ = Shear Strength (FL^{-2})

The resistance of the slab/subbase interface can perhaps be broken down into two segments one relating to interfacial adhesive bond (as may be represented by the cohesive strength of the subbase material) and the other related to interfacial sliding resistance. In this regard, two basic premises are stated:

1. The adhesive bond strength across the slab/subbase interface can be defined by the cohesive shear strength of the subbase layer (fc) which is determinable from laboratory tri-axial testing (Figure 37).
2. The coefficient of sliding friction (fF) can be defined by the tangent of the φ angle as again would be determined from tri-axial laboratory testing data (Figure 37).

Characterization of the interfacial adhesive bond between the slab and the subbase layer in this manner is considered to be a manifestation of the shear capacity of the subbase layer. Under field conditions, once the adhesive shear strength of the interface has been

exceeded, the sliding frictional resistance is in force and represented by the angle of friction (tan φ).

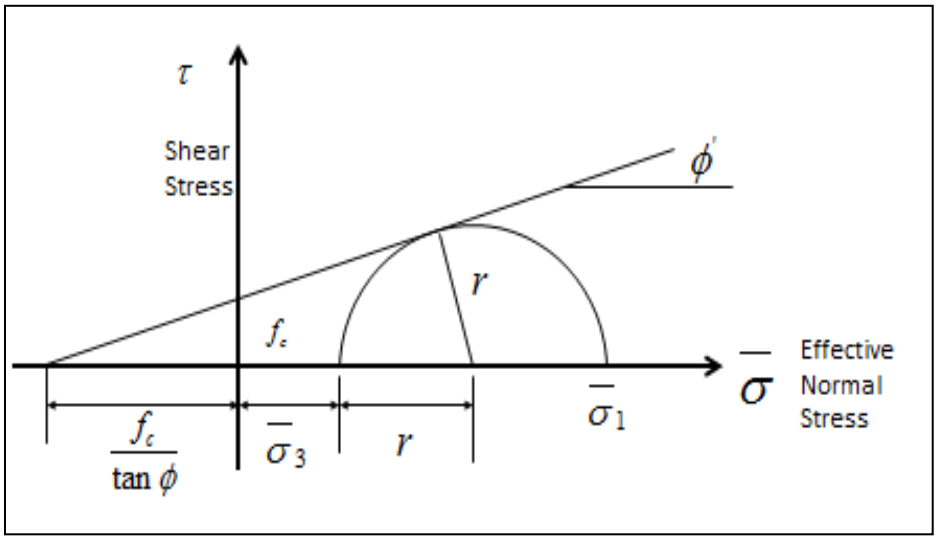

Figure 37 Shear Strength and Angle of Friction Determinations.

k_1 and k_2 are erosion damage coefficients that are determined using the calibration on field data. Interfacial shear stress can be determined as follows:

$$\boldsymbol{\tau_i = (1 - x_b)\ \frac{\partial \delta_{L_i}}{\partial X}\ \frac{E_{sb}}{2(1+\nu)}} \qquad (5\text{-}8)$$

Where

x_b = Degree of bond between slab and subbase

$\boldsymbol{\delta}L_i$ = Deflection from the load (Function of design load, modulus of subgrade reaction (k) and radius of relative stiffness (*l*)

X = Distance from the point of loading along the diagonal from the corner or from the edge of the slab

E_{sb} = Subbase modulus

$\boldsymbol{\nu}$ = Subbase Poisson's ratio

The equation clearly shows that the interfacial shear stress is a function of load level P, subgrade k-value, slab thickness (as affected by load transfer efficiency). Load transfer efficiency (LTE) is a factor included in the model through its effect on deflection and in the calculation of the shear stress which ultimately affects the amount of accumulated damage. It's well known that aggregate interlock and the use of dowels can significantly affect the capability of concrete slabs to resist erosion damage under load. Field observations have shown that slabs with dowels develop less faulting than those without dowels[41, 52]. Data from more than 100 LTPP jointed concrete pavement sections indicated that dowel bar usage significantly reduced joint faulting for all pavement age categories [51].

5.4 Computerization of the Model

The erosion model was automated in a computer code to facilitate analysis of a concrete pavement system with respect to the prediction of erosion and faulting related performance. The program considers key distress types that occur in concrete pavement systems and it can be used for both design purposes and in pavement management systems. Sensitivity analysis and field verification of the erosion model is subsequently discussed. One of the main advantages of this program is that it can be calibrated with

the local data if it is available. Figure 38 shows the main menu of the computer program. The program works in three steps; first the input data, secondly the calibration and thirdly the analysis. The output includes the faulting prediction during the design life; also the changes of load transfer efficiency and interfacial shear stress as well as a graph that shows how much fatigue cracking would develop in the concrete pavement.

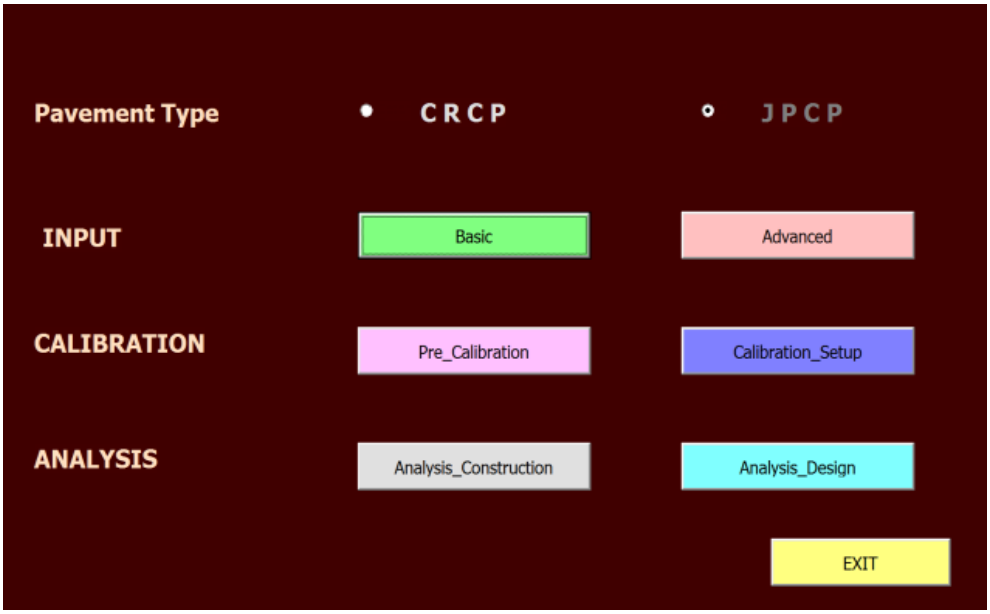

Figure 38 The Design Program Main Page.

5.5 Sensitivity Analysis

Sensitivity analysis has been performed on the model to evaluate the sensitivity of the outputs and demonstrate the utility of the analysis the program offers. The base pavement structure for this analysis is an eight inch concrete slab without a base layer jointed at 15 ft intervals with a 12 ft lane width. The subgrade layer has a k-value of 150

psi/in. The average annual daily truck traffic, ADTT, was set equal to 1200 with annual growth rate of 3% and number of wet days to 180 days in a year. The erosion model was calibrated based on pavement sections located in Texas. Table 11 shows the main input parameters for the base analysis.

Five cases were analyzed and compared to the base analysis. In each of these five cases only one variable is changed with the rest of input values held constant. Table 12 shows how variables for sensitivity study were defined. Figure 39 shows the effect of increasing the traffic level or adding the dowel bars on performance.

Table 11. Input Parameters for the Base Analysis.

Pavement Type	JPCP
Analysis Period	15 Years
Slab Thickness	8"
AADT	1200
Base Layer	No
Joint Spacing	15'
Lane Width	12'
Shoulder	No
Dowel Bar	No
Subgrade K value	150 pci
Wet Days	180
Coarse Aggregate	Limestone
Calibration Data	Texas

Table 12. Changed Parameter for Each of the Five Case Studies.

Case Number	Studied Input Parameter	Changed Value
Case 1	Slab Thickness	6.5" Concrete Slab
Case 2	Traffic (AADT)	1550
Case 3	Dowel Bars	20" Length,1.2" Diameter
Case 4	Base Layer	2" Asphalt Layer
Case 5	Wet Days	270 Days a year

Figure 39 shows that in the second case where the traffic level is raised from 1200 to 1550 amount of faulting increases. Figure 39 also illustrate the effect of adding dowels on the joints. Existence of dowels dramatically lowers the shear stress and faulting drops by 20%.

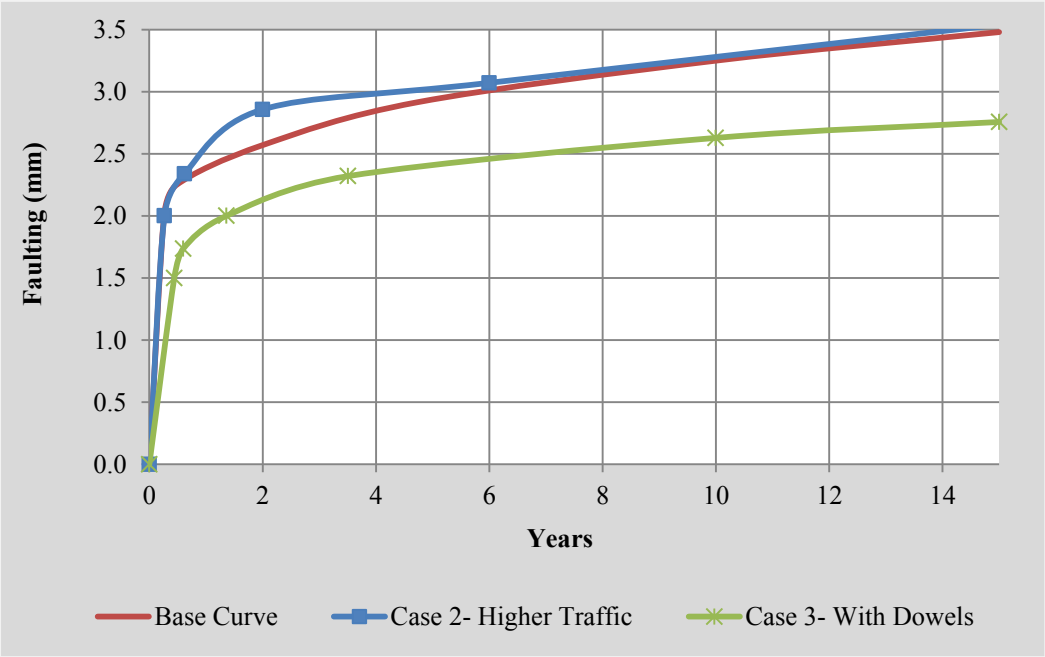

Figure 39 Sensitivity Analysis on Base Curve.

Figure 40 shows the changes of load transfer efficiency for cases with and without dowels. The load transfer efficiency after 15 years of service is still twice comparing to the case without dowels. The load transfer in base curve comes only from aggregate interlock. When load transfer is only a function of aggregate interlock it is susceptible to the width of the joint opening. Table 13 summarizes the results of the sensitivity analysis.

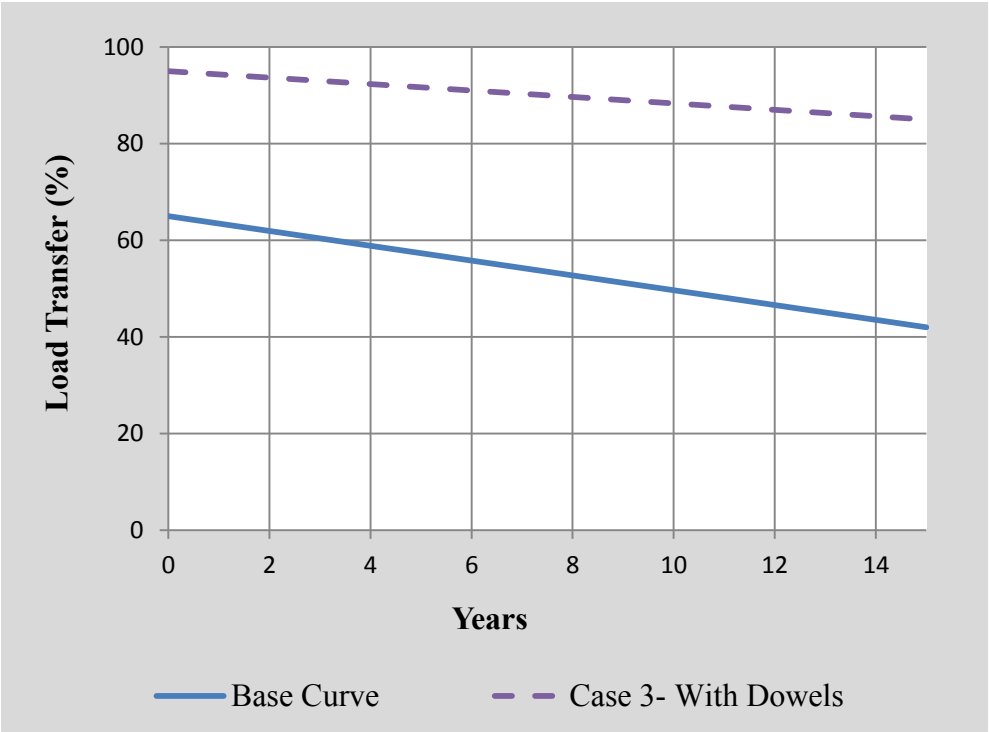

Figure 40 Changes of Load Transfer Efficiency With and Without Dowel Bars.

Table 13. Sensitivity Analysis Results.

Case Number	Faulting in 6 Yrs (mm)	% Change in 6 Yrs	Faulting in 10 Yrs (mm)	% Change in 10 Yrs
Base Curve	3	0.0%	3.27	0.0%
Case 1	3.4	13.3%	3.75	14.7%
Case 2	3.15	5.0%	3.38	3.4%
Case 3	2.4	-20.0%	2.64	-19.3%
Case 4	0.5	-83.3%	3.7	13.1%
Case 5	3.2	6.7%	3.3	0.9%

In first case the slab thickness has been lowered by 20%. As a result faulting was increased by approximately 15% and the average shear stress at the interface increased by 20%. A greater PCC slab thickness provides greater structural stiffness and lower shear stress which results in a lower deflection and less faulting. In case number 4, two inches of asphalt base layer was added that significantly lowers faulting. Last case shows how the moisture contributes to erosion. In a moist climate the probability of water on the slab/subbase interface is greater causing the erosion to increase and the amount of faulting.

5.6 Field Data

Data from the Long-Term Pavement Performance database (LTPP) were used to validate the model's results [62]. Table 14 shows construction and traffic information of the selected LTPP pavement sections included in this analysis. All sections are located in Texas. The subbase layers are all treated except for the one denoted by "G" that indicates granular base or subbase.

Section 48-4143 was used to calibrate the program. Figure 41 shows the fit to calibrate the model using LTPP section 48-4143. As a result of this calibration is to get k_1 and k_2 in order to define ultimate load to failure. k_1 and k_2 are damage coefficients that are determined using the calibration on field data.

Table 14. Construction Information on LTPP Sections.

SHRP ID	Slab Thickness (in)	Base Thickness (in)	Subbase Thickness (in)	AADT Truck
4143	10.4	4.5	5.5	279
3003	9.3	3.5	7	915
3699	10.2	6.2	6.1	1895
4152	11.4	6.4	6.6	312
B420	10	4.3	5.5	347
D410	11.4	6.4	6.6	341
E420	9.6	7.6	4	450

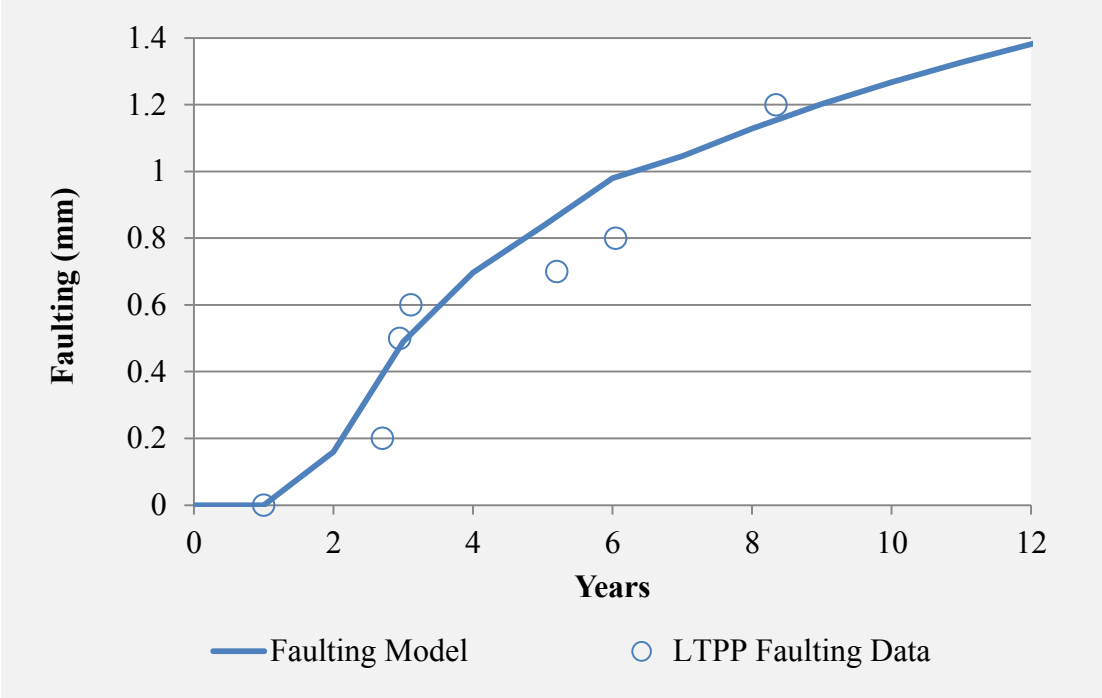

Figure 41 Calibration of the Model Using the Field Data.

The program was used accordingly to analyze pavement sections with the same specifications and to compare the results to real observed data in the field (All the sections were calibrated prior to analysis). The correlation between observed and model-fitted faulting is presented in Figure 42 (The section 4143 that was used for calibration is excluded). The R square value is 84%, which represents a very good fit to the data. It should be noticed that each section provides several data point that were collected during the service time. Table 15 shows the T-Test results for the data analysis. The null hypothesis of zero mean difference is accepted at a 95% confidence level as the P Value is much larger than 0.05.

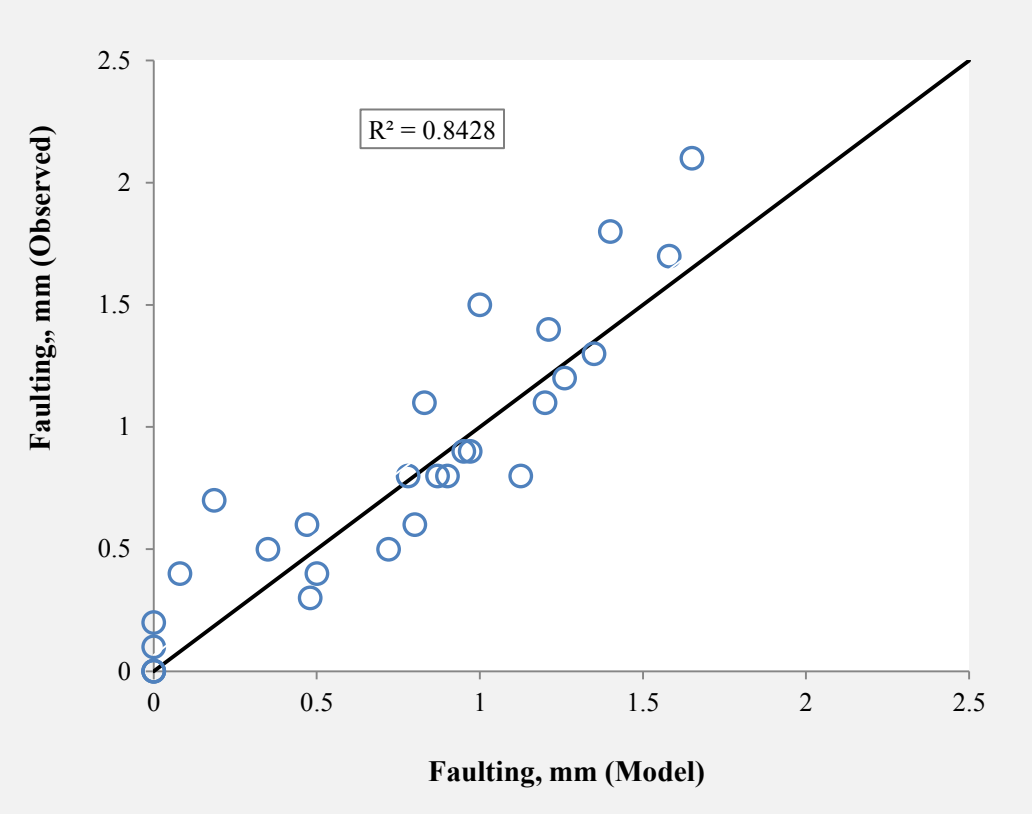

Figure 42 Modeled versus Measured Faulting of LTPP Data.

Table 15. Statistical Analysis for Sampled LTPP Faulting Data.

Statistical Quantity	Observed	Model
Mean	0.804	0.738
Variance	0.317	0.268
Observations	28	28
P Value	0.651	

5.7 Conclusions and Discussion

Faulting directly affects the serviceability of the pavement. It indirectly contributes to other major distress types that affect the performance of jointed concrete pavement. The mechanistic empirical model presented in this section can effectively analyze the faulting and erosion in JPCP's. The erosion resistance of materials were precisely defined and considered in this model. The mode is capable to be calibrated for local conditions as a distinct advantage over other faulting models. The model was successfully implemented and calibrated into a computerized format. Comparison of the model analysis versus the field data shows a great fit.

6. SUBBASE EROSION CHARACTERISTICS

One of the most important elements of concrete pavement construction has been the type and nature of the materials used in sublayers below concrete slabs. Subbase layers should provide a stable construction platform, uniformly increased slab support, erosion resistance, and a gradual vertical transition in layer stiffness. The features of an ideal subbase layer under a concrete slab might include sufficient strength with a moderate level of friction and sufficient erosion resistance but a conforming uniform support. A subbase layer should be adequately flexible to minimize curling and warping related stresses as well as potential for reflection cracking in the overlying concrete slab.

Many distresses in jointed concrete pavements occur when the sublayer loses its capability to provide enough support underneath the slab. According to field observations and lab tests, when this occurs, faulting is typically the major performance issue for jointed concrete pavements [51], however other distress may occur due to a lack of subbase supports as well such as cracking, corner breaking and ultimately slab failure.

Despite the importance of erosion in jointed concrete pavements, little development has taken place to measure material properties that pertain to erosive strength or the resistance of slab-subbase interface. In many cases, the question is if the subgrade material is of sufficient shear strength to be used underneath a concrete slab. If so, this may lead to more efficient design and save cost in raw materials, transferring, mixing and placing another sublayer since there is no benefit adding a layer of aggregate

base, or stabilizing the subgrade under the slab. Particularly in low volume roadways or parking lots, engineers need to appropriately design the underlying support layer in order to avoid extra expenses for construction of the pavement. Often local materials are available for construction; however engineers need a method to evaluate their future performance. For highly trafficked highways, aggregate bases and stabilized bases are commonly used to provide the needed performance, however for light duty pavements these materials may not be necessary. This research was conducted in order to develop a design process to assist the designer in making this determination specific to soil type, local climate, and specific traffic loading.

6.1 Material Selection

This study focused on the assessment of key erosion parameters related to the use of subgrade materials underneath the slab. Accordingly, eight different soil samples were collected from project sites across the United States. These samples cover all different soil types from high plasticity clay to non-plastic beach sand. Figure 43 shows the U.S. soil texture classification map [63] in which colors represent different soil types according to USDA soil triangle shown next to the map. As can be seen a lot of areas are covered with sand (non-cohesive soil), clay (cohesive soil) or combination of the two. Coastal areas, such as Florida, are an example of states with sandy soils and concentration of plastic clays can be seen in Texas, South Dakota or parts of California and Mississippi. Field samples collected in this study cover almost all the common soil types across the country.

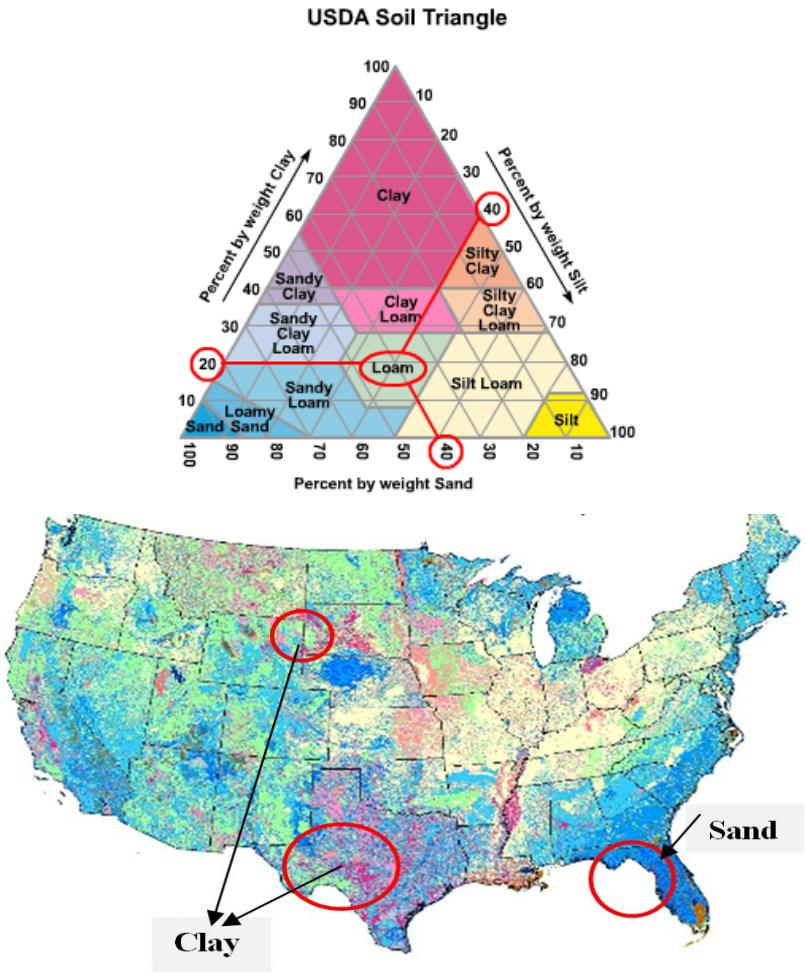

Figure 43 The Soil Classification Triangle and U.S. Soil Classification Map [63].

The Hamburg Wheel-Tracking Device (HWTD) was used in order to test the subgrade samples. The following sections detail the material properties, HWTD and testing plan. Finally the test results are presented in a database type form.

6.1.1 Gradation and Classifications

Dry and wet sieve analyses were performed on field soil samples to provide grading curves (ASTM D6913). Atterberg limits (liquid limit, plastic limit, and the

plasticity index) on the fine portion of soils were determined (ASTM D4318). Soils were then classified according to unified soil classification system (ASTM D2487) [64] [65] [66]. Results for the sieve analyses, grading curve and Atterberg limits for each sample are shown in Appendix A and Appendix B. Table 16 summarizes the eight sample gradations and classifications. Sand is defined as particles of soil that pass a No. 4 (4.75 mm) sieve and be retained on a No. 200 (75 μm) sieve. Particles retrained on No. 4 sieve (greater than 4.75 mm) are defined as gravel. Silt and clay are defined as particles that are smaller than 75 μm.[66]. Table 16 lists the samples in the order of increasing clay content and plasticity index.

Samples were divided in to four subcategories. The first two samples are considered pure sands with more than 90% of sand and they are both non-cohesive. The sand from Florida (Sample number two) is finer compared to the sand from North Carolina (sample number one). The second set is sandy soils containing silt. While the two samples in this set have similar grading, the plasticity index is significantly different between the two, with the sandy silt from South Carolina having a higher plasticity index than the silty sand from Texas. The third set is a combination of clay and sandy soils. The one from Houston (sample number six) has higher plasticity index compare to the one from San Angelo (sample number five). And finally the last two samples are clays with plasticity indexes of 20% and 40%, while containing almost 80% or more of minus 200 sieve particles.

Figure 44 shows a comparison between the poorly graded sand and fat clay regarding the significant differences in particle size. Figure 46 shows grading curves for

collected samples. Vertical dotted lines show the border between gravel-sand and sand-fine particles.

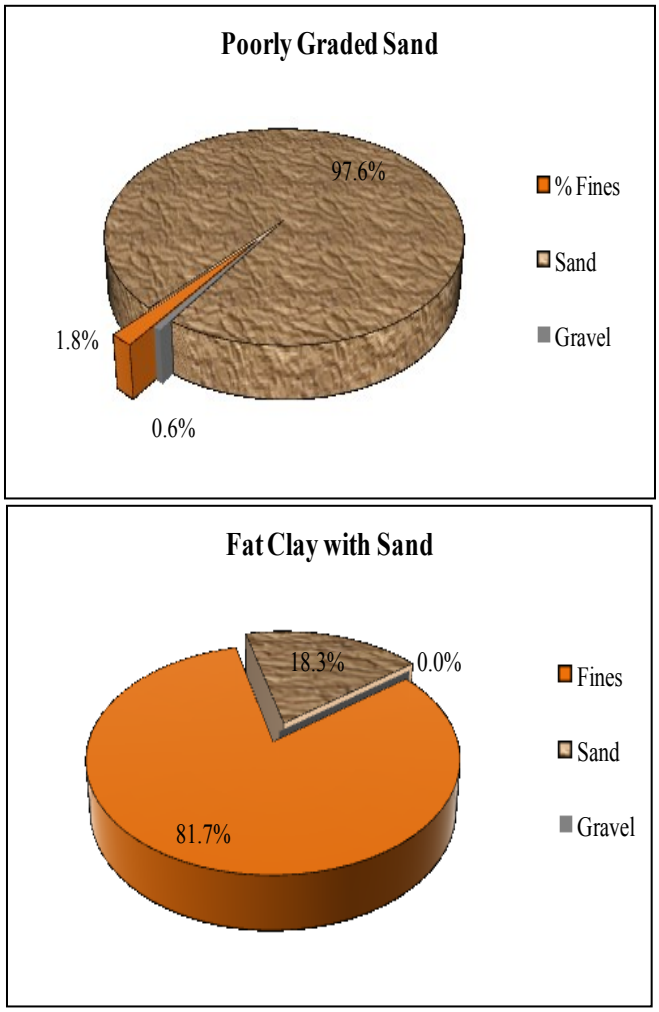

Figure 44 Comparison between Two of the Sample's Gradation.

Figure 45 shows the plasticity indexes, PI, and cohesiveness of the collected samples. As mentioned before, samples are listed in the order of increasing clay content, as well as the plasticity index. All these figures are used to demonstrate that these samples

represent most common soil types found in the United States and used for construction of pavements.

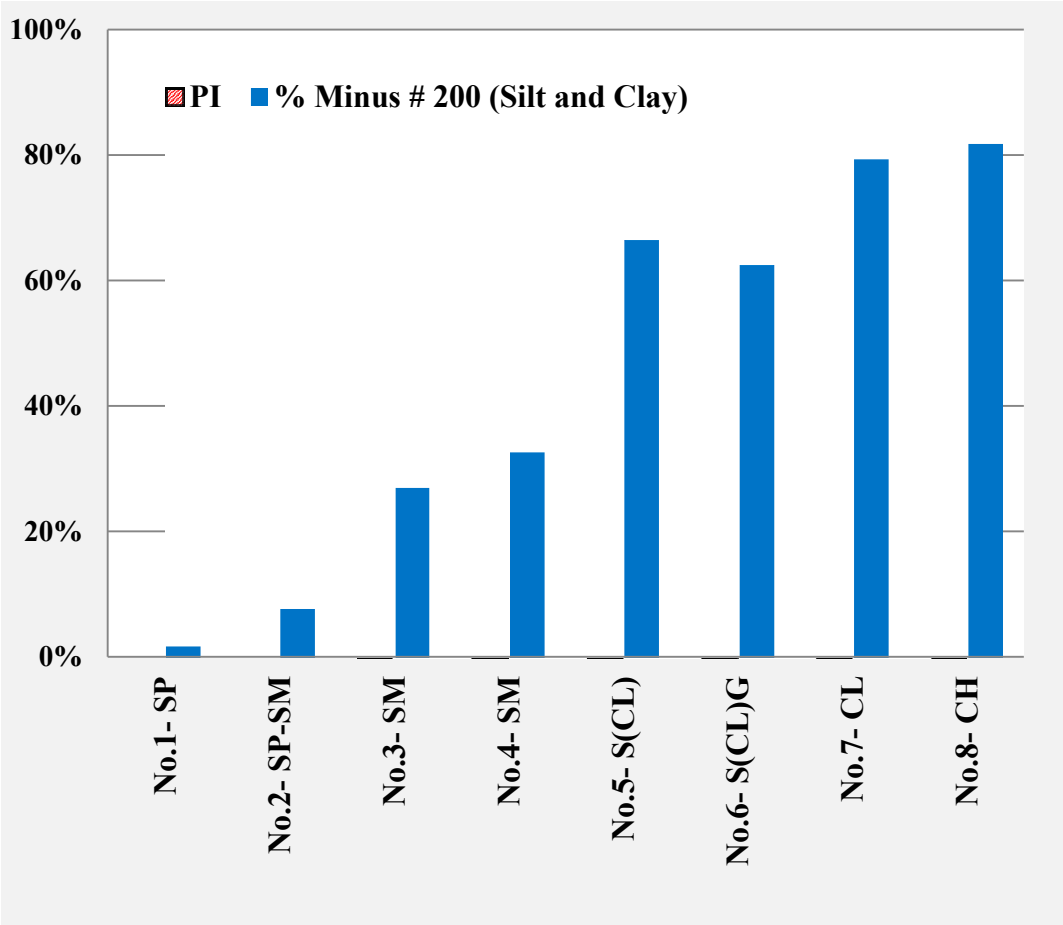

Figure 45 PI for Each Sample along with the Percent of Minus 200 (Silt and Clay).

Table 16 Soil Samples Location and Classification (NP for Non-Plastic).

No	Location	State	Group Symbol	Soil Category	Clay and Silt	Sand	Gravel	PI	Category for Fines
1	Greenville	NC	SP	Poorly Graded Sand	1.80%	97.60%	0.60%	NP	NP
2	Delray Beach	FL	SP-SM	Poorly Graded Sand with Silt	7.70%	91.80%	0.50%	NP	NP
3	College Station	TX	SM	Silty Sand	26.90%	69.30%	3.80%	2.09%	ML
4	Anderson	SC	SM	Sandy Silt	32.70%	63.70%	3.60%	9.91%	ML
5	San Angelo	TX	s(CL)	Sandy Lean Clay	66.30%	30.70%	3.00%	13.36%	CL
6	Houston	TX	s(CL)g	Sandy Lean Clay with Gravel	62.30%	22.60%	15.10%	17.34%	CL
7	Garland	TX	CL	Lean Clay with Sand	79.30%	20.70%	0.00%	19.17%	CL
8	Houston	TX	CH	Fat Clay with Sand	81.71%	18.29%	0.00%	39.96%	CH

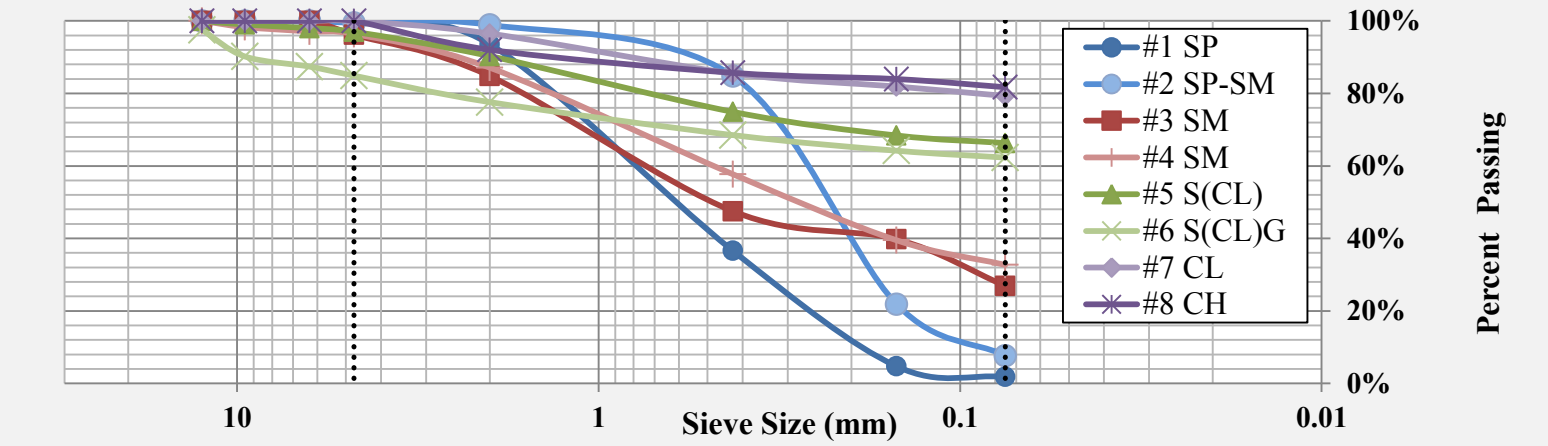

Figure 46 Grading Curves for Collected Samples.

6.1.2 Maximum Density and Optimum Moisture

Compaction tests have been performed for all three samples in order to determine optimum water content and maximum dry density using ASTM D1557 and ASTM D698 [67] [68] [69]. Table 17 shows the compaction test results, optimum moisture and maximum dry density for samples.

Table 17 Compaction Test Results for Samples.

No	Location	State	Group Symbol	Optimum Moisture	Max Dry Density (pcf)	Max Dry Density (Kg/m3)
1	Greenville	NC	SP	9.41%	114.3	1830.4
2	Delray Beach	FL	SP-SM	9.60%	109.9	1761.1
3	College Station	TX	SM	8.68%	127.6	2044.4
4	Anderson	SC	SM	21.62%	102.7	1644.9
5	San Angelo	TX	s(CL)	13.93%	110.5	1770.0
6	Houston	TX	s(CL)g	14.36%	117.9	1889.2
7	Garland	TX	CL	21.14%	101.4	1623.6
8	Houston	TX	CH	20.23%	111.2	1781.3

6.2 Method of Testing Erosion

6.2.1 Hamburg Wheel-Tracking Device

The Hamburg Wheel-Tracking Device (HWTD) was used in order to test the subgrade samples. The test consists of two component layers, the top is a concrete cap

and the other is the material of interest which is placed immediately under the concrete cap. Test devices and procedures are further summarized below.

HWTD testing is mainly conducted under a wet condition (sample is under water during testing) in which erosion occurs due to mechanical and hydraulic shearing on the underlying layer generated by slab movement under an applied load. The configuration of the test device is shown in Figure 47. The test configuration consists of a subgrade or base material 25.4 mm (1 in.) thick placed on a neoprene material below a jointed concrete block 25.4 mm (1 in.) thick. The device allows for testing a laboratory-compacted specimen or a core obtained from the field. A wheel load of 71.6 kg (158 lb) is applied at a 60-rpm load frequency. Measurements consist of the depth of erosion at 11 locations versus the number of wheel load passes [59] [60].

Samples are 6-inches in diameter and 1-inch thick. On top of the sample there is a concrete cap, the same size that has been split and sealed to simulate the joint. A wheel passes on the concrete cap causing deflection and erosion on the sample until the material fails.

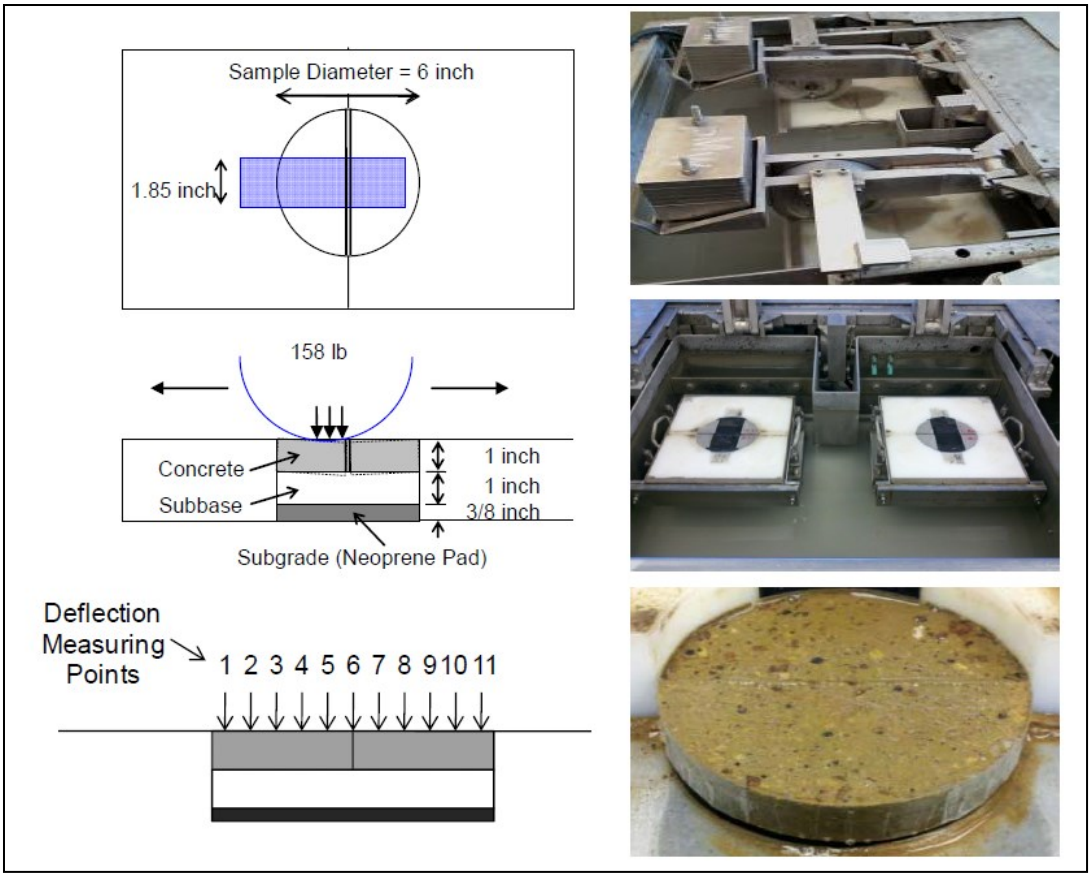

Figure 47 Hamburg Wheel-Tracking Device (HWTD) [59].

6.2.2 Test Program

Soil properties may change significantly when changing moisture contents. These changes also affect soil resistance against erosion. Water has significant role in erosion process. Saturated subgrade or base materials may not perform properly as a support underneath the slab. Cohesive soils such as clayey soils are more sensitive to moisture content but since they contain higher portion of fine particles, it take longer water inundation to make them saturated. The erosion testing was conducted in a way

to address the range of moisture contents experienced by subgrade materials and to simulate boundary conditions anywhere from completely dry to saturated condition.

Two types of erosion testing were performed using Hamburg Wheel-Tracking Device (HWTD): wet and dry conditions. As previously explained, the HWTD contains a tank where the sample is placed inside, and the wheels pass on top of that. Under the wet condition, the device tank is filled with water just before starting the test, so when the load is passing over, it can propel the water on top of the sample. The water level is at the concrete cap and soil interface. The wet condition represents periods of time when the joint is holding water under traffic loading while dry condition represents when the joint is not holding water.

Erosion testing was done according to the chart shown in Table 18. The test conditions represent different moisture conditions within the joint as well as the layer below. These conditions in the field are a function of the joint sealant effectiveness, prevailing weather conditions, as well as other factors such as drainage. The first test is the extreme case of heavy storm in which the subgrade can become over saturated. In the lab the wet HWTD was performed using saturated sample from moisture room. The second test simulates pavement condition just after the rain and the third test pertains to the drying period. The fourth test considers the totally dry condition for the subgrade.

Sandy soils have lower quantity of fine particles compared to cohesive soils such as clays which typically allows them to drain water much faster. Figure 48 schematically details the behavior of sand material versus clay when they are exposed to the same level of moisture. Since sands have larger pores the water can directly pass

through the soil. In clays, the pores are much smaller so the permeability is reduced which then does not allow the water to pass through the clay easily. Clays tend to absorb water and permeation happens very slowly. Due to the slower moisture transport in clay materials, clays were tested in wider range of moisture contents to simulate potential field conditions. Therefore, a range of four moisture content levels were performed on the two clayey samples (Samples number 7 and 8). For the rest of the materials, one wet and one dry test was carried out at optimum moisture conditions (Table 18).

Table 18 Erosion Tests Using Hamburg Wheel-Tracking Device (HWTD).

No	Test Type	Sample's Moisture Content	Material for the Test
1	Wet	Saturated	Clay Only
2	Wet	Optimal Moisture	All Soils
3	Dry	Optimal Moisture	All Soils
4	Dry	Dry	Clay Only

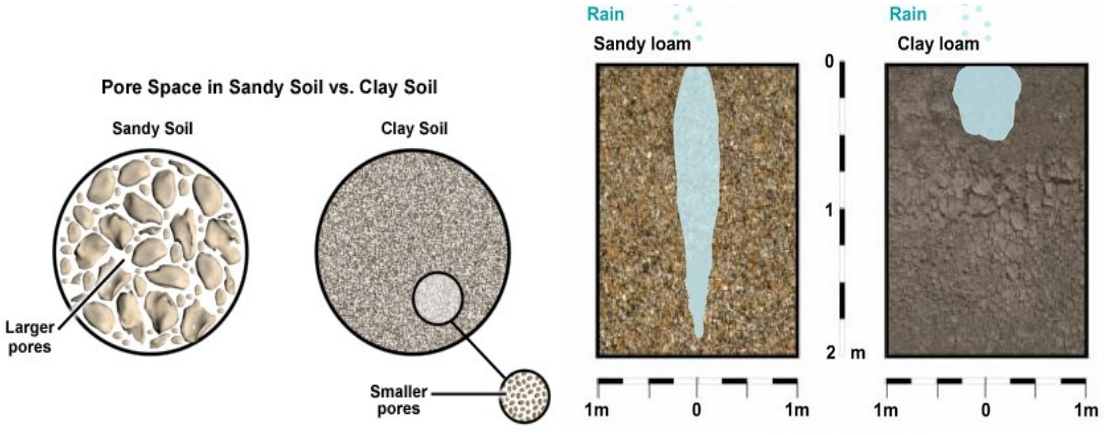

Figure 48 Schematic View to Compare the Permeability of Sand versus Clay.

6.2.3 Stabilized Samples

Clay has been used for many years in low volume roadway applications. However, water can dramatically change clay's performance behavior and strength. Most importantly, since clay can absorb a great amount of water it may swell and damage the pavement structure.

Stabilization of clay has been practiced as a method to improve clay performance as subbase layer. Soils can be stabilized when lime, cement, or other products are added to the soil which generates long-term strength gain through a pozzolanic reaction. Cement and lime have consistently been found to be among the most effective stabilizers for road and airfield applications [70].

In order to evaluate the effectiveness of such treatments against the erosion under concrete pavements, the two clay samples (lean clay and fat clay) were stabilized and tested using Hamburg Wheel-Tracking Device (HWTD). Four stabilized tests were performed for each of the two clay samples; three cement stabilized (3%, 5% and 7% cement) and one lime stabilized sample. Effective percent of lime was measured based on pH measurements (TXDOT-121E) and used to make lime treated samples [71]. The pH test determines the minimum percent lime needed for a soil-lime mixture to attain a pH of 12.4. Cation exchange occurs at this pH, resulting in modification of the soil particle structure to achieve improved workability and decrease swell and plasticity. Appendix C shows the pH test results for clays. The effective percent of lime was found to be 2% for the lean clay (based on field observations, this sample may have been treated with lime in the field prior to sampling) and 4% for the fat clay. Also, in order to

test how sand's behavior changes after stabilization, one of the sand samples was stabilized and tested under wet condition using HWTD.

6.3 Test Results

6.3.1 Dry and Wet Erosion Tests (At Optimum Moisture)

For each of the samples, a dry test and wet test (tank dry or full) was performed while the sample was initially compacted at optimum moisture condition (Table 18, Test numbers 2 and 3). Results were then plotted as number of passes versus measured deflection in millimeters. Erodibility of the sample is defined as slope of load repetition versus deflection and is defined with the unit of mm/1million repetition. The greater erodibility value is a result of a higher slope which means the material has less resistance against erosion.

For dry conditions, the moisture inside the sample remains constant during the test (sample at optimum moisture content), since the water tank of HWTD was totally dry. Under wet conditions, testing was conducted with the moisture level in the sample near optimum; and the water tank was full (water level at slab-subbase interface). Table 19 and Figure 49 show results of erosion tests for both dry and wet tests. The wet erosion rate was found to be on the average 20 times greater than the dry erosion rate for unstabilized subgrade samples. Figure 50 shows only the dry erosion test results and Figure 51 shows only the wet erosion test results.

Table 19 Results of Dry and Wet Erosion Tests (Optimum Moisture) for all Samples.

Sample	Soil Category	Dry Hamburg on $W_{Optimum}$ (mm/million)	Wet Hamburg on $W_{Optimum}$ (mm/million)
#1_SP	Poorly Graded Sand	90	4500
#2_SP-SM	Poorly Graded Sand with Silt	20	2400
#3_SM	Silty Sand	95	1600
#4_SM	Sandy Silt	130	1600
#5_s(CL)	Sandy Lean Clay	110	3000
#6_s(CL)g	Sandy Lean Clay with Gravel	130	3100
#7_CL	Lean Clay with Sand	60	900
#8_CH	Fat Clay with Sand	60	840

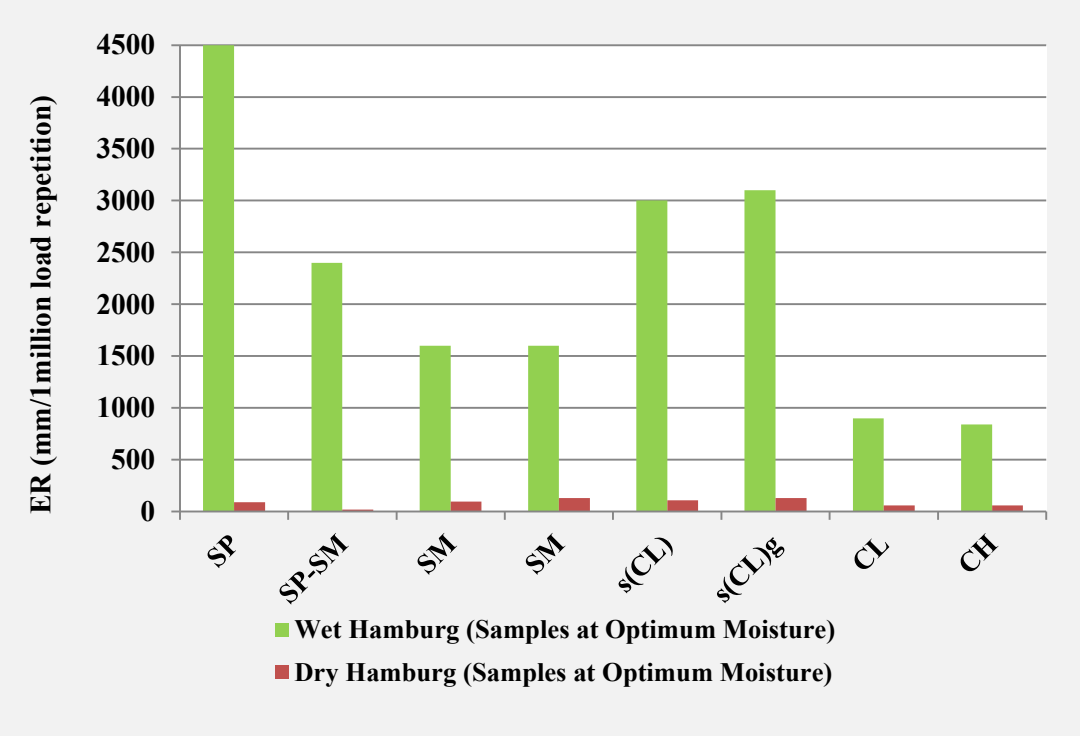

Figure 49 Erosion Tests Results for all Samples (Wet and Dry Tests).

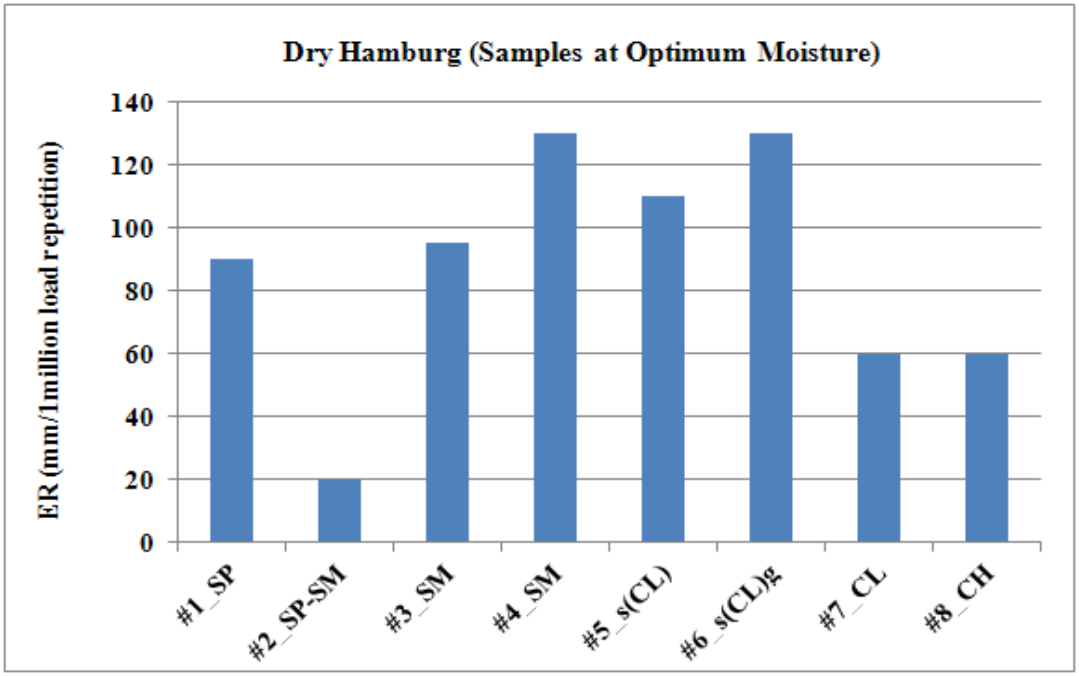

Figure 50 Dry Erosion Tests Results for all Samples.

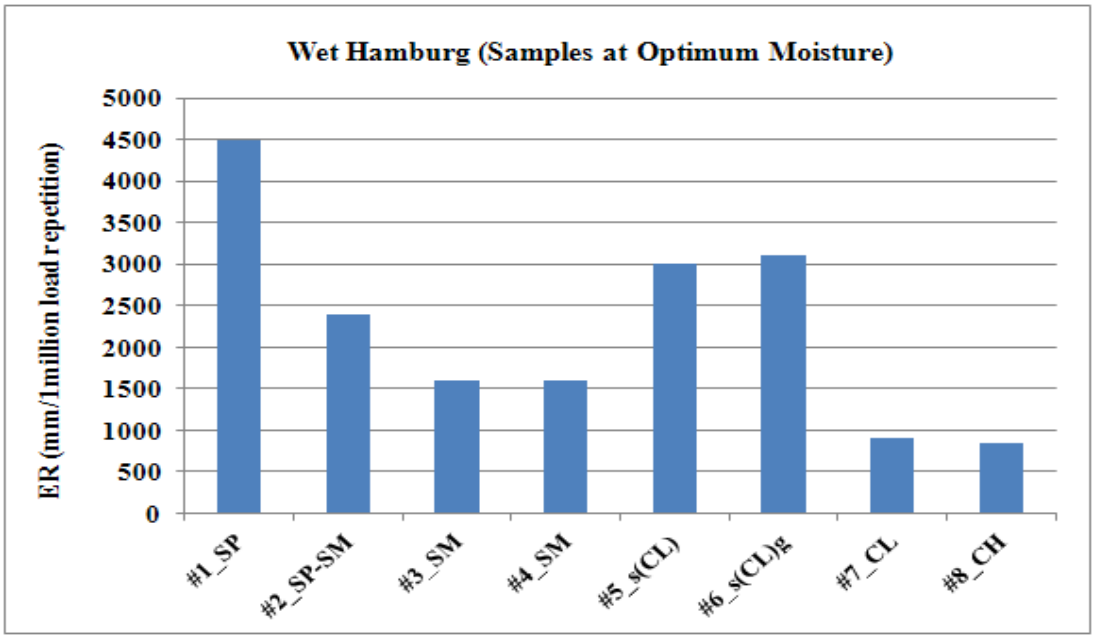

Figure 51 Wet Erosion Tests Results for all Samples.

As it was discussed previously, samples were prepared from four subcategories of soils: sand, combination of silt and sand, combination of sand and clay, and clayey soils. Except for the sand, the two samples of each of the other subcategories behave nearly the same under both wet and dry test conditions. While subgrades show relatively low erodibility in dry conditions, the rate of erosion is much higher in wet conditions. Figure 52 shows the results of HWTD tests for one sample from each subcategory (both dry and wet tests on the same graph). Figure 53 shows dry testing results for one sample from each soil subcategory and Figure 54 shows the results of wet test for one sample from each soil subcategory. Appendix D includes graphs of all erosion test results for collected samples.

The combination of traffic load and water can wash away abraded material below the concrete cap. Clearly, all subbase/subgrade materials are weaker in wet conditions since water significantly decreases the shear strength. Among all samples, clays (samples 7 and 8) are more resistant against erosion both in dry and wet conditions.

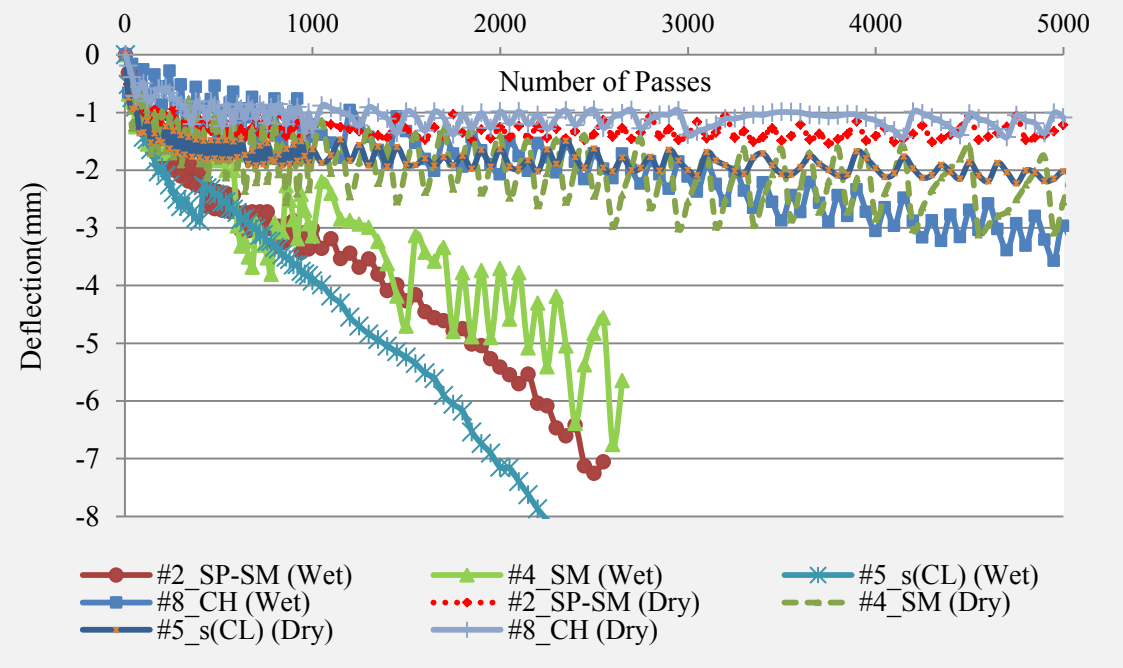

Figure 52 Hamburg Test Results for One Sample of Each Subcategory.

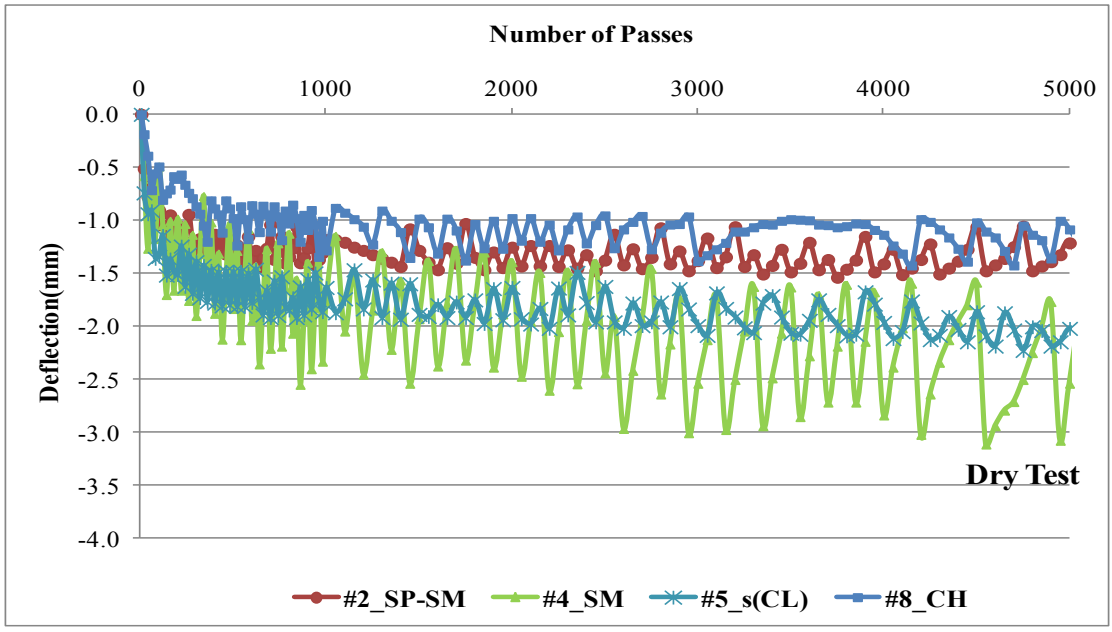

Figure 53 Dry Hamburg Test Results.

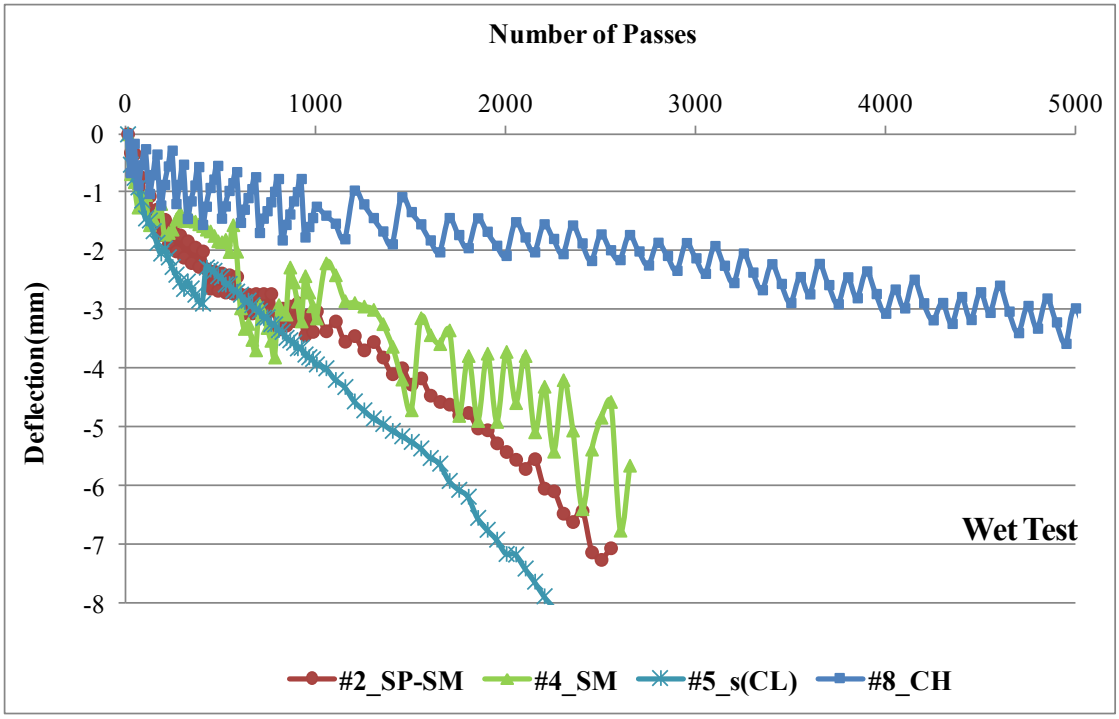

Figure 54 Wet Hamburg Test Results.

6.3.2 Erosion Tests on Clays

Clays generally show very good shear strength when dry but the strength characteristics change as a function of water content. Four moisture conditions were explored on each clay soil (Table 18). Two of them were discussed previously. Two more tests were performed where clay samples were exposed to extreme conditions: The first was created by oven drying the sample and testing under dry condition (tank empty) and another where the sample was completely saturated, and tested under wet condition (tank full).

Hence, clays have been tested under four different moisture conditions that make it possible to evaluate how the moisture content of the sample affects erodibility. Table 20 and Figure 55 show results for Hamburg test on lean and fat clay.

Table 20 Results for Hamburg Test on Lean Clay and Fat Clay.

Test Method	Dry Test	Dry Test	Wet Test	Wet Test
Sample's Moisture Content	Oven Dried	Optimum	Optimum	Saturated
ER for #7_CL (PI~20)	30	60	900	13600
ER for #8_CH (PI~40)	30	60	840	32400

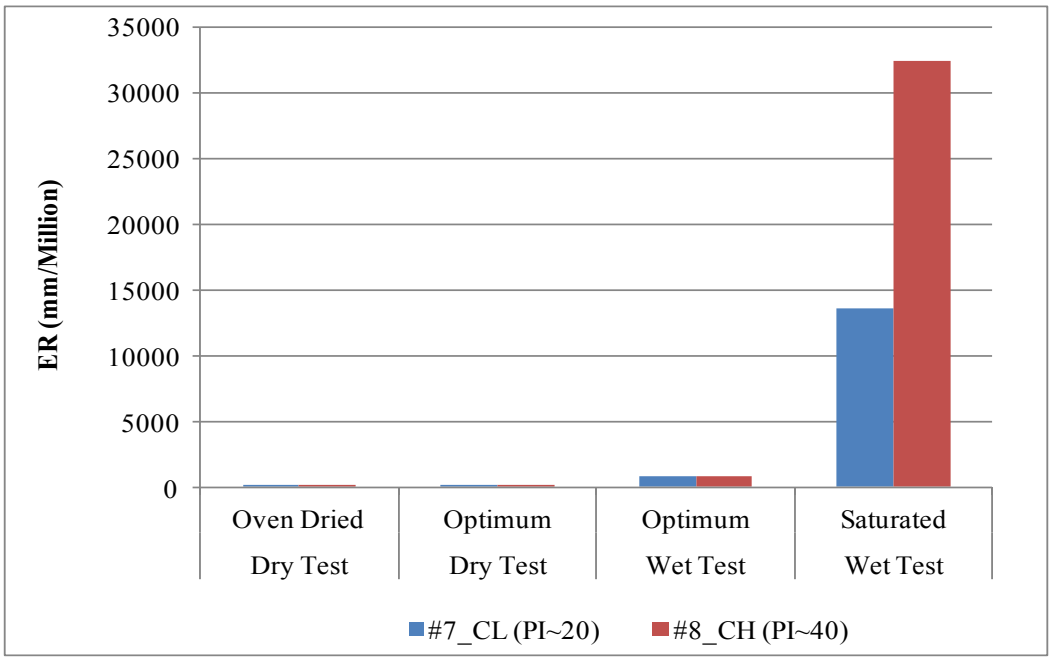

Figure 55 Results for Hamburg Test on Lean Clay and Fat Clay.

Results show that both clays behave similarly if they are not totally saturated. While dried clays are very resistant against erosion, clays are extremely weak against erosion when they become saturated. The sample with higher plasticity is weaker and the erodibility index is greater.

It should be noted that saturation of the whole clay layer rarely occurs unless pavement is in very WET climate with unsealed joints. In order to saturate these one inch thick samples, they were kept in the moisture room for a week prior to the test to achieve saturation. The saturation moisture content for lean clay is 49.20% and for the fat clay is 61.42%. Figure 56 and Figure 57 show the plot of Hamburg tests for lean and fat clay.

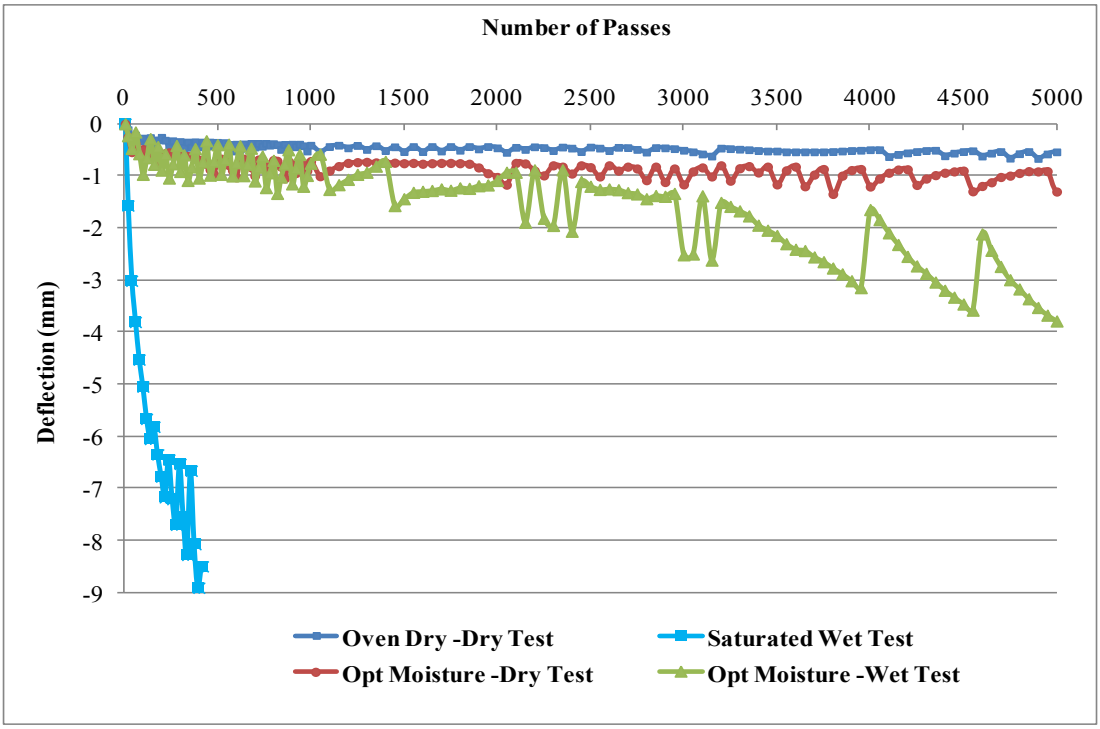

Figure 56 Hamburg Tests for Lean Clay, Sample Number 7.

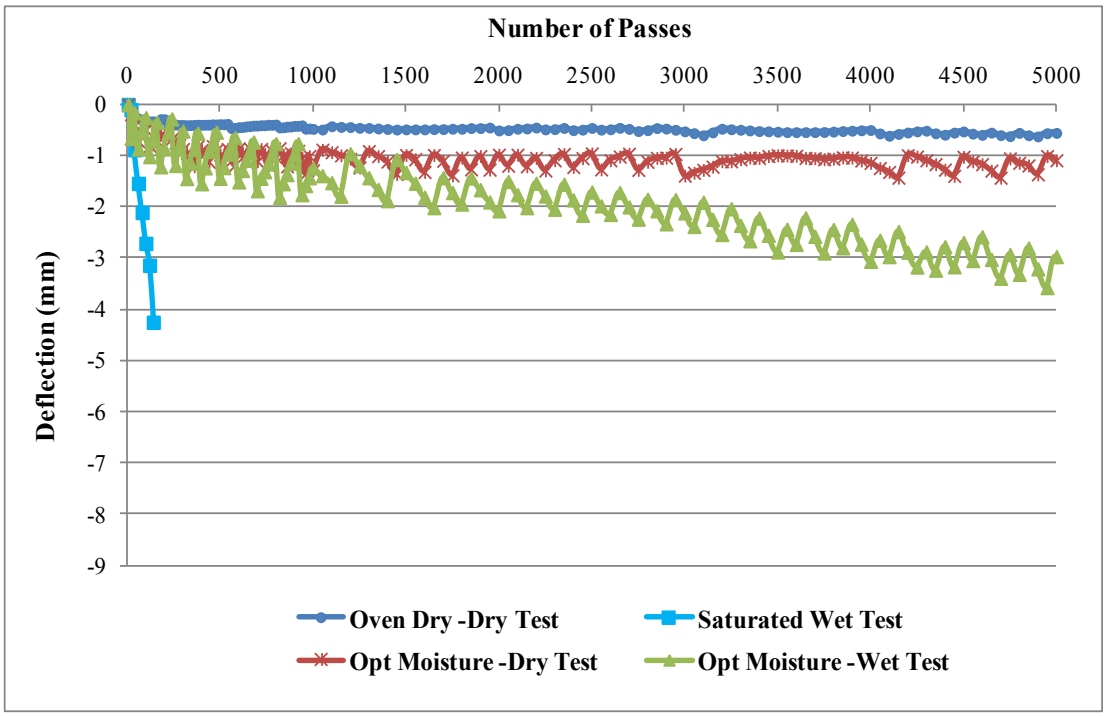

Figure 57 Hamburg Tests for Fat Clay, Sample Number 8.

6.3.3 Stabilized Clay Samples

In order to evaluate the effectiveness of soil stabilization, four stabilized conditions were tested for each of the two clay samples described above; three cement stabilized (3%, 5% and 7% cement) and one lime stabilized sample. Samples were cured for 28 days and were all tested right after moisture room at completely saturated moisture levels. If the samples were tested in drier conditions, the erosion rate would have been minimal; therefore those conditions were not tested. Effective percent of added lime was measured based on pH measurements (TXDOT-121E) and used to make lime treated samples [71]. The effective percent of lime was found to be 2% for the lean

clay (based on field observations, this sample may have been treated with lime in the field prior to sampling) and 4% for the fat clay (Appendix C). Table 21 and Figure 58 show results for HWTD testing on stabilized clays. Figure 59 and Figure 60 shows the plot of test results for stabilized lean clay and fat clay.

Table 21 Results for Hamburg Test on Stabilized Clays.

Test Method	Wet Test in Saturation	Wet Test in Saturation	Wet Test in Saturation	Wet Test in Saturation	Wet Test in Saturation
% Stabilized	0% Cement	3% Cement	5% Cement	7% Cement	Effective % of Lime
ER for #7	13600	6400	3500	1100	3400
ER for #8	32400	8200	5300	2200	4200

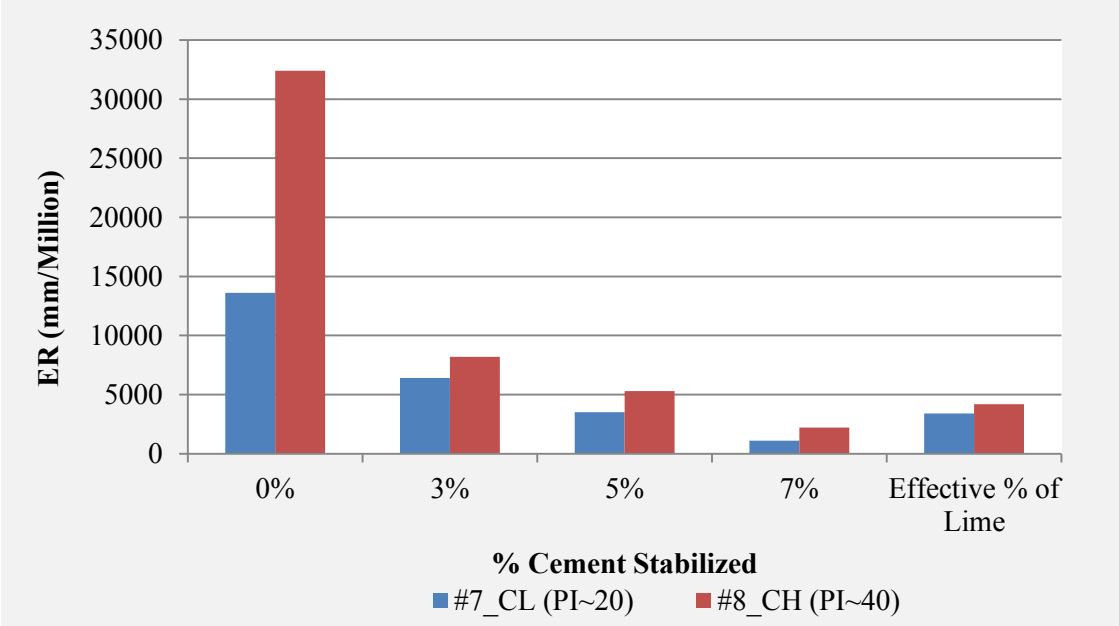

Figure 58 Results for Hamburg Test on Stabilized Clays.

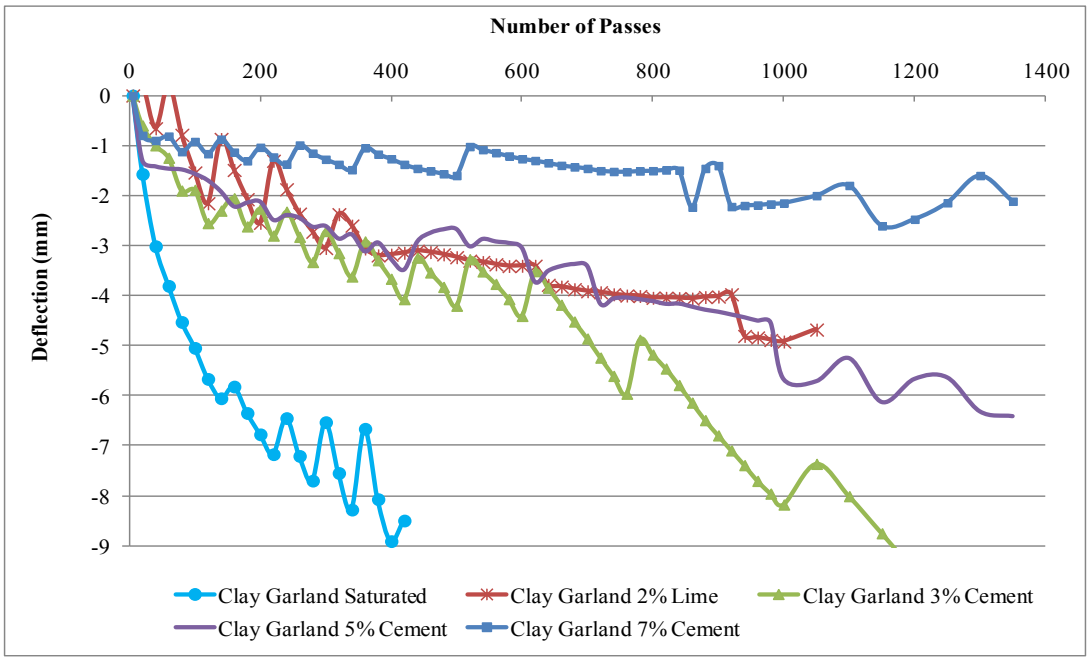

Figure 59 Hamburg Tests for Stabilized Lean Clay, Sample Number 7.

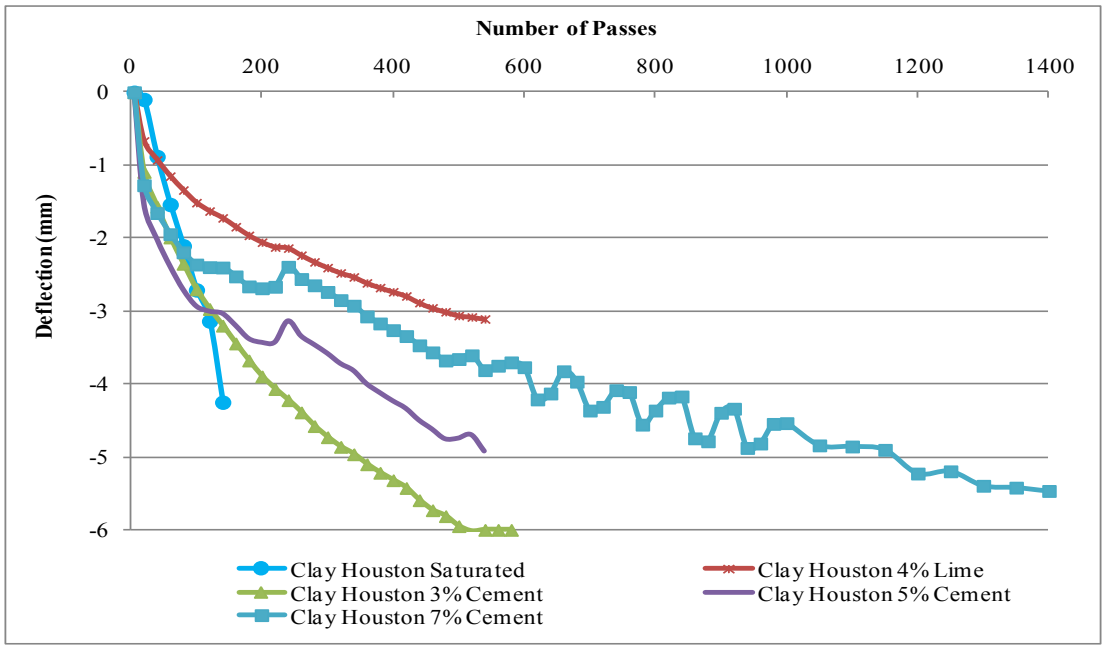

Figure 60 Hamburg Tests for Stabilized Fat Clay, Sample Number 8.

As it was expected, stabilization significantly improved the resistance of the samples against erosion. Clays with less plasticity are stronger against erosion in extreme wet conditions. Even though high plastic clays have higher cohesiveness compared to low plastic clays, they absorb more water when saturated, hence the reverse effect that water has on cohesiveness weakens the high plastic clay.

6.3.4 Stabilized Sand Samples

Three sand-stabilized samples were tested on sample number one, the beach sand from North Carolina using 6% lime, 6% cement and 3% cement added with 3% lime. Samples were cured for 14 days and were all tested right after moisture room, at saturated moisture levels. Table 22 and Figure 61 show results for Hamburg test on stabilized clays. Figure 62 shows the plot of Hamburg tests for stabilized poorly graded sand, sample number one.

Table 22 Results for Hamburg Test on Stabilized Sand.

Test Method	Wet Test in Saturation	Wet Test in Saturation	Wet Test in Saturation	Wet Test in Saturation
% Stabilized	Non-Stabilized	6% Lime	3% Lime +3%Cement	6% Cement
ER for #1_Sand (SP)	4500	3100	2500	1070

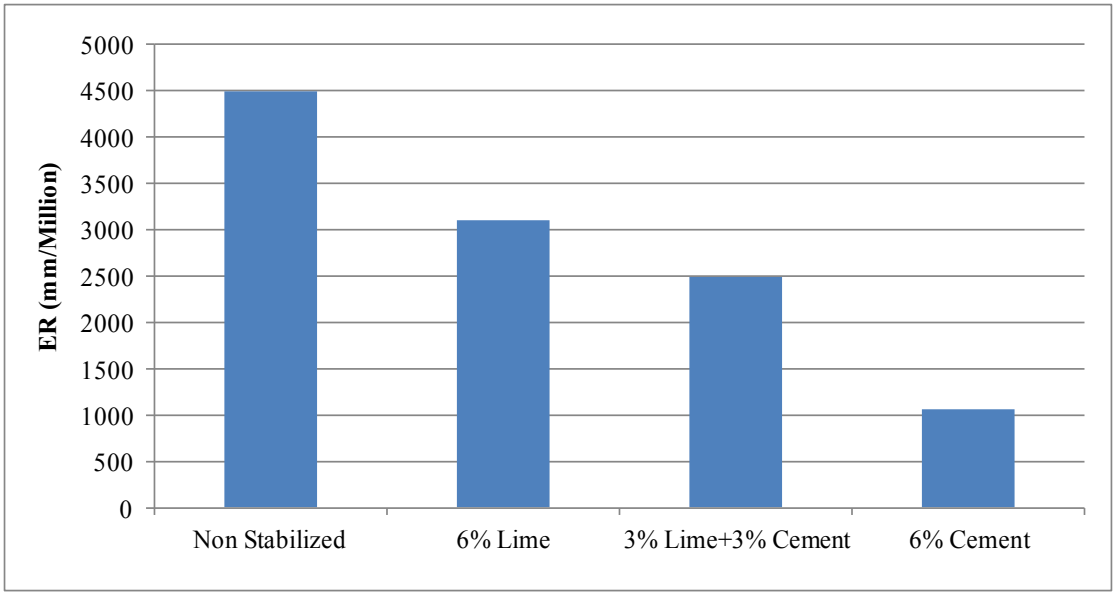

Figure 61 Results for Hamburg Test on Stabilized Sand.

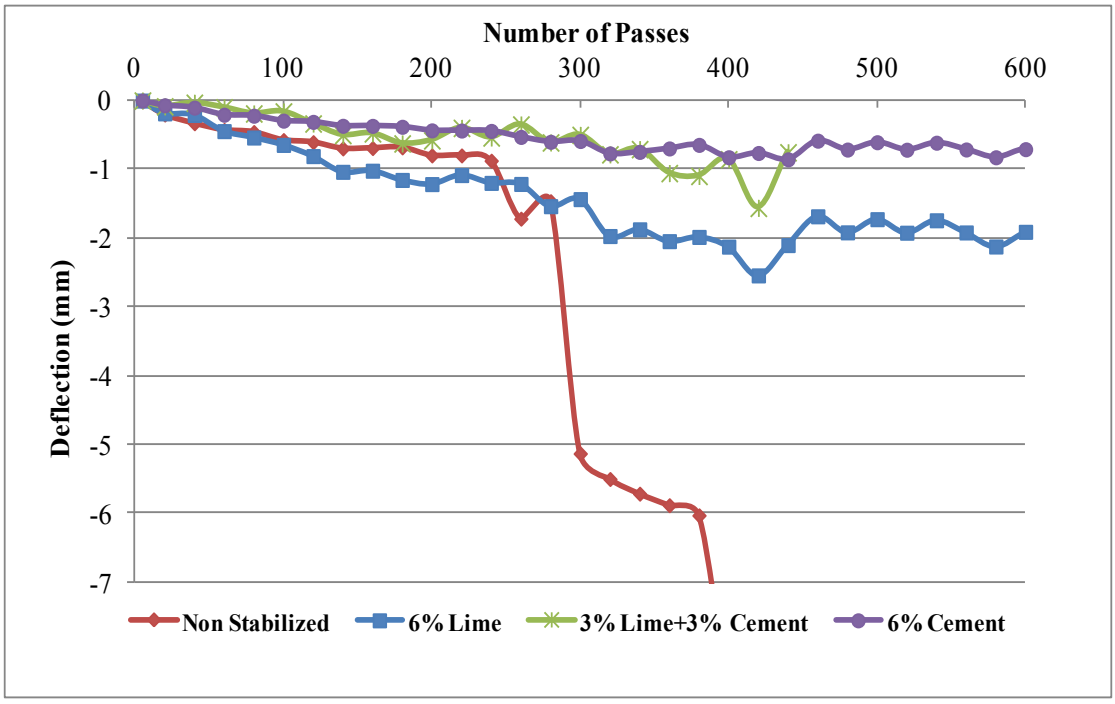

Figure 62 Hamburg Tests for Stabilized Sand, Sample Number 1.

Stabilization improved the resistance of sand against erosion. Cement stabilization showed better erodibility resistance as compared to lime stabilization. Also stabilization has greater impact on clay as compared to sands mainly because of faster and stronger chemical reactions of clay particles.

7. CONCLUSIONS AND DISCUSSIONS

Past and present joint sealing practice was reviewed and critiqued. Different sealant types was discussed and compared. Brief review on sealant failure mechanism was provided and a review of previous studies and observations on the subject were presented.

An experimental program on sealant effectiveness in regards to water infiltration was performed. Several important conclusions can be drawn from the results of this test program. Valuable data was collected during the field testing of joint sealant effectiveness. The experimental results showed that if joint seals are properly installed, they can be very effective in preventing moisture infiltration. Unsealed joints have significantly higher flow rates compared to joints with damaged sealants. Moreover, results showed that different joint seals start to infiltrate greater and greater amounts of water at different threshold widths. Preformed sealants have better resistance to infiltration and have historically showed longer service periods. The test results in this study have also demonstrated the effect of proper sealant installation on performance. The water infiltration rates for dirty joints were as high as the amount of water that was infiltrated for the joints with 50% debonding. In comparison to a clean joint with a 3mm joint opening, the infiltration rate was more than 5 times the infiltration rate of that allowed for dirty joints. The sensitivity of the sealants to poor installation is more dramatic when the joint openings are wider that perhaps is the case in climatic conditions experiencing a wide range of temperature change.

A mechanistic definition for the number of wet days was developed and analyzed. Most definitions relate the number of wet days only to climatic factors such as rainfall. But the actual number of days that water exists underneath the slab is not only a factor of rainfall. Several other factors such as surface and subsurface drainage, joint sealants and subbase permeability must be taken into consideration when defining the actual number of wet days. As an example for a certain pavement section in a high rainfall region a clay subgrade can hold water but a granular subbase may drain the water. Therefore, number of wet days for the pavement with clay subgrade is greater even though they are both in a same climatic region. Number of wet days was analyzed and formulated in order to be used for design purposes.

An intensive erosion test program was performed on different subbase/subgrade materials. Several important conclusions drawn from this test program are summarized as follows:

- The presence of water is a critical factor in the process of erosion underneath a slab. Subgrade materials when exposed to water show considerably less resistance against erosion compared to when they are dry. Existence of water significantly decreases the shear strength at the slab/subbase interface therefore it greatly increases the potential for erosion to occur. The erosion rate under wet condition was found to be on the average 20 times greater than the dry erosion rate for tested subgrade samples.

- All the subbase samples showed acceptable performance in the absence of water. Even though erosion occurred in dry tests, the rate of dry erosion was very low for all samples.
- Sands found to be highly erodible, particularly when the slit and clay content is lower. Sandy soils are not as cohesive which contributes to the sand relatively weak performance against erosion. Clays on the other hand were found to be more resistant against erosion.
- While dried clays are very resistant against erosion, clays are extremely erodible when they become completely saturated. It should be noted that complete saturation of the clay material as a sublayer rarely occurs unless pavement is in an extremely wet climate with unsealed joints and poor drainage system. Tested samples that were only one inch thick were held in a moisture room over a week to get saturated.
- These results suggest that clays could be used as a subbase under dry conditions for low volume roads or parking lots but using clays as a subbase should be avoided in places with heavy rain and unsealed joints.
- Stabilization significantly improved the resistance of the clay samples against erosion. Seven percent cement caused a decrease in erodibility index by 14 times in fat clay. Stabilization also improved the resistance of sand materials against erosion.

- Cement stabilization showed better erodibility resistance as compared to lime stabilization. Also, both types of stabilization had greater impact on clay materials as compared to sands mainly because of mineralogy of clay materials.

Faulting directly affects the serviceability of the pavement. It indirectly contributes to other major distress types that affect the performance of jointed concrete pavement. A model for faulting was developed and presented. The presence of water on the interface along with the effect of traffic and erodibility are the three main elements of the erosion/faulting process. Traffic, the erosion resistance of materials, and number of wet days were precisely defined and considered in this model. The mechanistic empirical model presented in this dissertation can effectively analyze the faulting and erosion in jointed concrete pavements. The model is capable of calibration for local conditions as a distinct advantage to any other faulting model found in the literature. The model was successfully calibrated and implemented as part of a computerized format. Results show that the model fits well with the field data and can be implemented for design and maintenance management purposes.

By using the model, the effectiveness of sealant on pavement sustainability can be ascertained. A valuable outcome of this study is the demonstration mechanistically of the role of joint seal effectiveness on service life of jointed concrete pavements. Sealants, by limiting water infiltration into the pavement sublayers, can improve concrete pavement performance.

REFERENCES

1. Hall, K.T., J.A. Crovetti, and T.E. Hoerner, *Effectiveness of Sealing Transverse Contraction Joints in Concrete Pavements – Final Report*. 2008, U.S. Department of Transportation, Federal Highway Administration: McLean, VA.

2. Teller, L.W. and E.C. Sutherland, *The Structural Design of Concrete Pavements: Part 4A, Study of the Structural Design of Several Types of Transverse and Longitudinal Joint Designs.* Journal of Public Roads, 1936. 17(7): p. 143-149.

3. Ioannides, A.M., A.R. Long, and I.A. Minkarah, *Joint Sealant and Structural Performance at the Ohio Route 50 Test Pavement.* Transportation Research Record: Journal of the Transportation Research Board, 2004. 1866(1): p. 28-35.

4. Morian, D.A. and S. Stoffels, *Joint Seal Practices in the United States: Observations and Considerations.* Transportation Research Record: Journal of the Transportation Research Board, 1998. 1627(1): p. 7-12.

5. Olson, R.C. and R. Roberson, *Edge Joint Sealing as a Preventive Maintenance Practice*. 2003, Minnesota Department of Transportation, Office of Materials Road Research: Saint Paul, MN.

6. Lynch, L., R. Steffes, and J. Chehovits, *Joint and Crack Sealing Challenges, Transportation in the New Millennium*. 2000, Committee on Sealants and Fillers for Joints and Cracks, Transportation Research Board: Washington, D.C.

7. ASTM-D5078, *Standard Specification for Crack Filler, Hot-Applied, for Asphalt Concrete and Portland Cement Concrete Pavements*. 2011, American Society for Testing and Materials: West Conshohocken, PA.

8. ASTM-D5893, *Standard Specification for Cold Applied, Single Component, Chemically Curing Silicone Joint Sealant for Portland Cement Concrete Pavements*. 2010, American Society for Testing and Materials: West Conshohocken, PA.

9. ASTM-D2628, *Standard Specification for Preformed Polychloroprene Elastomeric Joint Seals for Concrete Pavements*. 2011, American Society for Testing and Materials: West Conshohocken, PA.

10. Neshvadian Bakhsh, K., D.G. Zollinger, and Y.S. Jung, *Evaluation of Joint Sealant Effectiveness on Moisture Infiltration and Erosion Potential in Concrete Pavement*, in *Transportation Research Board 92nd Annual Meeting*. 2013, Transportation Research Record: Washington, D.C. p. 42-48.

11. Smith, K.L. and A.R. Romine, *LTPP Pavement Maintenance Materials: SHRP Crack Treatment Experiment, Report No. FHWA-RD-99-143*. 1999, Federal Highway Administration, : Washington, D.C.

12. Bautista, F.E., *Caltrans-Industry Joint Sealing Field Review*. 2012, California Department of Transportation: Sacramento, CA.

13. Brown, H.E., *Joint Sealant Materials for Concrete Pavement Repairs*. 1991, Virginia Transportation Research Council: Charlottesville, VA.

14. Lynch, L.N., J.G. Chehovits, and D.G. Luders, *Ten-Year Field Performance Evaluation of Joint Reseating Project.* Transportation Research Record: Journal of the Transportation Research Board, 2002. 1795(1): p. 40-48.

15. ARA, *Arizona SPS-2 PCC Joint Seal Performance* in *ARA Technical Memorandum*. 2013, Applied Research Associates: Albuquerque, NM.

16. Eacker, M.J. and A.R. Bennett, *Evaluation of Various Concrete Pavement Joint Sealants*. 2000, Michigan Department of Transportation: Lansing, MI.

17. Lynch, L.N., J.G. Chehovits, and D.G. Luders, *Joint Resealing Project at Fairchild Air Force Base, Washington.* Transportation Research Record: Journal of the Transportation Research Board, 2013. 2361(1): p. 98-105.

18. Scofield, L., *Relative Cost of Concrete Highway Features: Final Report 12-27-10*. 2010, American Concrete Pavement Association: Rosemont, IL.

19. Shober, S.F., *The Great Unsealing: A Perspective on Portland Cement Concrete Joint Sealing.* Transportation Research Record: Journal of the Transportation Research Board, 1997. 1597(-1): p. 22-33.

20. Li, Q., *Development of Testing System for Analysis of Transverse Contraction Joints in Portland Cement Concrete Pavement*. 2012, University of Florida: Gainesville, FL.

21. Gurjar, A.H., T. Tang, and D.G. Zollinger, *Evaluation of Joint Sealants of Concrete Pavements.* Journal of The National Aeronautics and Space Administration, 1997(19990008235).

22. Gurjar, A., D.G. Zollinger, and T. Tang, *Strain and Age Effects on Behavior of a Concrete Pavement Joint Sealant Material.* Transportation Research Record: Journal of the Transportation Research Board, 1996. 1529(1): p. 95-100.

23. Gurjar, A., H.B. Kim, and E. Moody, *Laboratory Investigation of Factors Affecting Bond Strength in Joint Sealants.* Transportation Research Record: Journal of the Transportation Research Board, 1998. 1627(-1): p. 13-21.

24. Hawkins, B.K., A.M. loannides, and I.A. Minkarah, *To Seal or Not to Seal? A Field Experiment to Resolve An Age-Old Dilemma.* Transportation Research Record: Journal of the Transportation Research Board, 2001. 1749(1): p. 38-45.

25. Cho, Y.K., *Advanced Cleaning Device to Remove Debris and Chemicals for Crack/Joint Sealing in Pavement- Final Report*, in *Highway IDEA Project 159*. 2013, Transportation Research Board Lincoln, NE.

26. Cook, J. and I.A. Minkarah, *Pavement Design Features and Their Effect on Joint Seal Performance.* Transportation Research Record, 1980(752).

27. Morian, D.A., N. Suthahar, and S. Stoffels, *Evaluation of Rigid Pavement Joint Seal Movement.* Transportation Research Record: Journal of the Transportation Research Board, 1999. 1684(1): p. 25-34.

28. Weisgerber, F.E. and C.P. Wang, *Stress Distributions in Highway Joint Seals.* Science and Technology of Building Seals, Sealants, Glazing, and Waterproofing, Second Volume, 1992: p. 213.

29. Woo Lee, S. and S.M. Stoffels, *Analysis of In-Situ Horizontal Joint Movements in Rigid Pavements.* Transportation Research Record: Journal of the Transportation Research Board, 2001. 1778(1): p. 9-16.

30. Tons, E., *Factors in Joint Seal Design.* Highway Research Record, 1965(80).

31. Ray, G.K., *Effect of Defective Joint Seals on Pavement Performance.* Transportation Research Record, 1980.

32. Dunn, K.H., *The Effect of Sealed versus Unsealed Joints on the Performance of Jointed PCC Pavement*. 1987, Wisconsin Department of Transportation: Madison, WI.

33. Burke Jr, M.P. and J.W. Bugler. *The Long-Term Performance of Unsealed Jointed Concrete Pavements*. in *Transportation Research Board 81nd Annual Meeting*. 2002. Washington, D.C.: Transportation Research Board.

34. Hall, K.T. and J.A. Crovetti, *LTPP Data Analysis: Relative Performance of Jointed Plain Concrete Pavement with Sealed and Unsealed Joints*. 2000, Transportation Research Board, National Research Council: Washington, D.C.

35. Curt Dunn, B. and K.E. Fuchs, *Practice of Unsealed Joints in New Portland Cement Concrete Pavements*. 2009, North Dakota Department of Transportation: Bismarck, ND.

36. Cedergren, H.R., *Seepage, Drainage, and Flow Nets*. Vol. 16. 1997, New York, NY: John Wiley & Sons.

37. Forsyth, R.A., G.K. Wells, and J.H. Woodstrom, *Economic Impact of Pavement Subsurface Drainage.* Transportation Research Record: Journal of the Transportation Research Board, 1987(1121): p. 77-85.

38. Huang, Y.H., *Pavement Analysis and Design*. 2 ed. 2003, Saddle River, NJ: Prentice Hall.

39. AASHTO, *Guide for Design of Pavement Structures*. 1998, American Association of State Highway and Transportation Officials,: Washington, D.C.

40. NCHRP, *Mechanistic-Empirical Pavement Design Guide*. 2004, National Cooperative Highway Research Program: Champaign, IL.

41. Jung, Y.S. and D.G. Zollinger, *New Laboratory-Based Mechanistic-Empirical Model for Faulting in Jointed Concrete Pavement.* Transportation Research Record: Journal of the Transportation Research Board, 2011. 2226(1): p. 60-70.

42. DRIP, *Drainage Requirements in Pavements Version 2.0*. 2002, Federal Highway Administration, US Department of Transportation: Washington, D.C.

43. Marek, M., *Roadway Design Manual*, in *TxDOT Manuals*. 2010, Texas Department of Transportation: Austin, TX.

44. Cedergren, H.R., J.A. Arman, and K.H. O'Brien, *Development of Guideline for the Design of Subsurface Drainage Systems for Highway Pavement Structural Sections*. 1973, Federal Highway Administration: Washington, D.C.

45. Reddi, L.N., *Seepage in Soils: Principles and Applications*. 2003, New York, NY: John Wiley & Sons.

46. Ridgeway, H., *Infiltration of Water Through the Pavement Surface.* Transportation Research Record, 1976(616): p. 98-100.

47. Ridgeway, H.H. *Pavement Subsurface Drainage Systems*. in *NCHRP Synthesis of Highway Practice*. 1982. Washington, D.C.: National Cooperative Highway Research Program (NCHRP).

48. Oldfield, D. and T. Symes, *Long Term Natural Ageing of Silicone Elastomers.* Polymer Testing, 1996. 15(2): p. 115-128.

49. Munson, B.R., D.F. Young, and T.H. Okiishi, *Fundamentals of Fluid Mechanics*. 1990, New York, NY: John Wiley & Sons.

50. Keefer, D.L. and S.E. Bodily, *Three Point Approximations for Continuous Random Variables.* Management Science, 1983. 29(5): p. 595-609.

51. Selezneva, O., J. Jiang, and S.D. Tayabji, *Preliminary Evaluation and Analysis of LTPP Faulting Data-Final Report*. 2000, Federal Highway Administration: Washington, D.C.

52. Byrum, C.R. and R.W. Perera, *The Effect of Faulting on IRI Values for Jointed Concrete Pavements*. 2005, Texas Transportation Institute: College Station, TX.

53. Jung, Y.S., D.G. Zollinger, and T.J. Freeman, *Evaluation and Decision Strategies for the Routine Maintenance of Concrete Pavement*. 2009, Texas Transportation Institute: College Station, TX.

54. Freeman, T.J. and D.G. Zollinger, *Guidelines for Routine Maintenance of Concrete Pavement*. 2008, Texas Transportation Institute: College Station, TX.

55. Neshvadian Bakhsh, K., *Evaluation of Bond Strength between Overlay and Substrate in Concrete Repairs*. 2010, KTH University (The Royal Institute of Technology): Stockholm, Sweden.

56. ACI, *Guide for Design of Jointed Concrete Pavements for Streets and Local Roads*, in *ACI 325-12R-02*. 2002, American Concrete Institute: Farmington Hills, MI.

57. De Beer, M., *Aspects of Erodibility Lightly Cementitious Materials*, in *South African Council for Scientific Industrial Research.* . 1989, Flexible Pavement Program: Cape Town, South Africa.

58. Tex-242-F, *Standard for Hamburg Wheel Tracking Test*. 2009, Texas Department of Transportation: Houston,TX.

59. Jung, Y.S., D.G. Zollinger, and A.J. Wimsatt, *Test Method and Model Development of Subbase Erosion for Concrete Pavement Design.* Transportation Research Record: Journal of the Transportation Research Board, 2010. 2154(1): p. 22-31.

60. Zollinger, D.G., B.H. Cho, and A.J. Wimsatt, *Subbase and Subgrade Performance Investigation and Design Guidelines for Concrete Pavement*. 2012, Texas Transportation Institute: College Station, TX.

61. Neshvadian Bakhsh, K. and D. Zollinger. *Faulting Prediction Model for Design of Concrete Pavement Structures*. in *Geo-Shanghai 2014*. 2014. Shanghai,China: American Society of Civil Engineers.

62. LTPP-Database. *Long-Term Pavement Performance Program*. Federal Highway Administration Research and Technology [Web] 2013 [cited 1 March 2013; Pavement Performance Database : Inventory and Monitoring Data]. Available from: http://www.ltpp-products.com/.

63. USDA-Webpage. *USDA/The COMET Program*. [Web] 2012 [cited 10 September 2012; Basic Hydrologic Science Course, Runoff Processes,Section Four: Soil Properties]. Available from: http://www.meted.ucar.edu.

64. ASTM-D6913, *Standard Test Methods for Particle-Size Distribution (Gradation) of Soils Using Sieve Analysis*. 2009, American Society for Testing and Materials: West Conshohocken, PA.

65. ASTM-D4318, *Standard Test Methods for Liquid Limit, Plastic Limit, and Plasticity Index of Soils*. 2010, American Society for Testing and Materials: West Conshohocken, PA.

66. ASTM-D2487, *Standard Practice for Classification of Soils for Engineering Purposes (Unified Soil Classification System)*. 2011, American Society for Testing and Materials: West Conshohocken, PA.

67. ASTM-D698, *Standard Test Methods for Laboratory Compaction Characteristics of Soil Using Standard Effort (12 400 ft-lbf/ft3 (600 kN-m/m3))*. 2007, American Society for Testing and Materials: West Conshohocken, PA.

68. ASTM-D1557, *Standard Test Methods for Laboratory Compaction Characteristics of Soil Using Modified Effort (56,000 ft-lbf/ft3(2,700 kN-m/m3))*. 2009, American Society for Testing and Materials: West Conshohocken, PA.

69. ASTM-D2216, *Standard Test Methods for Laboratory Determination of Water (Moisture) Content of Soil and Rock by Mass*. 2010, American Society for Testing and Materials: West Conshohocken, PA.

70. Kawamura, M. and S. Diamond, *Stabilization of Clay Soils Against Erosion Loss*. 1975, Purdue University/Indiana Department of Transportation: West Lafayette, IN.

71. Tex-121-E, *Standard for Soil Lime Testing*. 2002, Texas Department of Transportation: Houston, TX.

72. Engineering-Toolbox. *Evaporation from the Water Surface*. [Web] 2014 [cited 1 June 2014; Tools and Information for Engineering and Design]. Available from: http://www.engineeringtoolbox.com/.

73. Rajput, R., *Engineering Thermodynamics: A Computer Approach (SI Units Version)*. 2009, Sudbury, MA: Jones & Bartlett Publishers.

APPENDIX A. SOIL SAMPLES CLASSIFICATIONS

Sample Number 1.

Location: Greenville, North Carolina, Color: White-Gray

Non-Plastic (LL= 14.2%, PL: Not Applicable)

Coefficient of Uniformity (Cu) = 4.44, Coefficient of Curvature (Cc) = 0.85

Category: Poorly Graded Sand, Group Symbol: SP

Table 23 Gradation Table for Sample No. 1, Poorly Graded Sand.

Sieve mesh size (mm)	Sieve Number	Percent Retained	Percent Passing	Particles	
9.52	3/8"	0.00%	100.0%	Gravel	0.6%
4.750	4	0.57%	99.4%		
2.000	10	5.85%	93.6%	Sand	97.6%
0.425	40	57.00%	36.6%		
0.150	100	31.83%	4.7%		
0.075	200	2.95%	1.8%		
Pan	Pan	1.79%	0.0%	Fines	1.8%

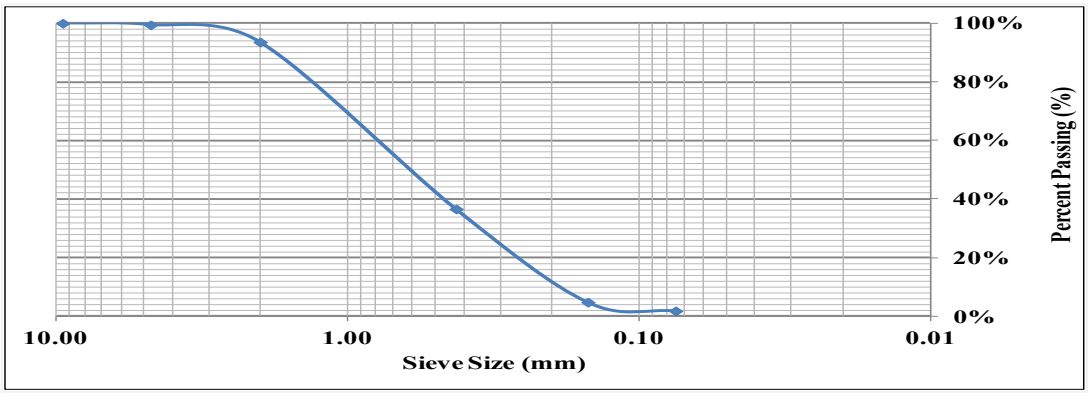

Figure 63 Gradation Curve for Sample No. 1, Poorly Graded Sand.

Sample Number 2.

Location: Delray Beach, Florida, Color: Very Dark Brown

Non-Plastic (LL= 16.1%, PL: Not Applicable)

Coefficient of Uniformity (Cu) = 2.78, Coefficient of Curvature (Cc) = 1.36

Category: Poorly Graded Sand with Silt, Group Symbol: SP-SM

Table 24 Gradation Table for Sample No. 2, Poorly Graded Sand with Silt.

Sieve mesh size (mm)	Sieve Number	Percent Retained	Percent Passing	Particles	
6.300	1/4"	0.0%	100.0%	Gravel	0.5%
4.750	4	0.5%	99.5%		
2.000	10	0.6%	98.9%	Sand	91.8%
0.425	40	14.1%	84.8%		
0.150	100	62.9%	21.9%		
0.075	200	14.2%	7.7%		
Pan	Pan	7.7%	0.0%	Fines	7.7%

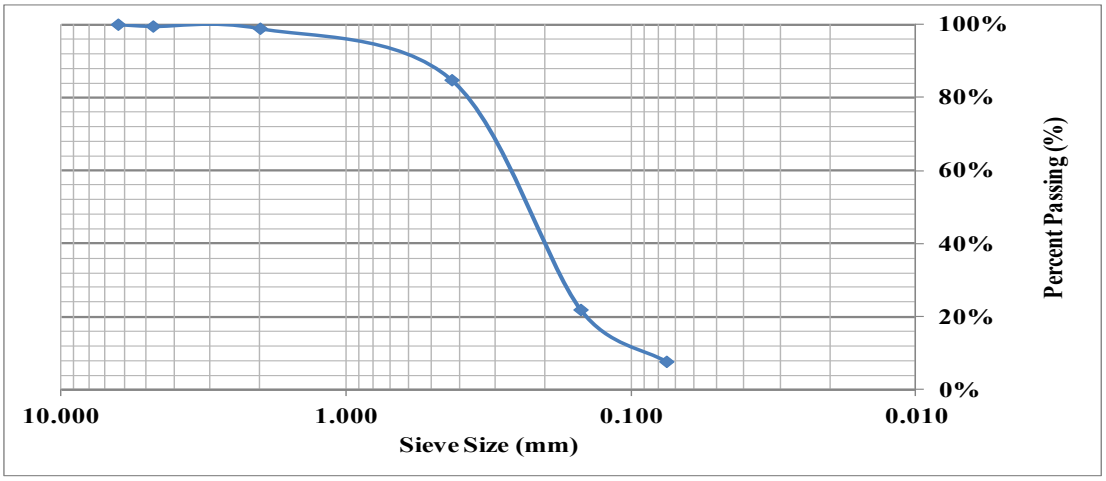

Figure 64 Gradation Curve for Sample No. 2, Poorly Graded Sand with Silt.

Sample Number 3.

Location: College Station, Texas, Color: Light Brown

PI= 2.09%, (LL= 20.01%, PL: 17.92%)

Classification of Fine Portion: Low Plasticity Silt (ML)

Category: Silty Sand, Group Symbol: SM

Table 25 Gradation Table for Sample No. 3, Silty Sand.

Sieve mesh size (mm)	Sieve Number	Percent Retained	Percent Passing	Particles	
12.50	1/2"	0.00%	100.00%	Gravel	3.8%
4.750	4	3.80%	96.20%		
2.000	10	11.40%	84.80%	Sand	69.3%
0.425	40	37.30%	47.50%		
0.150	100	7.70%	39.80%		
0.075	200	12.90%	26.90%		
Pan	Pan	26.90%	0.00%	Fines	26.9%

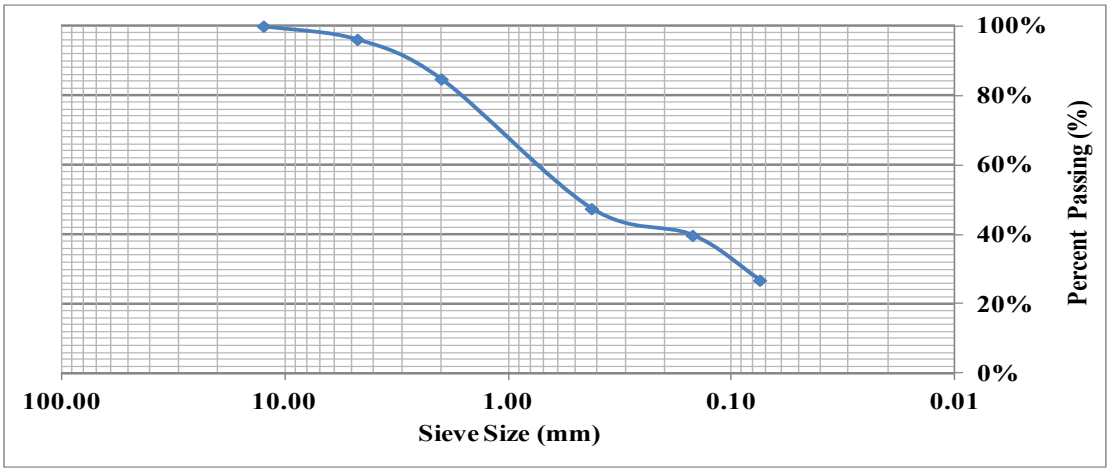

Figure 65 Gradation Curve for Sample No. 3, Silty Sand.

Sample Number 4.

Location: Anderson, South Carolina, Color: Brick Red

PI= 9.91%, (LL= 41.99%, PL: 32.08%)

Classification of Fine Portion: Low Plasticity Silt (ML)

Category: Sandy Silt, Group Symbol: SM

Table 26 Gradation Table for Sample No. 4, Sandy Silt.

Sieve mesh size (mm)	Sieve Number	Percent Retained	Percent Passing	Particles	
9.52	3/8"	0.80%	99.2%	Gravel	3.6%
4.750	4	2.80%	96.4%		
2.000	10	9.30%	87.1%	Sand	63.7%
0.425	40	29.40%	57.7%		
0.150	100	18.20%	39.5%		
0.075	200	6.80%	32.7%		
Pan	Pan	32.70%	0.0%	Fines	32.7%

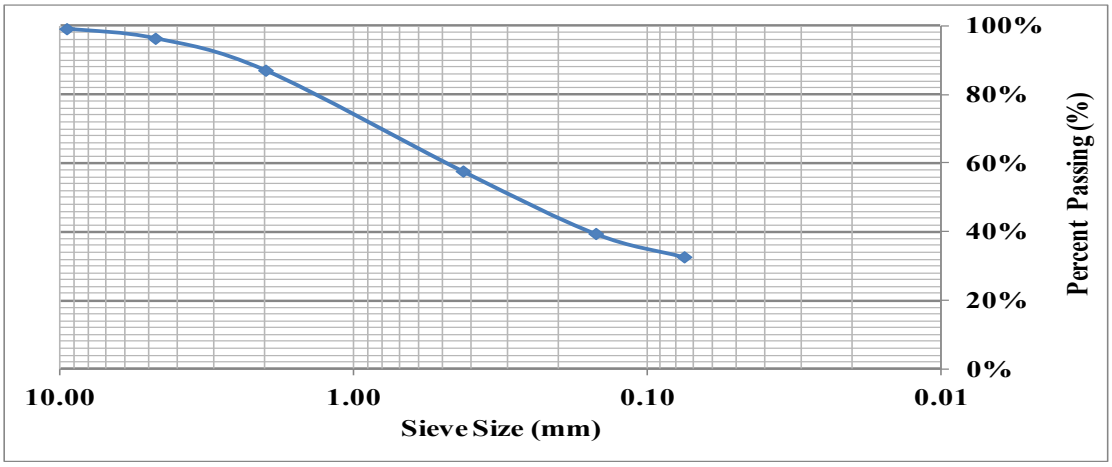

Figure 66 Gradation Curve for Sample No. 4, Sandy Silt.

Sample Number 5.

Location: San Angelo, Texas, Color: Dark Brown

PI= 13.36%, (LL= 32.36%, PL: 19.00%)

Classification of Fine Portion: Low Plasticity Clay (CL)

Category: Sandy Lean Clay, Group Symbol: s(CL)

Table 27 Gradation Table for Sample No. 5, Sandy Lean Clay.

Sieve mesh size (mm)	Sieve Number	Percent Retained	Percent Passing	Particles	
12.50	1/2"	0.0%	100.0%	Gravel	3.0%
4.750	4	3.0%	97.0%		
2.000	10	6.7%	90.3%	Sand	30.7%
0.425	40	15.4%	74.9%		
0.150	100	6.5%	68.4%		
0.075	200	2.1%	66.3%		
Pan	Pan	66.3%	0.0%	Fines	66.3%

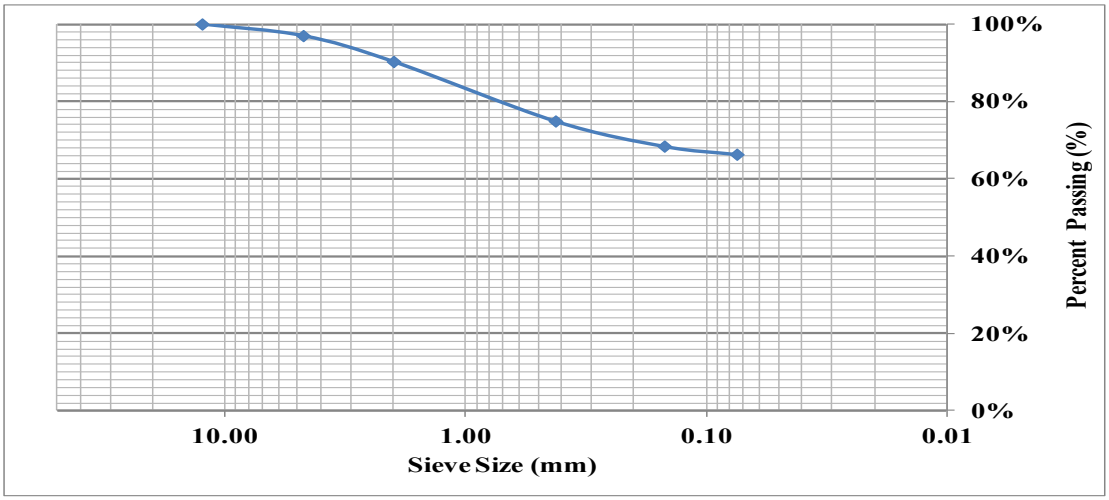

Figure 67 Gradation Curve for Sample No. 5, Sandy Lean Clay.

Sample Number 6.

Location: Houston, Texas, Color: Brown

PI= 17.34% (LL= 33.59%, PL: 16.25%)

Classification of Fine Portion: Low Plasticity Clay (CL)

Category: Sandy Lean Clay with Gravel, Group Symbol: s(CL)g

Table 28 Gradation Table for Sample No. 6, Sandy Lean Clay with Gravel.

Sieve mesh size (mm)	Sieve Number	Percent Retained	Percent Passing	Particles	
12.50	1/2"	2.5%	97.5%	Gravel	15.1%
4.750	4	12.6%	84.9%		
2.000	10	7.3%	77.6%	Sand	22.6%
0.425	40	9.1%	68.5%		
0.150	100	4.3%	64.2%		
0.075	200	1.9%	62.3%		
Pan	Pan	62.3%	0.0%	Fines	62.3%

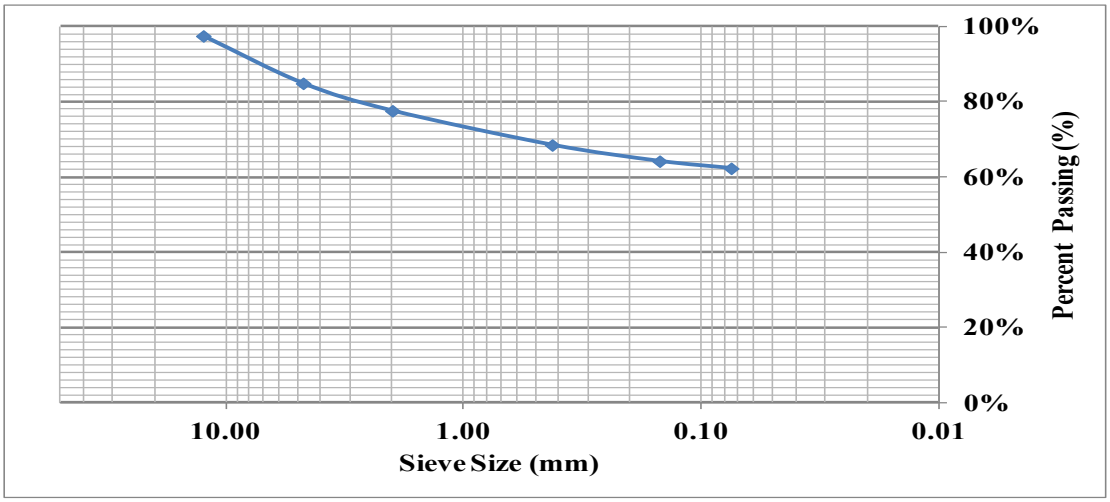

Figure 68 Gradation Curve for Sample No. 6, Sandy Lean Clay with Gravel.

Sample Number 7.

Location: Garland, Texas, Color: Grayish Brown

PI= 19.17% (LL= 41.78%, PL: 22.61%)

Classification of Fine Portion: Low Plasticity Clay (CL)

Category: Lean Clay with Sand, Group Symbol: CL

Table 29 Gradation Table for Sample No. 7, Lean Clay with Sand.

Sieve mesh size (mm)	Sieve Number	Percent Retained	Percent Passing	Particles	
12.50	1/2"	0.00%	100.0%	Gravel	0.0%
4.750	4	0.00%	100.0%		
2.000	10	3.50%	96.5%	Sand	20.7%
0.425	40	11.00%	85.5%		
0.150	100	3.60%	81.9%		
0.075	200	2.60%	79.3%		
Pan	Pan	79.30%	0.0%	Fines	79.3%

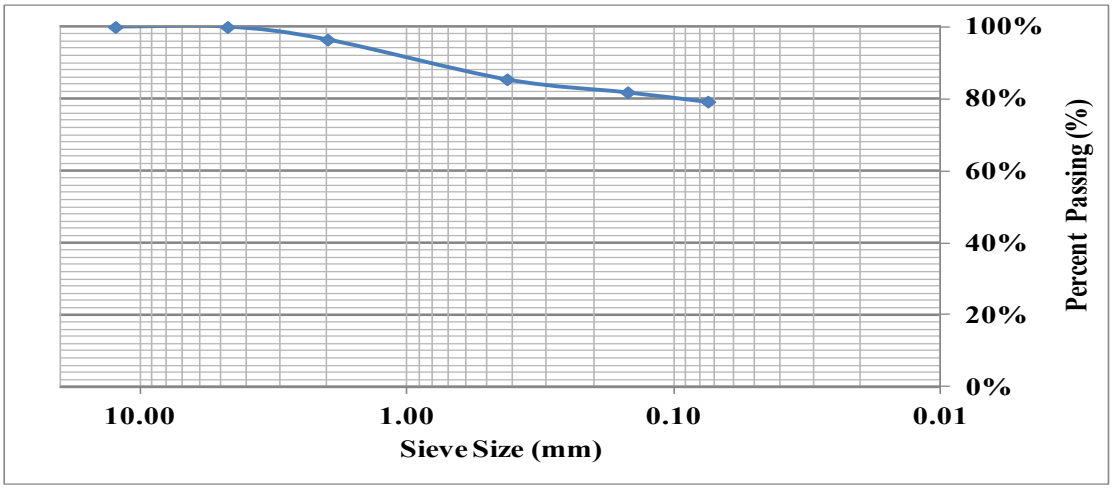

Figure 69 Gradation Curve for Sample No. 7, Lean Clay with Sand.

Sample Number 8.

Location: Houston, Texas, Color: Dark Grayish Brown

PI= 39.96% (LL= 61.48%, PL: 21.52%)

Classification of Fine Portion: High Plasticity Clay (CH)

Category: Fat Clay with Sand, Group Symbol: CH

Table 30 Gradation Table for Sample No. 8, Fat Clay with Sand.

Sieve mesh size (mm)	Sieve Number	Percent Retained	Percent Passing	Particles	
12.50	1/2"	0.00%	100.0%	Gravel	0.0%
4.750	4	0.00%	100.0%		
2.000	10	7.96%	92.0%	Sand	18.29%
0.425	40	6.36%	85.7%		
0.150	100	1.72%	84.0%		
0.075	200	2.25%	81.7%		
Pan	Pan	81.71%	0.0%	Fines	81.71%

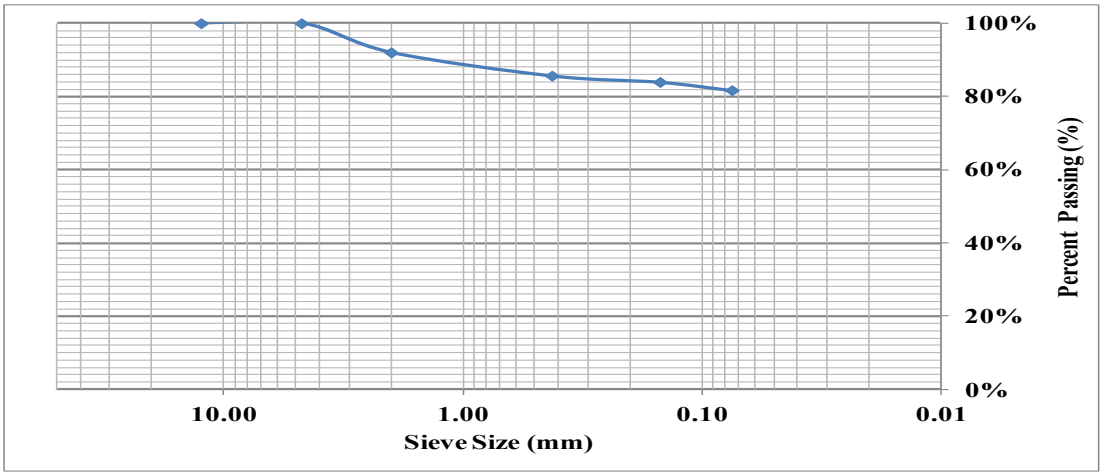

Figure 70 Gradation Curve for Sample No. 8, Fat Clay with Sand.

APPENDIX B. SOIL SAMPLES ATTERBERG LIMITS

Table 31 Atterberg Limits for Samples.

No	Location	State	Category	LL(%)	PL(%)	PI(%)	Category for Fines
1	Greenville	NC	Poorly Graded Sand	14.20	NP	NP	NP
2	Delray Beach	FL	Poorly Graded Sand with Silt	16.10	NP	NP	NP
3	College Station	TX	Silty Sand	20.01	17.92	2.09	ML
4	Anderson	SC	Sandy Silt	41.99	32.08	9.91	ML
5	San Angelo	TX	Sandy Lean Clay	32.36	19.00	13.36	CL
6	Houston	TX	Sandy Lean Clay with Gravel	33.59	16.25	17.34	CL
7	Garland	TX	Lean Clay with Sand	41.78	22.61	19.17	CL
8	Houston	TX	Fat Clay with Sand	61.48	21.52	39.96	CH

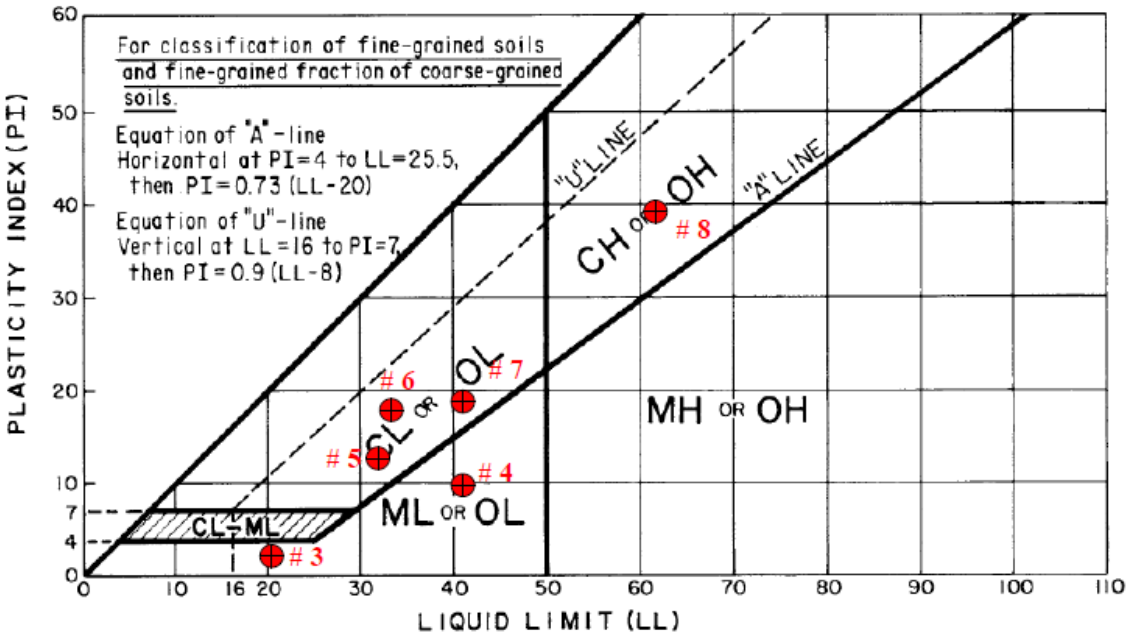

Figure 71 Fine Particles Classifcation for Samples (ASTM D2487).

APPENDIX C. LIME STABILIZATION ON CLAY SAMPLES

The PH test determines the minimum percent lime needed for a soil-lime mixture to attain a PH of 12.4. Cation exchange occurs at this pH, resulting in modification of the soil particle structure to achieve improved workability and decrease swell and plasticity. Series of 30 g samples of soil were placed in separate containers. Series of lime equivalent to 0, 2, 4, 6, 8, and 10% of the 30 g soil samples were added to the soil and mixed with 150 ml (5 fl. oz.) of distilled water to each combination, and stirred vigorously. The PH was measured for each sample and recordings were plotted to find the effective percent of added lime for the soil. Figure 72 shows the PH measurement device. Figure 73 and 74 show the plotted graph for lean and fat clay in this study (sample number 7 and 8). The effective percent of lime is 2% for the lean clay and 4% for the fat clay.

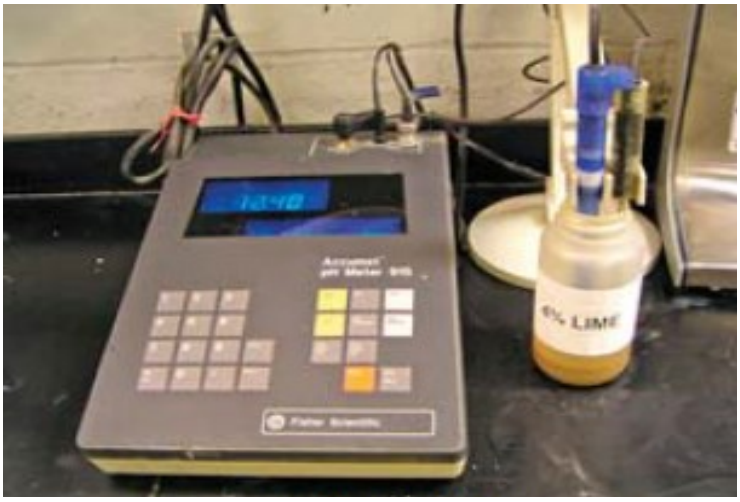

Figure 72 PH Measurement Device.

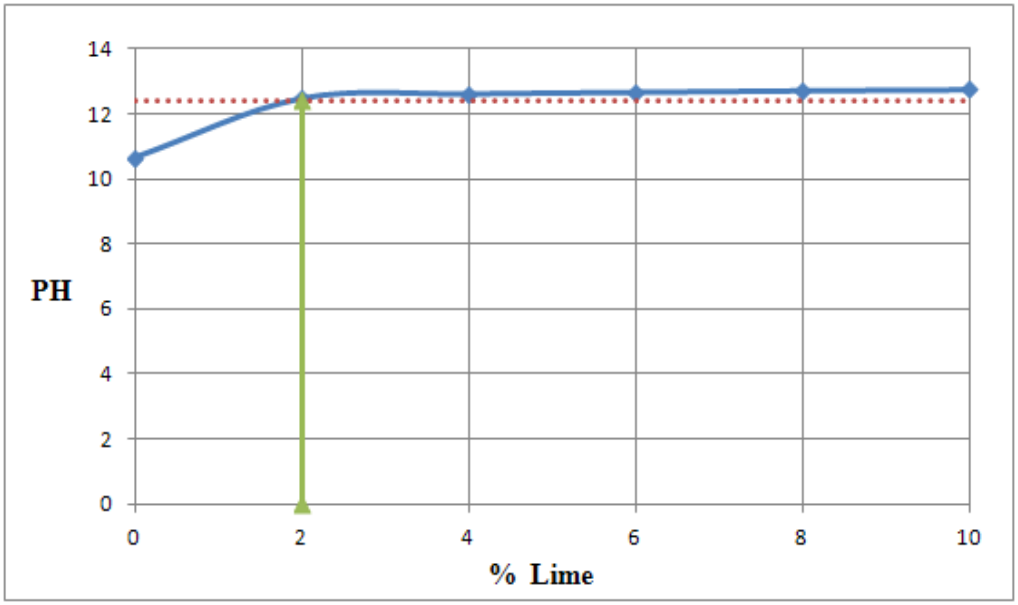

Figure 73 PH Test Plot for Lean Clay, Sample No. 7.

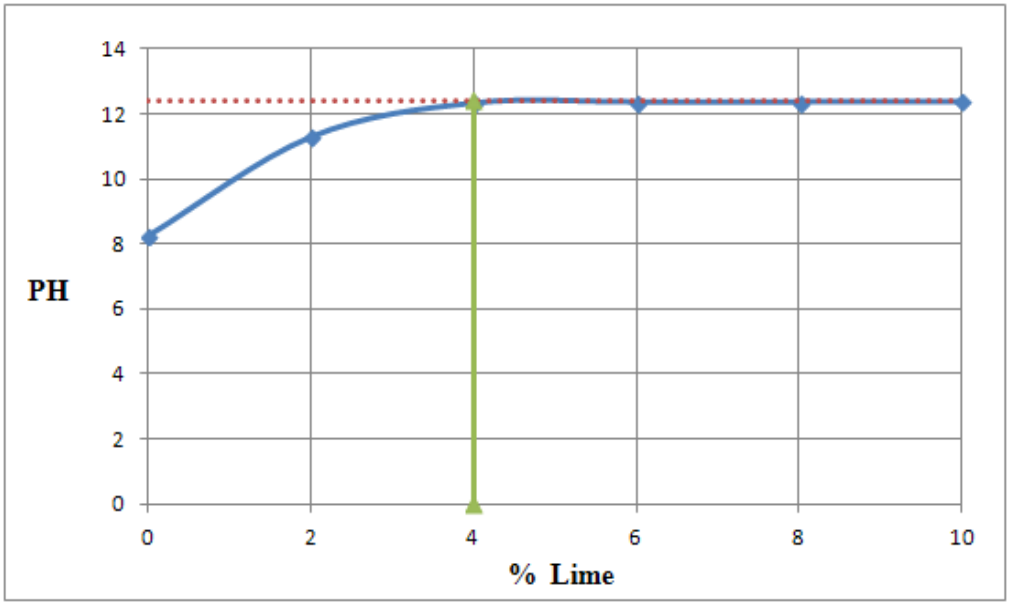

Figure 74 PH Test Plot for Fat Clay, Sample No. 8.

APPENDIX D. HAMBURG TEST RESULTS

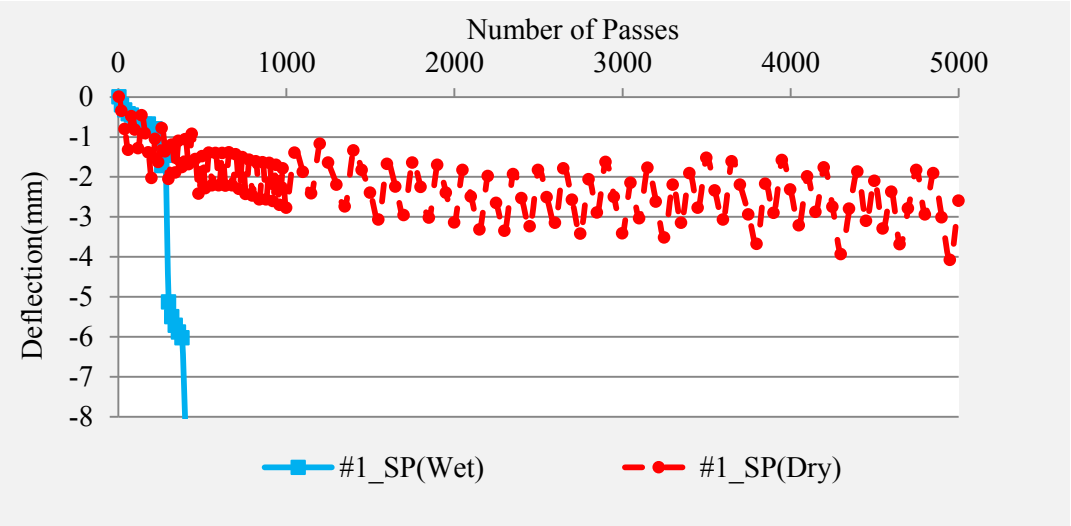

Figure 75 Erosion Test Results for Poorly Graded Sand.

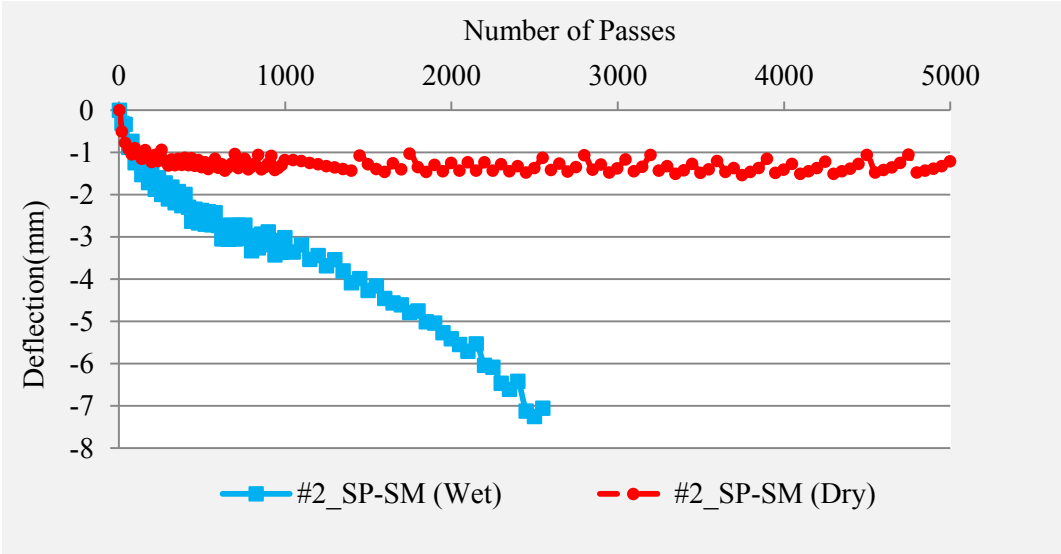

Figure 76 Erosion Test Results for Poorly Graded Sand with Silt.

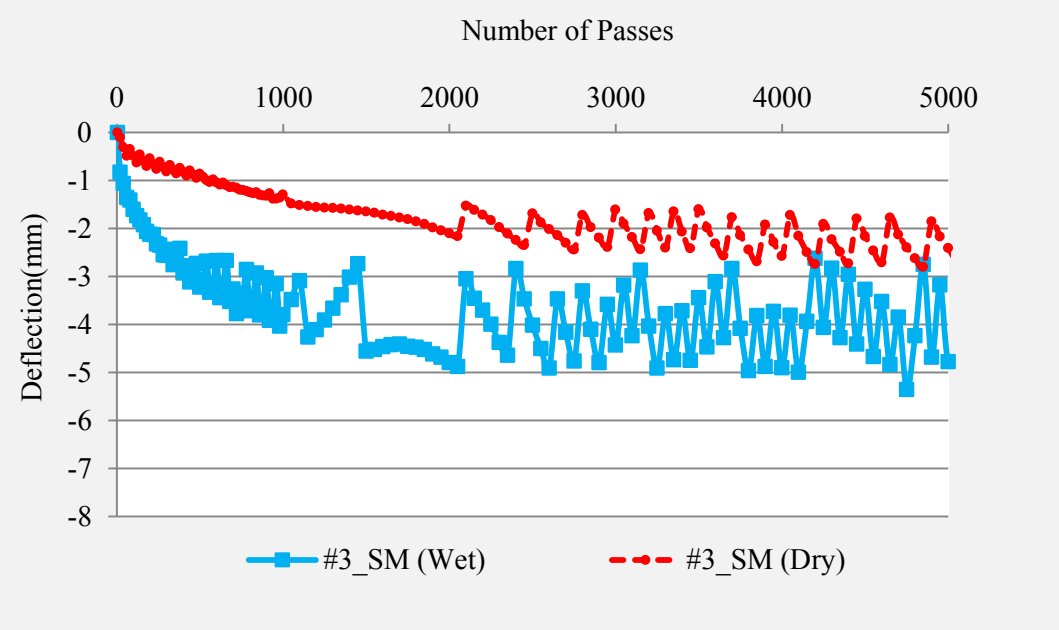

Figure 77 Erosion Test Results for Silty Sand.

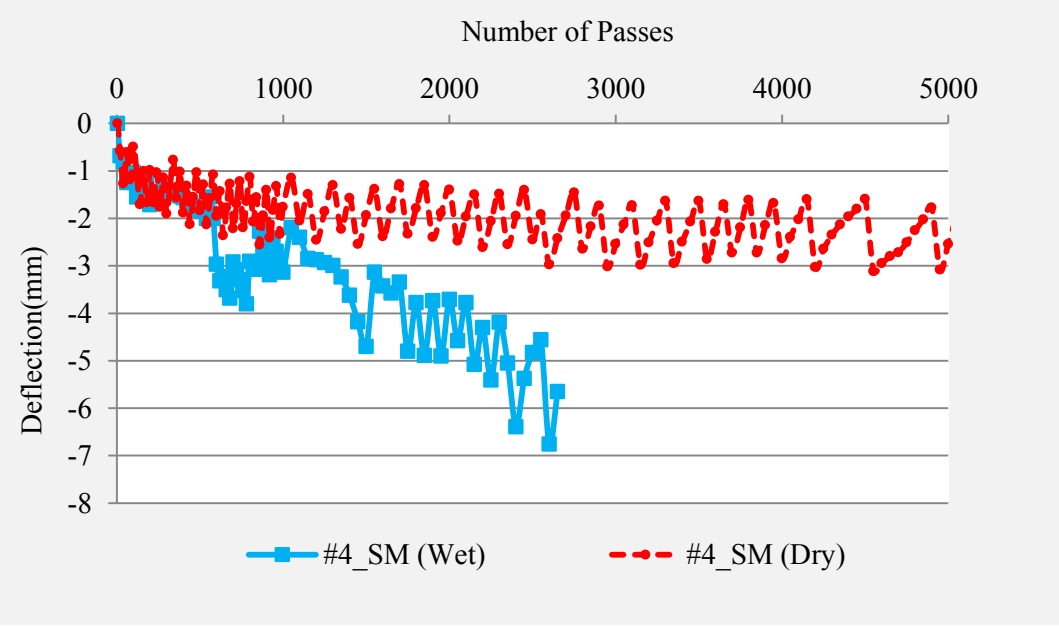

Figure 78 Erosion Test Results for Sandy Silt.

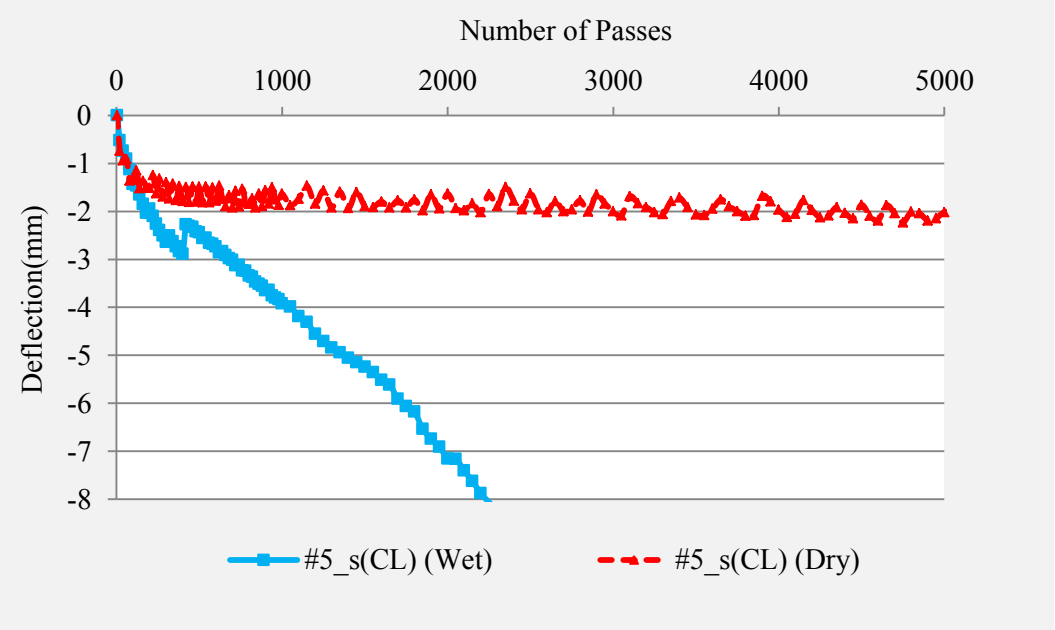

Figure 79 Erosion Test Results for Sandy Lean Clay.

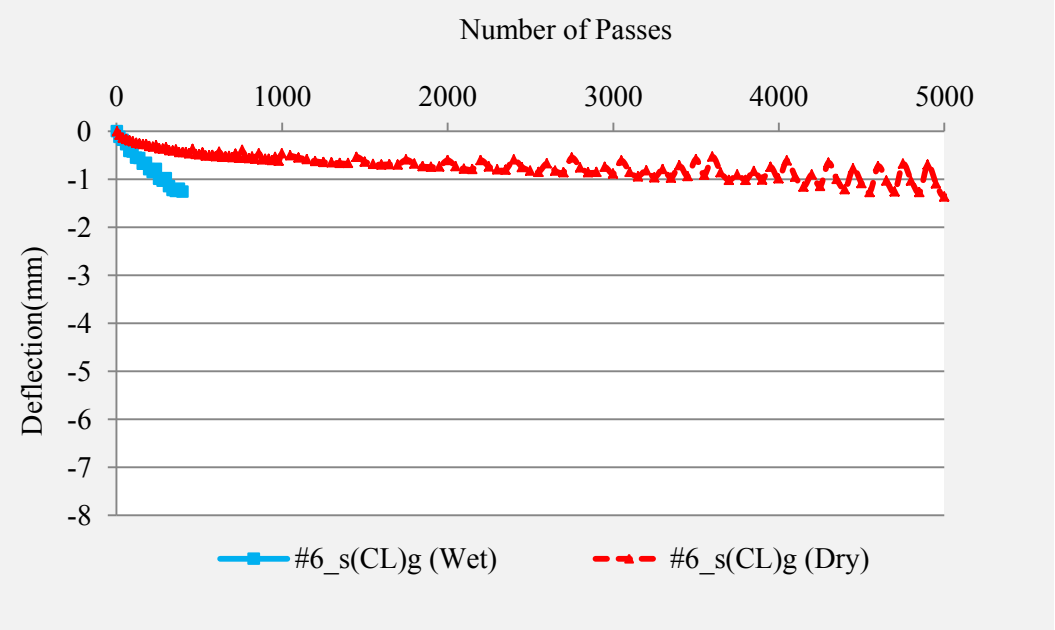

Figure 80 Erosion Test Results for Sandy Lean Clay with Gravel.

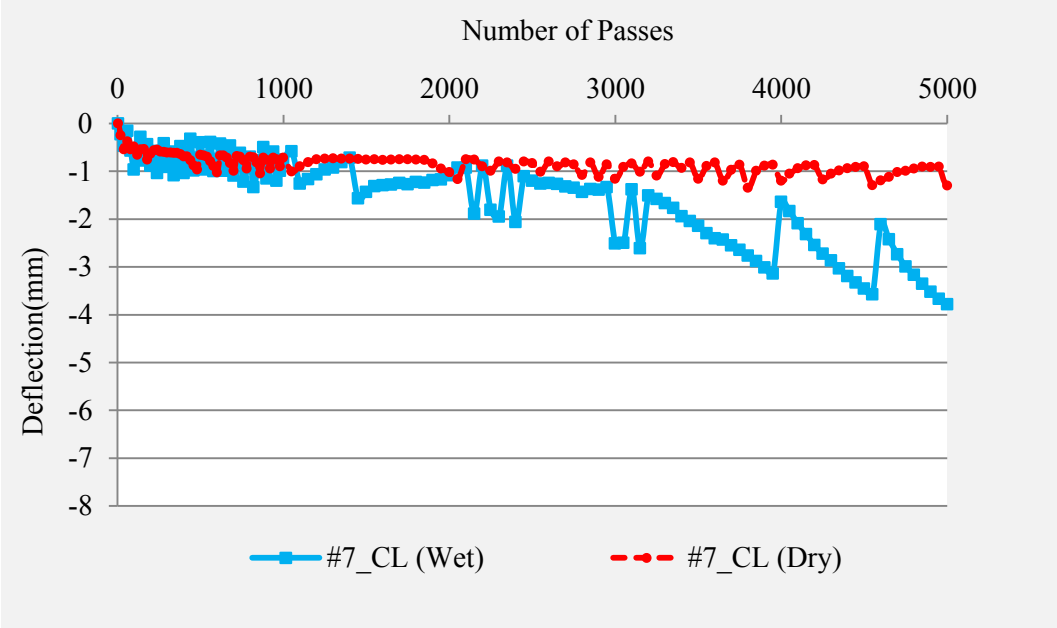

Figure 81 Erosion Test Results for Lean Clay with Sand.

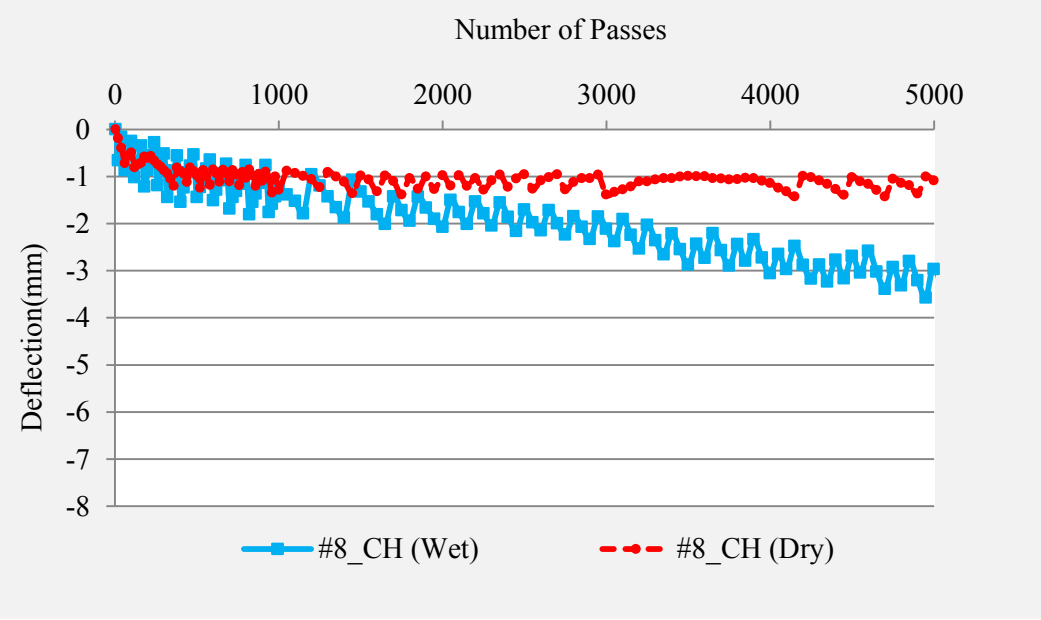

Figure 82 Erosion Test Results for Fat Clay with Sand.

APPENDIX E. EVAPORATION OF TRAPPED WATER IN A JOINT WELL

Water inside the joints is exposed to evaporation. The amount and rate of evaporation depends on the joint surface area, the temperature, the relative humidity and the wind velocity (Figure 83).

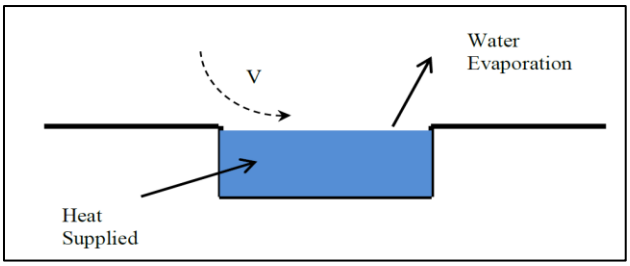

Figure 83 Evaporation of Trapped Water in a Joint.

Evaporation rate factor can be defined using following experimental equation [72, 73];

$$E_h = \theta . A . (x_S - x) \quad \text{(E-1)}$$

where

E_h = amount of evaporated water per hour (kg/h)

$\boldsymbol{\theta}$ = $(25 + 19\ v)$ = evaporation coefficient (kg/m^{2}h)

v = velocity of air above the water surface (m/s)

A = water surface area (m^2)

x_S = humidity ratio in saturated air (kg/kg), (kg H2O in kg Dry Air)

x = humidity ratio in the air (kg/kg), (kg H2O in kg Dry Air) [73]